https://doi.org/10.1016/j.enconman.2021.115175

A comprehensive review of solid oxide fuel cells operating on various promising fuels

Qidong Xu[a], Zengjia Guo[a], Lingchao Xia[a], Qijiao He[a], Zheng Li[a], Idris Temitope Bello[a], Keqing Zheng[b,*], Meng Ni[a,*]

[a] *Department of Building and Real Estate, Research Institute for Sustainable Urban Development (RISUD) & Research Institute for Smart Energy (RISE), The Hong Kong Polytechnic University, Hung Hom, Kowloon, Hong Kong, China*

[b] *School of Electrical and Power Engineering, China University of Mining and Technology, Xuzhou, China*

Corresponding authors:

Email: meng.ni@polyu.edu.hk (M. Ni); keqingzheng@cumt.edu.cn (K.Q. Zheng)

Abstract:

Solid oxide fuel cells (SOFCs) are very promising clean power generation devices due to their high efficiency and low emission. Unlike low temperature fuel cells, SOFCs can operate on various promising alternative fuels involving hydrocarbons, alcohols, solid carbon and ammonia. Currently, several excellent reviews on SOFC developments are available in the literature but a review dedicated to alternative fuels-fed SOFCs is lacking. Herein, we comprehensively review the electrochemical performances and stabilities of SOFCs operating on various fuels. Although comparable maximum power densities to hydrogen are frequently obtained for these fuels, some degradation problems influence the long-term stable operation of SOFCs. Therefore, various degradation mechanisms are firstly reviewed, followed by strategies from three perspectives of thermodynamics, kinetics and structure as the potential solutions to degradation issues. It is found that suitable operating conditions, specific novel anode materials or optimized anode structures are likely to enhance the lifetime and performance of SOFCs, while remaining challenges and future prospects of SOFCs fed by each fuel are separately elaborated for further improvements. Generally, the new engineering designs, material developments and latest knowledge presented in this review could provide useful guidance for the development and practical commercialization of SOFCs using promising fuels.

Keywords: Solid oxide fuel cell; Fuel flexibility; Durability; Degradation Suppression; Power generation.

Highlights:

- The degradation issues related to SOFCs operating on hydrogen substitutes are critically analyzed.
- Effective approaches to improve cell durability are comprehensively reviewed from perspectives of thermodynamics, kinetics and structure.
- Remaining challenges and future promises of alternative fuels-fed SOFCs are outlined.

1. Introduction

Traditional fossil fuels (coal, oil and natural gas) have been the world's principal energy sources to cope with the economic development and rapid urbanization [1]. Due to serious issues like inefficiency and severe environmental pollution related to the current electricity generation technology [2], cleaner and more effective energy conversion devices directly utilising fossil fuels have become essential for future energy sustainability and environmental issues mitigation. Solid oxide fuel cells (SOFCs) are promising means for directly converting chemical energy into electricity power through electrochemical reactions with higher conversion efficiency than conventional thermal power plants. In order to ensure the moderate ionic conductivity of solid ceramic electrolyte, SOFCs normally operate at the temperature from 600 to 1000 ℃ to overcome much higher activation energy [3]. High operating temperature brings numerous advantages to SOFCs over other types of fuel cell, such as higher tolerance to fuel impurities [4]; the use of low-cost nickel catalyst instead of prohibitively expensive platinum group metals [5]; the electrochemical utilization of carbon monoxide, one reducing gas species which may be catastrophic to other lower temperature fuel cells like PEMFCs (proton exchange membrane fuel cells); and feasible occurrences of internal reforming or decomposition reaction of combustible fuels thereby producing direct electrochemical fuels (hydrogen and carbon monoxide). In addition, the efficiency of hybrid system can be over 70% when the high-quality waste heat generated from SOFCs is recovered by gas turbine, CHP (combined heat and power) application [6,7] or other thermodynamic cycles [8,9].

Hydrogen has been globally identified as the ideal fuel for fuel cells [10,11], because hydrogen could be efficiently electrochemically oxidized without any greenhouse gases emission [12,13]. Besides, higher heating value (HHV) of hydrogen can be up to 141.9 MJ kg^{-1} which is the highest compared to any existing fossil fuel except nuclear energy [14]. However, although the share of hydrogen production from renewable technologies such as biomass-based approaches [1] and water electrolysis driven by alternative energies [15] is continuously increasing [16], the global hydrogen production mainly relies on fossil fuel feedstock nowadays, accounting for more than 90% [17]. In addition, extremely strict requirements for the storage and transportation of hydrogen also impede the wide-scale application of hydrogen [18]. Moreover, the low ignition energy and wide flammability range of hydrogen impose an undesired risk to the fuel cell community [19]. Therefore, due to these unsolved problems and drawbacks of hydrogen as well as innate promising traits of SOFCs, more and more researchers have shifted their focus to the direct operation of SOFCs on other promising fuels.

The topic of SOFCs operating on alternative fuels has received numerous attentions, which could be evidenced by many excellent review articles [20–29]. The fuel cell stability was frequently discussed in these review articles, because some potential degradation problems could seriously restrict the stable performance and thus implementation of SOFC technology when SOFCs operate on alternative fuels. However, most of them were mainly focusing on one specific fuel such as methane [22,23], alcohols [24–26], ammonia [29] or solid carbon [27,28], and very limited attention has been paid to the durability assessment of SOFCs fed by various alternative fuels [20,21]. Ge et al. [20] summarized the developments of SOFCs for direct hydrocarbon utilization, but the anode material advances were the focus of discussion. Boldrin et al. [21] reviewed the strategies and materials for carbon and sulfur tolerant fuel cells from heterogeneous catalysis. Besides, inspired by the research work conducted by Wang et al. [22], we found that the approaches for deterioration suppressions and performance enhancements could be achieved from perspectives of thermodynamics, kinetics and structure. Therefore, in this review, the degradation mechanisms of SOFCs on promising hydrogen substitutes involving hydrocarbons, alcohols, solid carbon and ammonia are discussed. In addition, based on the latest advances in oxygen-ion-conducting SOFCs, strategies from three perspectives for solving the degradation issues so as to enhance the cell stability were separately elaborated. Finally, remaining challenges and promises of SOFCs operating on these alternative fuels are concluded.

2. Structure, Principle, and Materials of SOFCs

SOFCs consist of an ion-conducting solid ceramic electrolyte sandwiched between the porous fuel electrode (anode) and porous air electrode (cathode) [30] (Fig. 1). Similar to other types of fuel cells, SOFCs are supplied with the fuel in the anode and the air in the cathode which are physically separated by the dense impermeable electrolyte film. Oxygen molecules are reduced to oxygen anions at TPB (triple phase boundary) sites of the cathode (Eq.(3)) by electrons from the anode via external circuit, and due to the gradient of oxygen chemical potential, ions are transported through the ceramic electrolyte (ion conductor) into TPB sites of the anode, where fuels can be electrochemically oxidized to release electrons which flow through external circuit to the cathode to generate usable electricity power (Eqs. (1) and (2)). As long as the fuel and air are continuously supplied to SOFCs, the external load can operate continuously because of continuous electrochemical reactions.

$$H_2 + O^{2-} \rightarrow H_2O + 2e^- \quad (1)$$

$$CO + O^{2-} \rightarrow CO_2 + 2e^- \quad (2)$$

$$0.5O_2 + 2e^- \rightarrow O^{2-} \quad (3)$$

Based on the principle of the SOFC and functions of each component, the anode, cathode, and electrolyte need to be equipped with specific properties by fabricating particular materials. The latest material advances of these three components could be found in various excellent review papers available in the literature [31–35], so only several frequently used materials will be briefly introduced in this section.

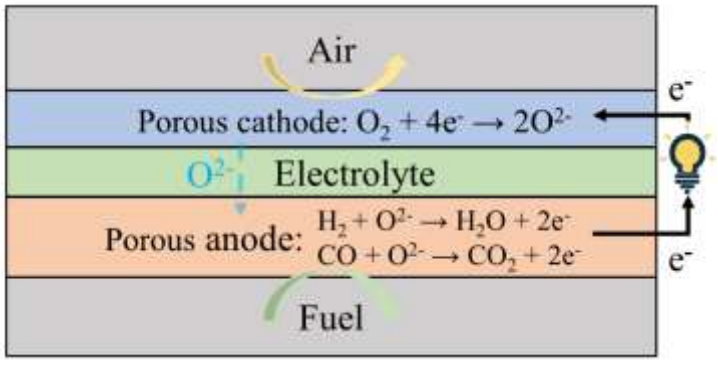

Fig. 1. The schematic of SOFC

2.1. Electrolyte material

For the electrolyte, the permeability must be sufficiently low in order to separate gases of both sides of the gas-tight layer. Besides, the high ionic conductivity and extremely low electronic conductivity which minimizes the leakage current need to be maintained at high operating temperature, strong reducing (anode side) and oxidizing (cathode side) environments.

State-of-the-art material for electrolyte is YSZ (yttria-stabilized zirconia), which is commonly used in the high-temperature SOFCs (HT-SOFCs, >850℃) [36]. Typically, anode-supported YSZ-based SOFCs need to operate at temperature above 973 K in order to overcome the overpotential and thus achieve feasible ionic conductivity (0.01 S cm^{-1} at 700 ℃) when the typical electrolyte thickness of 10 μm is assumed [32]. However, for the lower working temperature, doped-ceria is one of the most successful materials for the electrolyte, such as SDC (samarium doped ceria, $Sm_xCe_{1-x}O_2$) and GDC (gadolinium doped ceria, $Gd_xCe_{1-x}O_2$), which show higher conductivity particularly in the low or intermediate temperature range from 500 to 750 ℃. However, doped-ceria is likely to suffer from chemical instability at lower oxygen fugacity (fuel electrode side) due to the redox cycle of cerium cation, which causes substantial electronic conductivity leading to the internal shorting and thus lower OCV (open-circuit voltage) [37]. Different from the doped ceria, the lanthanum strontium gallium magnesium (LSGM, Sr and Mg-doped $LaGaO_3$) with the perovskite structure possesses adequate ionic conductivity and negligible electronic conductivity at relatively low oxygen pressure, and the minimum operating temperature for LSGM is the same as that of GDC (550 ℃) [38]. However, some material compatibility problems hinder the application of thin LSGM, such as nickel interdiffusion and La loss [32]. Fortunately, these issues mentioned-above related to doped ceria and LSGM could be well addressed by the bi-layer electrolytes structure, which could incorporate best properties of each electrolyte materials [32].

The electrolyte normally contributes the most of ohmic resistance of the SOFC due to the inefficiency of ionic conduction, so the thickness reduction of the electrolyte and the utilization of higher ionic conductivity electrolyte materials enable SOFCs to operate on lower temperature, which could offer numerous benefits to fuel cell system. Firstly, a wide range of materials for the components could be used with simpler and more economical fabrication approaches; secondly, lower temperature means quick start-up or shut-down time and also ease the problems such as sintering or grain growth of metallic phase in the anode, which in turn improves the thermal stability and prolongs the lifetime of fuel cells. Furthermore, intermediate temperature and low temperature SOFCs (IT-SOFCs, 650 to 850 ℃ and LT-SOFCs, 400 to 650 ℃) show great potentials in the application of transportation and portable devices with significant long-term economic and environmental benefits [4].

2.2. Cathode material

The oxygen reduction reaction (ORR) takes place in the cathode, so the cathode material possessing wonderful catalytic effect can truly improve the performance of SOFCs since the biggest polarization loss in SOFCs is related to ORR. LSM perovskite-type oxide (strontium-

doped lanthanum manganite, $La_xSr_{1-x}MnO_3$) is the most commonly used material for the cathode of HT-SOFCs, because LSM shows excellent catalytic effect and high electronic conductivity in the temperature from 800 to 1000 ℃ [39]. However, LSM does not seem to be the optimal choice for intermediate or low temperature because of the higher activation energy and increased polarization resistance due to insufficient catalytic activity below 700 ℃ [40]. Therefore, for the temperature from 500 to 700 ℃, the cobalt-containing MIEC (mixed ionic/electronic conducting) materials like strontium-doped lanthanum ferro-cobaltite (LSCF, $La_{1-x}Sr_xCo_{1-y}Fe_yO_{3-\delta}$) [41] and strontium-doped barium ferro-cobaltite (BSCF, $Ba_{1-x}Sr_xCo_{1-y}Fe_yO_{3-\delta}$) [42] have received more attention due to their enhancements of cathode reaction kinetics and higher ionic conductivity at intermediate or low temperature. In addition, the distinguished feature of the MIEC cathode material is that the TPB region is intrinsically expanded to the entire gas-cathode interface because of mixed ionic/electronic conductive property [40]. Although LSCF cathode shows greater reactivity with YSZ electrolyte, forming the $La_2Zr_2O_7$ insulation layer, this problem could also be mitigated by inserting a ceria-based buffer layer into the cathode/electrolyte interface to form the bi-layer electrolytes structure since ceria shows more stable compatibility with the LSCF cathode [3].

2.3. Anode material

Anode is the component where the fuel oxidation (e.g., hydrogen oxidation reaction) or reforming reactions occur. Therefore, requirements for the anode involve sufficient ionic and electronic conductivities as well as active catalytic effect for chemical/electrochemical reactions [30]. Similar to the cathode, anode is also a porous composite electrode consisting of electronic conductor and ionically conductive ceramic. Nickel metal is the most advanced material for the electronic phase of the anode because of high intrinsic electronic conductivity of the metal, excellent electrocatalytic activity and low cost. Besides, nickel is also the best reforming catalyst for many carbon-containing fuels, so the internal reforming reaction is possible if SOFCs operate on other promising fuels. Preferred ionic phase of the anode is YSZ or doped-ceria which provides enough ionic conductivity into the depth of the anode layer and also lowers the thermal expansion coefficient (TEC) of the composite anode to achieve good thermal compatibility with YSZ or doped-ceria electrolyte since Ni has a relatively higher TEC than that of these electrolytes [30]. In addition, the presence of ionic phase in the anode can present a framework as a sintering inhibitor to prevent the grain growth of Ni particles since the agglomeration or interdiffusion of Ni grains is likely to occur at elevated temperature [3].

The optimizations of microstructure and composition of the anode is also important to improve the performance of SOFCs by achieving the lowest overpotential losses [43].

Although the Ni metal has a high electronic conductivity (about 20,000 S cm^{-1} at 1000 ℃), the conductivity of Ni-YSZ can be more than a factor of 10 lower than that of bulk nickel metal because of the possible not well-connected metallic phase, porosity, tortuosity and the nature of the composite electrode. Therefore, 30-60 vol% Ni is typically recommended since the cermet cannot meet the requirement of sufficient electronic conductivity and suffers from higher ohmic polarization resistance if the content of Ni phase is less than 30 vol% of anode solid phase [44]. In addition, the optimum volume of gas phase is essential to facilitate the easy diffusion of direct fuel gases into electrochemical active sites and the better transportation of reaction products away from the anode to minimize concentration overpotential loss. Gas phase is also one important component of the TPB, which is directly related to the rate of electrochemical reactions. Therefore, for efficient functioning, Ni-YSZ porous anode is expected to be constituted by 30-35 vol% porosity [6]. In general, good chemical and thermal stability as well as the excellent performance make Ni-YSZ cermet anode still attractive presently [33,45].

However, despite tremendous advantages of Ni-YSZ composite cermet, several serious deactivation issues could be caused if SOFCs directly operate on alternative fuels, which will be detrimental to the performance and durability of anode catalyst [30]. For example, carbon deposition has been considered as one of the serious issues when SOFC is fed by carbon-containing fuels [5]. Therefore, to tackle this shortcoming of the anode, numerous strategies have been employed to enhance the coking resistance and thus increase the cell lifetime. These approaches and coking problem as well as other issues associated with non-hydrogen fuels will be discussed in the following sections.

3. Operation of SOFCs on promising fuels

Since oxygen ions transferred from the cathode could oxidise any reductive fuels and relatively higher operating temperature of SOFCs benefits the kinetics of electrode electrochemical/chemical reactions, in principle, it is possible to utilize a wide range of fuels, including gaseous state fuels such as the gaseous alkanes and ammonia, liquid fuels like alcohols and liquid alkanes, or even solid phase fuels including activated carbon, coal and biomass. However, several degradation issues involving carbon deposition, sulfur poisoning, agglomeration, re-oxidation and nitriding of the nickel metal etc. could deactivate functions of the anode and thereby threaten the cell stability when these promising fuels are used as the fuel for SOFCs. In order to solve these issues above, degradation mechanisms of SOFCs are firstly summarised, depending on the fuel used. Then, particular attention is given to the suppression strategies from thermodynamics, kinetics and structure to improve the operation stabilities of SOFCs, involving the control of operating temperature, fuel mixture composition, specific current density, anode material and structure design etc. Besides, the future development directions of this competitive energy technology are identified.

3.1. Hydrocarbons

3.1.1. Fundamentals of hydrocarbon-fuelled SOFCs

Direct utilization of Hydrocarbons

The internal process is complex when hydrocarbon fuel is directly fed into SOFC system without substantial amounts of oxygen-carrying species. On one hand, due to the excellent catalytic effect of the anode and thus the faster electrochemical kinetics, the direct electrochemical oxidation of hydrocarbon is possible to occur if hydrocarbon fuel could reach the electrochemical active sites. On the other hand, under SOFCs high temperature operating conditions, hydrocarbon is likely to decompose into lighter hydrocarbon or hydrogen before reaching the electrochemical active sites, and this chemical process can be improved due to the presence of anode catalyst [26]. Although the direct electrochemical oxidation is probably the most effective way for fuel conversion, it is not likely to take place in one step, because even for the simplest hydrocarbon, methane, the process of electrochemical oxidation involving eight electrons could be more sluggish than others reactions such as the thermal decomposition reactions and the afterward electrochemical reactions [46,47]. Besides, the steam or dry reforming of hydrocarbon may take place when the steam or carbon dioxide is generated as electrochemical products. Therefore, based on the information and analysis available, direct electrochemical oxidation of hydrocarbon is unlikely to be the main reaction of the anode, while the internal anodic reactions should be the combination of several *in-situ* reactions

including direct electrochemical oxidation, reforming and decomposition reactions. According to McIntosh [5] and Mogensen [48], the process that the hydrocarbon is directly fed into the anode channel of the SOFCs with negligible or no oxygen, steam or other oxide gases should be referred as direct utilization or direct conversion of hydrocarbons rather than the direct electrochemical oxidation.

Reforming of the hydrocarbon

Other than the direct utilization, there are also other operation modes for hydrocarbon, such as the external reforming, steam reforming (Eq. (4)), dry reforming (Eq. (5)), partial oxidation (Eq. (6)) and auto-thermal reforming. Here, we use methane as an example.

External reforming is a kind of operation that the fuel is processed in the separate reforming chamber after desulfurization process, and then the reformed synthesis gas (mixture of carbon monoxide and hydrogen) is afterwards supplied to SOFC without the stringent gas cleaning system (e.g., water gas shift reactors) that converts most of carbon monoxide to hydrogen and then removes residual carbon monoxide to low ppm (parts per million) level, since high temperature fuel cells even with traditional Ni-based anodes are likely to be free of CO poisoning problem, thus avoiding deactivations of carbon deposition and sulfur poisoning [26]. Besides, due to the endothermic nature of reforming process, heat needs to be supplied to the external reactor, which will result in extra capital. Therefore, because of the complexity of whole system and additional operating cost, external reforming may be only appropriate for large-scale stationary SOFCs usually combined with CHP applications [3]. However, for the small-scale devices especially for the portable or transport systems, internal steam and dry reforming as well as the partial oxidation are much prevalent.

$$\mathrm{CH_4 + H_2O \leftrightarrow 3H_2 + CO} \qquad \Delta H^0_{298} = +206\ \mathrm{kJ\ mol^{-1}} \tag{4}$$

$$\mathrm{CH_4 + CO_2 \leftrightarrow 2H_2 + 2CO} \qquad \Delta H^0_{298} = +247\ \mathrm{kJ\ mol^{-1}} \tag{5}$$

$$\mathrm{CH_4 + 0.5O_2 \leftrightarrow 2H_2 + CO} \qquad \Delta H^0_{298} = -36\ \mathrm{kJ\ mol^{-1}} \tag{6}$$

$$\mathrm{CO + H_2O \leftrightarrow H_2 + CO_2} \qquad \Delta H^0_{298} = -41\ \mathrm{kJ\ mol^{-1}} \tag{7}$$

Steam or dry reforming reaction is a highly endothermic process that convert the methane and steam or carbon dioxide into the synthesis gas mixture, normally followed by water gas shift reaction (Eq. (7)), generating more hydrogen. When reforming reaction takes place inside the anode of SOFCs, the generated syngas could be subsequently consumed electrochemically for producing electricity and steam as well as the carbon dioxide which will further promote the reforming process, thereby improving the conversion of methane and leading to higher fuel utilization. Meanwhile, the heat due to the irreversible loss of electrochemical reactions and

also the ohmic resistance largely from the electrolyte can be well used by endothermic reforming process, thus reducing the requirement for active cooling which is normally implemented by oversupplying the air to the cathode side [4], and also the need for providing additional energy to the reforming process, so the thermal coupling of electrochemical reactions and reforming process could significantly improve the overall efficiency of SOFC system. Although rapid reforming reactions, especially in the high catalytic effect of the metal-based anode, may lead to severe local cooling usually at the entrance of the anode, mechanically damaging the cell system due to steep thermal gradient [49], thermal neutral state could be achieved if the operating condition is well-optimized, minimizing the possibility of mechanical failure due to the poor thermal management. Most recently, experimental and simulation results on the methane multiple-reforming (MMR) in SOFCs showed the feasibility of thermal neutral state, which provides very meaningful guidance to the heat management of cell stack [50]. In addition to the mechanical instability mentioned-above, dilution effect caused by the introduction of steam or carbon dioxide could lower the output performance of SOFCs through decreasing the partial pressure of syngas and practical OCV. Furthermore, the dry and steam reforming may be both problematic when the system is operating at partial load state, especially at the start-up or open circuit condition, because the heat produced from cell inefficiencies could be insufficient to sustain the thermal demands of reforming reactions [3]. Although the simpler apparatus of the SOFC system towards dry reforming can be achieved due to the fact that carbon dioxide is easier to handle than steam [51], dry reforming may pose more serious degradation threats to the anode than steam reforming from the perspective of carbon tolerance [52]. Despite these, as the major components of biogas, the utilization of methane and carbon dioxide from renewable resources could be a very promising route to achieve the carbon-neutral electric power generation [53].

Different from the endothermic nature of steam and dry reforming reactions, the partial oxidation process of methane is slightly exothermic ($\Delta H_{298}^{0} = -36\ \mathrm{kJ\ mol^{-1}}$) because part of total chemical energy available in methane fuel is lost as heat which could be evidenced by the partial oxidation chemical equation (Eq. (6)): products of per mole methane is only capable of producing 6 mole electrons which is 25% less than that of dry or steam reforming reactions. Besides, because air has been used as the main oxygen source due to its availability, nitrogen will be inevitably carried into the fuel mixture, leading to some undesirable consequences such as the efficiency loss because of non-negligible heat absorption (e.g., latent heating), potential production of N_2O (greenhouse gas) [54]. Therefore, the energy loss and the introduction of nitrogen could decrease the overall efficiency of SOFC system. For example, OCV was found

to decrease with the increase of added air flow rate, which will consequently has an negative effect on the output power density [55]. In addition to the open-circuit voltage, higher concentration of oxygen may also result in other detrimental issues such as agglomeration or migration of the metal catalyst due to the local temperature increase [49], potential delamination of the anode layer due to re-oxidation of nickel metals [55] and inhibition of oxygen transport from the cathode side because of lower oxygen chemical gradient [56]. Therefore, the oxygen to methane ratio needs to be well-optimized, since keeping highly reducing atmosphere in the anode is extremely essential to the durability of metal catalysts and integrity of the structure. In spite of these above, the rapid start because of the exothermic process still makes the partial oxidation process more appropriate for small-scale portable fuel cells since this type of system normally pays attention to the quick response, instead of the system efficiency [7].

Auto-thermal reforming is a process that combines the partial oxidation and steam reforming, so auto-thermal reforming may have synergistic benefits and thus achieve higher hydrogen yield and efficiency than partial oxidation, and simpler requirements for thermal management than steam reforming. Besides, it is possible for SOFC system to operate at from full load to zero power output since the energy demand for steam reforming at zero load condition could be partially or completely provided by the exothermic partial oxidation according to the fuel mixture composition.

Degradation issues of hydrocarbon-fuelled SOFCs

The nickel-based cermet is still most popular anode when SOFCs are operating on hydrocarbon fuels because of its superior properties in electronic conductivity and catalytic activities of electrochemical and reforming reactions. However, high temperature, and complicated gas environment have posed a harsh threat to the fuel electrode. Generally, there are four different kinds of degradation for nickel-based anode of hydrocarbon-fuelled SOFCs, including nickel coarsening, sulfur poisoning, coking (carbon formation), and redox instability [22]. All these degradation processes may cause changes of anode micro- and macro-structures or surface morphology, and thus the reduction of the TPB length or poor fuel diffusion ability, thereby leading to the poor performance and even complete failure of SOFCs.

Carbon formation

Among all these degradation mechanisms, carbon formation on the cermet anode is the most serious reason of catalyst deactivation and it may be even inevitable in any operation involving hydrocarbons or other carbon-containing fuels [57]. In general, when hydrocarbon is supplied

to SOFCs as fuel, carbon could be formed from hydrocarbon decomposition (Eq. (8)), Boudouard (Eq. (9)), and reversed H_2O gasification (Eq. (10)) reactions [58]. Boudouard reaction and reversed H_2O gasification reaction are favourable thermodynamically at lower temperature, whereas hydrocarbon decomposition reaction is favored at high temperature [21].

$$C_nH_m(g) \leftrightarrow m/2H_2(g) + nC(s) \quad (8)$$

$$2CO(g) \leftrightarrow CO_2(g) + C(s) \quad (9)$$

$$CO(g) + H_2(g) \leftrightarrow H_2O(g) + C(s) \quad (10)$$

Fully understanding the mechanism of carbon deposition is essential to develop anode materials and optimize micro- and macro-structures. According to the literature, two kinds of mechanism have been accepted by majority of scholars based on whether the catalytic metal exists or not [5,21,45], since two peaks of Raman Shift (D-band at 1350 cm^{-1} and G-band at 1580 cm^{-1}) are usually observed in the Raman spectroscopy after stability tests. Firstly, the growth of graphite carbon (G-band at 1580 cm^{-1}) on the active metal surface such as Ni is the main source of carbon deposition [57]. Dissolution-precipitation process is main mechanism for carbon deposits on the presence of active metals, involving adsorption of carbon on the surface of metals, dissolution of carbon into the metal bulk, and finally precipitation of carbon as a whisker (graphite fibre). Carbon deposition on the surface of metals may block pores or encapsulate catalytic sites, leading to the increased mass-transport resistance. Fortunately, deposited carbon could be oxidised after the oxygen-temperature programmed oxidation (TPO) process which means that this kind of deactivation is reversible. However, with further formation of carbon on the surface of catalytical active metals, carbon may dissolve and plug into the metal bulk, leading to the volume expansion and even pushing metal particles off the support, which can cause structural failure and thus permanent deactivation of catalysts [21]. Besides, metal particle size [59], preparation method [60,61], metal content [62] and second phase [63] of the catalyst could influence the behaviours of carbon formation. For example, based on the thermodynamic analysis of methane dry reforming process, the ideal catalyst particle size to avoid considerable carbon formation was found to be below 5 nm at optimal operating conditions [64]. Secondly, amorphous carbon (D-band at 1350 cm^{-1}) could form in the gas phase even without the metal catalyst through these three potential chemical reactions. Normally, amorphous carbon would deposit at the outer surface of the anode or the exhaust exist via gas flow [65], which is less deactivating [21]. The deactivation process is likely to fill the pores of the anode, resulting in higher concentration polarization loss. Furthermore, different from the carbon catalytically formed on metal particles, the carbon formed by gas-

phase does not cause mechanical failure of the anode cermet due to no introduction of structural stress [5]. Because of more reactive nature [66], the amorphous form of the carbon is more likely to convert into the graphitic form at elevated temperature [57].

Sulfur poisoning

Another crucial issue is the sulfur poisoning not only to anode but cathode, because some hydrocarbon fuels or even commercial fuels may contain certain amount of sulfur-based constituent as impurity [67] or as an additive [68], which will deactivate the Ni-based cermet anode even at low ppm level [69], and the sulfur compound in the much polluted air can also lead to serious degradation of the strontium-based cathode if SOFCs are installed in the urban environment [70,71]. Sulfur compounds in hydrocarbon fuels are more likely to be converted into the most thermodynamically stable gaseous hydrogen sulphide (H_2S) in the environment of anode compartment, which is also why H_2S is usually directly used to be the source of sulfur compounds in many laboratory experiments [72]. From the anode perspective, although the degradation behaviour of cermet related to H_2S impurity mainly depends on various factors such as operating temperature, current density, H_2S concentration and anode structure [73], possible mechanisms of sulfur poisoning on the anode have been summarised by numerous studies [73–76]. Generally, the rapid initial drop of output power density had been observed in many research studies, which have been referred as short-term effect by some scholars. The fast decrease of power output at the beginning is mainly because of the adsorption of sulfur (Eq. (11)) on the nickel surface which will cause the decrease of TPB length and the increase of anode polarization resistance, subsequently leading to lower cell performance [73]. Depending on operating conditions, performance degradation caused by the short-term effect can be partially or completely eliminated after the switch of H_2S-free fuel for performance recovery, especially for lower H_2S concentration and higher temperature [77]. With the increasing of exposure time, long-term effect of sulfur poisoning may behave differently at different H_2S concentrations, operating temperatures, or even current densities. For example, sulfidations of Ni (Eqs. (12) and (13)) are more likely to occur at lower temperature or higher H_2S concentration, which may change the morphology of Ni phase and thereby deactivate the local electrocatalytic capacity [78]. Besides, oxidation of Ni is also an important reason for the long-term behaviour of surfur poisoning when SOFCs is operating under high current density [69], because when adsorbed sulfur blocks electrochemical sites, more flux of O^{2-} because of high current density will oxidise Ni particles instead of direct fuels owing to insufficient active sites, and formed NiO may not only diminish the nickel amount but induce the stress in the

anode as a consequence of the bigger molecular structure of NiO, leading to microcrack or even interface delamination. Despite different processes caused by various operating conditions, the main influence of the long-term sulfur poisoning effect may be related to the micro-structure of the anode, which can have a permanent negative effect on the SOFC performance.

$$H_2S_{(g)} \leftrightarrow HS_{(ads)} + H_{(g/ads)} \leftrightarrow S_{(ads)} + H_{2(g/ads)} \quad (11)$$

$$H_2S + Ni \leftrightarrow NiS + H_2 \quad (12)$$

$$xH_2S + 3Ni \leftrightarrow Ni_3S_x + H_2 \quad (13)$$

Sintering of metal phase in the anode and redox instability of SOFCs

Carbon formation and sulfur poisoning are both possible degradation phenomena when hydrocarbon fuels are utilized. Unlike these two degradations, redox instability and nickel coarsening are more common since no matter what kinds of fuel are fed, they may occur. Ni-based anodes are expected to operate under a reducing environment in order to keep Ni in a metallic form, because when oxygen or air flow into the anode due to some reasons such as unintentionally interrupted supply of the fuel, or leakage of the air, Ni can be oxidized to sponge-like NiO accompanied with 69% volumetric expansion [79], resulting in lower electrochemical performance, and even the malfunction of whole fuel cell because of microstructure changes caused by the volume expansion [6]. In addition to the redox instability, nickel coarsening is another frequent problem which could also lead to microstructure change especially at higher temperature due to the thermally favourable sintering process and relatively lower melting point of the nickel metal [80]. Besides, smaller Ni particle seems to have higher surface energy, and agglomeration of these particles could decrease this energy. Therefore, bigger metal particles are likely to be formed during this agglomeration process, which may degrade the function of the anode by decreasing the electrical conductivity and TPB length because of the Ni-Ni contact loss [81].

3.1.2. Strategies to suppress degradation issues of methane-fuelled SOFCs

Methane (CH_4), the main component of natural gas, coal-bed gas and biogas, is the simplest alkane with the highest hydrogen to carbon ratio (4:1) among HCs which can lower the carbon dioxide emission per unit of electricity power generated during its oxidation process [82]. Therefore, methane has been considered as the most beneficial alternative gaseous fuel for SOFC system and also widely studied by many researchers (Fig. 2).

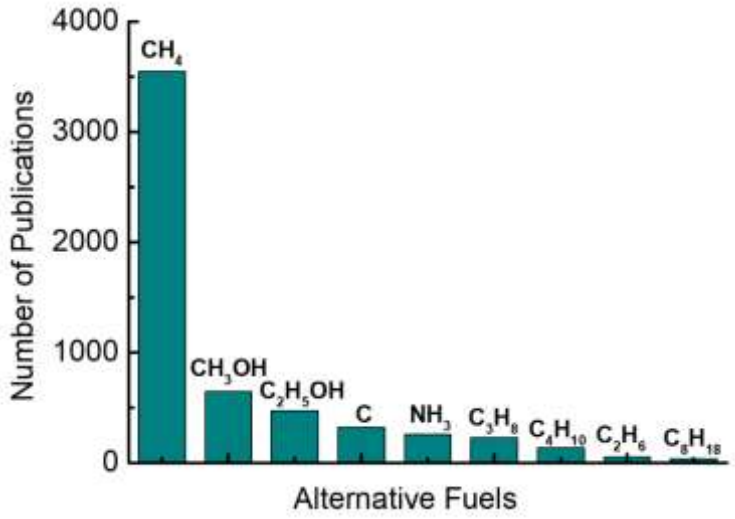

Fig. 2. Number of publications for SOFCs combined with various alternative fuels from 2001 to 2021. Data source: Scopus.

As discussed previously, Ni-based cermet has still been the most suitable anode material for hydrocarbon-fuelled SOFCs since Ni-based anodes generally achieved relatively higher P_{max} (maximum power density) compared to others such as copper- or oxide-based anodes. However, the most serious problem related to SOFCs operating on hydrocarbon fuels is the rapid degradation because of carbon formation at the anode as demonstrated in last section. In the literature, there are lots of articles which have reviewed the development of durable methane-fuelled SOFCs especially with the focus on the anode material design [20–22]. Therefore, we mainly introduce the latest progress of SOFCs on methane fuel since methane-fuelled SOFCs have received lots of attraction in recently years. According to the literature, strategies to suppress carbon deposition over nickel cermet anode could be implemented from three perspectives: thermodynamics, kinetics, and structure. Actually, in most laboratory experiments, combined strategies are normally adopted to achieve better performance towards electricity output and long-term stability. Related electrochemical characteristics of methane-fuelled SOFCs are summarized in Table 1. In addition to the carbon formation, other degradation problems (e.g., sulfur poisoning, re-oxidation of Ni and metal sintering) will also be involved in the following discussion.

Thermodynamics

Taking the carbon formation mechanism into account, the methane cracking reaction would be the main reason for the degradation of nickel-based anodes, especially at high working temperature. In order to eliminate the cracking reaction, the promotion of reforming reactions could be a promising way. Therefore, the most effective way to tackle the carbon formation is through thermodynamic approaches, including the addition of oxygen-containing agents,

operation on higher current or special temperature region which does not favour the methane cracking reaction. Due to the reducing nature of deposited carbon, the utilization of pyrolytic carbon could also be another special thermodynamic method to eliminate the negative effects of accumulated carbon.

Fig. 3 illustrates the C-H-O triangle diagram based on the thermodynamic calculation of chemical equilibrium mixture composition of H_2O, C (graphite), CO, CO_2, CH_4, H_2 and O_2, demonstrating equilibrium deposition and non-deposition areas of the graphitic carbon regarding the anodic feeding composition at different temperatures [83]. From the perspective of thermodynamics, the methane-rich mixture composition will shift into the non-coking area when oxygen-containing gases are added. For example, mixing with the steam, carbon dioxide or oxygen moves the fuel equilibrium composition into non-deposition area (the lines with rows in Fig. 3). It is worth noting that thermodynamic equilibrium calculation is the indication of OCV state in the SOFC operation, and more oxygen content will be transferred to the anode side when SOFC is under current swap state, which may result in other unfavourable problems such as delamination due to nickel particle re-oxidation because additional oxygen content required to eliminate coking issue in the OCV state is higher than that of the electricity output state [55].

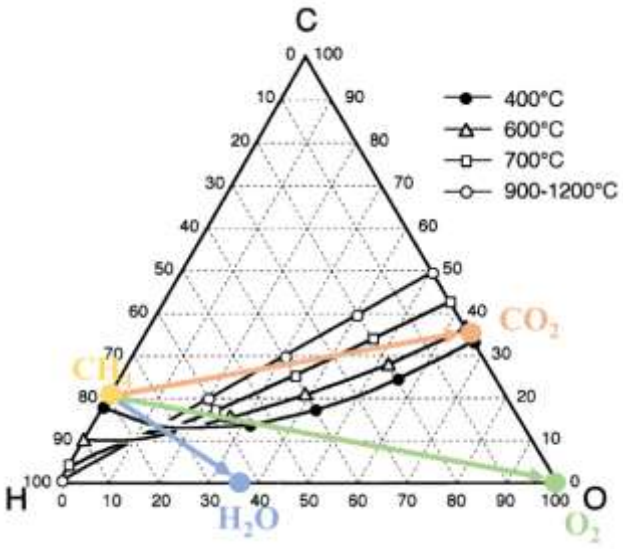

Fig. 3. Calculated carbon deposition region in the ternary diagram of O, C and H elements at 1 atm. This figure is redrawn from ref [83].

According to gas composition lines of methane mixing with oxygen-containing gases in Fig. 3, the simplest and most effective way to reduce carbon deposition is to add steam to methane which could be subsequently converted into the syngas through internal steam reforming reaction. For example, Zhang et al. [65] investigated effects of S/C (steam to carbon) ratio on

the long-term stability of direct-methane flat-tube SOFC with the Ni-YSZ anode and symmetric double-sided cathodes at specific current density (0.257 A cm^{-2}), and it was found that when S/C ratio was 2, SOFC achieved stable operation more than 190 h at the temperature of 750 ℃, while rapid deteriorations were observed due to the deposited carbon in less steam added cases. However, according to the results from experimental study [84], no carbon was formed on Ni-YSZ catalyst via steam reforming of methane at the temperature higher than 950 ℃ and inlet S/C ratio of 3.0/1.0. Despite different operation conditions and structures, such a significant discrepancy is mainly because the thermodynamic calculation of carbon deposition only provides a general guideline and does not account for the kinetics effect [83]. Therefore, the exact steam demand required for a SOFC system is dependent on various operation conditions, such as electricity output, structure, fuel flow rate and others [26]. In addition, thermodynamic calculation cannot predict the negative impact induced by excessive added gas. Zhang et al. [65] also found that current dropped suddenly after the 90 h stable performance when the fuel with S/C ratio of 3 was supplied, which was caused by the break of electron conducting network due to the gradual oxidation of nickel particles.

Similarly, oxygen and carbon dioxide could be also added into methane fuel to tackle the carbon issue for achieving long-term stable performance [49,55]. Baldinelli et al. [49] conducted systematic experiments to find the optimal O/C (oxygen to carbon) ratio through feeding the air-diluted natural gas and CO_2-seperated biogas to the anode-supported button SOFC with the configuration of Ni-YSZ/8YSZ/GDC-LSCF and found that when the current was set to 0.5 A cm^{-2}, 0.8 and 0.4 were best O/C ratios with considering the durability and material degradation for diluted natural gas and upgraded biogas cases, respectively. The inconsistency of optimal oxygen contents between these two oxygen carriers might be as a consequence of opposing thermodynamic natures of these processes, though there were no explanations about the reason in that study. Using typical NiO-YSZ anode, Aslannejad et al. [55] studied the optimal flow rate of air to achieve the best dilution. However, the addition of 350 SCCM air to 500 SCCM methane showing high tolerance towards carbon formation under OCV condition leaded to increased anode polarization due to severe delamination shown in the SEM (scanning electronic microscopy) image when SOFC was operating at 800 mA, while the 1:5 additional ratio (100 SCCM air) was confirmed to maintain the stable power density for 100 h operation afterwards. The results of studies [55,65] show the significance of relationship between additional oxygen agent amount and operation condition, especially the current density due to the fact that typical current density is also the thermodynamic method to prevent carbon formation which will be discussed more in the following paragraph. Because added

oxygen carrier and transferred oxygen anion (current density) are both sources of oxygen content, the balance of these two sources is essentially important for the durability of SOFCs concerning the carbon deposition as a result of insufficient oxygen amount and the re-oxidation of Ni metals owing to excessive oxygen content. Therefore, disequilibrium will be triggered if one of these conditions changes, leading to undesirable consequences.

Current density and operating temperature can also be thermodynamic strategies to maintain long-term output of SOFCs while directly using dry methane since during the operation the oxygen content (in forms of carbon dioxide and steam) could also drive fuel composition away from the coking region (Fig. 3), especially for higher current density and lower operation temperature [85]. The most plausible mechanism of carbon suppression by current density is that electrochemical reactions products promote reforming processes of methane (Eqs. (4) and (5)), reversed Boudouard reaction (Eq. (9)) and H_2O gasification reaction (Eq. (10)), thus deterring the cracking reaction or eliminating deposited carbon. Also, some researchers thought that high O^{2-} flux transferred because of high current density is the reason to prevent carbon formation since O^{2-} can react with deposited carbon and also release electrons, which is the same as the electrochemical oxidation of solid carbon in the direct carbon SOFC. In author's opinion, it depends on the structure of SOFC. According to the literature [3,5,86–89], it is widely accepted that electrochemical reactions mainly take place in a narrow region of the porous anode called functional layer, which is an active zone within approximate 10-20 μm from the anode-electrolyte interface. Therefore, when the design of anode-supported is used, higher concentrations of electrochemical products are the dominated reason for carbon prevention owing to the fact that less or even no O^{2-} will be transferred beyond this narrow region. However, due to the high oxygen anion content in the thin anode layer of electrolyte- or cathode-supported SOFC structure, the directly oxidation of deposited carbon will be possible, which can be evidenced by the phenomenon that only slight current density (1 mA cm^{-2}) could significantly reduce the amount of deposited carbon compared to the OCV condition (nearly 12 times) when the Ni-YSZ anode with the thickness of 25 μm was fabricated [86]. In addition, electrolyte-supported cell experienced a slower degradation rate than the anode-supported counterpart, which is shown in Fig. 4 [90]. Besides, no carbon in the adjacent region close to the electrolyte in cracked anode was detected after few hours operation on the same power output (1 mA cm^{-2}), though the partial pressure of methane decreased along the depth of the anode [85]. Despite good structurally intrinsic carbon tolerance on the current sweep condition, configurations of electrolyte- and cathode-supported cells suffer higher ohmic resistance because of thick electrolyte support layer and larger concentration

polarization due to better diffusion capacities of anodic gases than that of the cathodic counterpart under same structural conditions [91], respectively. Therefore, anode-supported structure has still been the most popular configuration of SOFC except some certain circumstances, such as the use of oxide or perovskite materials as anode.

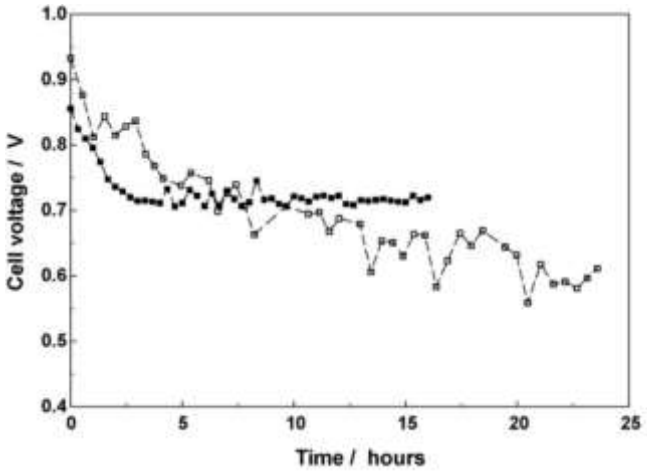

Fig. 4. Durability test in pure methane at 1023 K for the anode-supported SOFC at 100 mA cm^{-2} (□), and for the electrolyte-supported SOFC at 50 mA cm^{-2} (■). Figure reproduced from ref. [90] with permission from Elsevier.

In addition, the main reason of carbon formation, methane cracking reaction, can be limited at the temperature less than 700 ℃ [85,92]. It was found that critical current densities (J_c, the minimum current density to maintain long-term operation) became 0.8 A cm^{-2}-1.2 A cm^{-2} for 750℃ and 1.4 A cm^{-2}-1.8 A cm^{-2} for 800℃, respectively, from 0 A cm^{-2}-0.1 A cm^{-2} for both 650 ° and 700 ℃, which demonstrates that there is no or less methane pyrolysis at the temperature less than 700 ℃ and methane cracking reaction rate will be accelerated at the temperature higher than 700 ℃. Besides, Lin et al. [85] concluded except the working temperature, other factors such as the methane flow rate, anode thickness and porosity had slight impacts on J_c, when the Ni-YSZ anode-supported SOFC was running on the dry methane.

The fuel cell that utilizes deposited carbon based on the SOFC is called pyrolytic carbon air fuel cell (P-CAFC) [93], or rechargeable direct carbon fuel cell (RDCFC) [94–96]. The basic configuration of the P-CAFC or RDCFC is the same as that of SOFC, and the power is generated from the carbon deposited on the anode by feeding dry hydrocarbon (e.g., methane) at OCV condition. Different from the pulverized solid carbon fuel, pyrolytic carbon is formed by the gaseous hydrocarbon which could diffuse deeply into the porous anode, even reaching close to the functional layer [93], mitigating the diffusion problem of pulverized solid carbon. The reaction mechanism (Fig. 5) of deposited carbon fuel in RDCFC was concluded by

Hasegawa et al. [96]. Besides, six charging/discharging cycles operation demonstrated higher stability of RDCFC mode, as shown in Fig. 6a. However, due to intermittent electricity output of the RDCFC mode, intermittent fuel supply (IFS) mode was proposed, which could be considered as a hybrid of the continuous fuel supply mode and RDCFC mode [97]. In this mode, much more smooth and prolonged power output could be achieved (Fig. 6b), though there were other residual active gases such as hydrogen, carbon monoxide and methane, other than deposited carbon in the anode. Intermittent methane supply could be thought to be a promising method to utilize the deposited carbon, indirectly address the carbon accumulation.

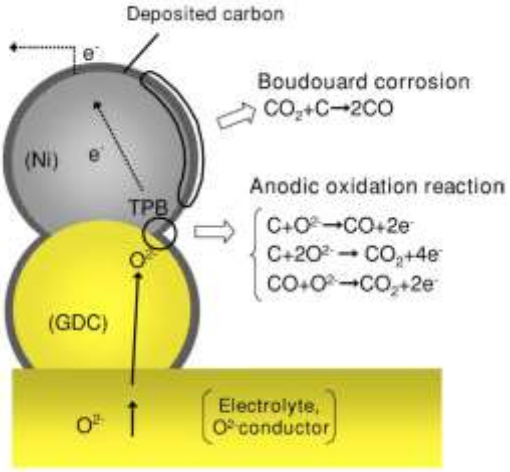

Fig. 5. Mechanisms of Anode reactions in a RDCFC. Figure reproduced from ref. [96] by permission of The Electrochemical Society.

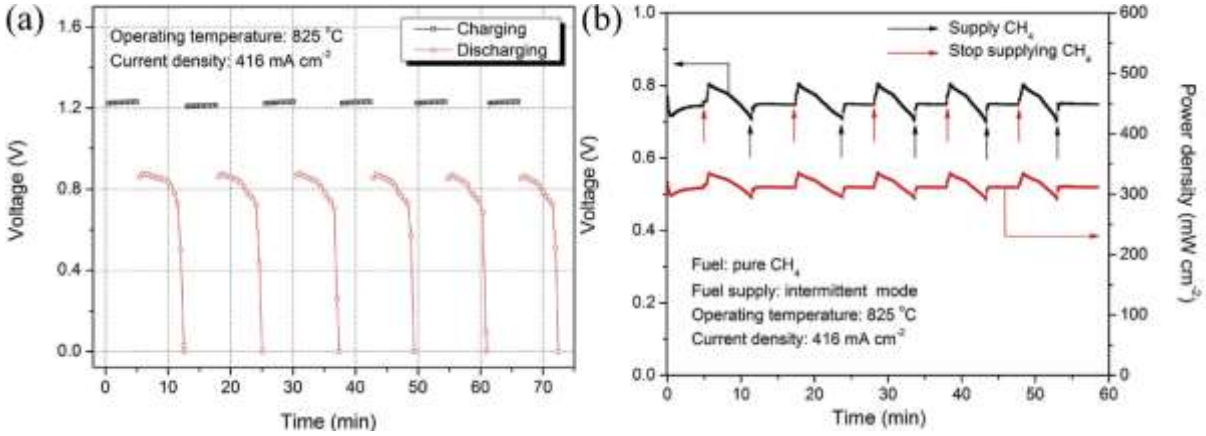

Fig. 6. (a) Voltage as a function of time in RDCFC mode; (b) Power density or voltage as a function of the time in intermittent methane supply mode. Figure reproduced from ref. [97] with permission from Elsevier.

Kinetics

The SOFC with the Ni-cermet anode operating on carbon-containing fuels inevitably causes carbon formation problem because nickel metal catalyses methane cracking. Therefore, in

order to improve the carbon tolerance of nickel cermet anodes, kinetic methods related to the material science provide lots of alternatives, involving the modifications of the Ni-cermet by incorporating or replacing other metals or oxides, or even the development of Ni-free anodes such as oxide- or copper-based anode.

Incorporating or alloying other metals could be an effective way to modify the tolerance ability towards carbon deposition as well as electrochemical performance of the Ni-based cermet anode. Despite high cost of noble metals involving Au, Ru, Ag and Pd, the enhancement of stable operation may partially compensate the increased manufacturing cost since addition of certain amount of these metals is likely to improve the carbon tolerance. Thermogravimetric analysis in the research conducted by Niakolas et al. [98] showed that commercial Ni-GDC ($Gd_{0.1}Ce_{0.9}O_2$) modified by Au nano-particles through deposition precipitation method achieved better carbon formation mitigation than pristine anode under dry methane feeding condition. In addition, SOFC with the Au-Ni-GDC anode ran stably over 200 hours with a output performance of 0.41 W cm^{-2} when fuel cell was operating on the methane rich fuel (three consecutive fuel operations: mixture of steam and methane with a molar ratio of 3/2, mixture of steam and methane with a molar ratio of 1/2 and dry methane), while for the Ni-GDC counterpart, 0.3 mV h^{-1} voltage degradation was observed even for the fuel condition of methane and steam mixture with a molar ratio of 1/2. Besides, the OCV for Au modification case was 0.15 V higher than that of the cell with pristine anode under methane steam reforming condition. These results demonstrate that the addition of Au leads to the improvement of carbon tolerance without sacrificing the SOFC electrochemical performance. Besides, Garcia-Garcia et al. [99] had drawn a same conclusion that small amount of gold doping could effectively prolong the lifetime of fuel cell system by suppressing carbon deposition. Fig. 7 shows that SOFC with the anode of Au-Ni-GDC achieved much more stable electricity output for nearly 200 hours without noticeable degradation than the Ni-GDC counterpart and the corresponding current density was 0.05 A cm^{-2} higher under the internal steam reforming condition at 800 °C and 0.7 V. This improvement of the current density may be attributed to the excellent catalytic effect of Au-modified anode towards methane steam reforming reaction since the OCV [98] and *i-V* curve [99] under hydrogen fuel were nearly identical for both SOFCs with un-doped and Au-doped Ni-GDC anodes, and anode properties such as conductivities, reducibility as well as microstructure rather than the catalytic activity are related to the electrochemical performance of SOFC under hydrogen fuel [100]. Furthermore, It was reported that the tolerance to H_2S was also enhanced by the addition of Au because the formation of Au-Ni alloy could hinder the formation of strongly bonded sulphur [101]. In addition to the Au metal, Ru

and Ag could serve as useful additives to be added into the Ni-based anode to improve the anti-coking ability and thus the lifespan of the system when methane is directly fed into SOFC system [102]. For example, when simulated biogas was used as the fuel in galvanostatic experiments, the Ag-doped cell only degraded at the rate of 7.93×10^{-4} V h^{-1} in 50 h long-term stability test, while the cell with pure Ni-YSZ anode completely failed after 19 h. Different from the electrochemical performance of SOFC with Au-modified anode, better P_{max} was achieved for both hydrogen and biogas fuels when 1 wt% Ag is impregnated into Ni-YSZ bulk anode [102]. However, another noble metal, palladium (Pd), shows less positive effect towards carbon resistance [103,104]. Although Pd nano-particles contributed to large promotion of the Ni-GDC activity, filament carbon fibres were still observed in methane fuel case, which indicated the poor carbon suppression of Ni-based anode impregnated by Pd metal. Although the addition of precious metals could improve the cell stability, high-cost nature primarily rules out the applications of noble metals-modified Ni-based anode on a wide scale, which has driven researchers to search for other cheaper alternative metals. Therefore, some transition or base metals such as Fe, Co, Cu and Sn have been extensively studied to investigate their modification effects on coking resistance as well as SOFC performance. Different from some researchers' stereotyped impression that introduction of most transition metals may compromise or sacrifice corresponding catalytic activities, recent studies have shown that small amount addition of those metals contributed to a higher P_{max} and better alleviation of carbon deposition. Jiang et al. [102] found that Sn with the loading of 1 wt% with respect to Ni metal amount greatly increased the power density of the SOFC in dry biogas compared to Sn-free Ni-YSZ anode (Fig. 8). Besides, the durability of the SOFC with Sn-modified anode was correspondingly enhanced (voltage degradation rate of 2.98×10^{-4} V h^{-1}), which is even lower than that of noble metal (Ag) counterpart. Furthermore, the stability could be further improved by increasing the mole ratio of Sn (Fig. 9) [105]. In addition to Sn, Co, Cu and Fe tend to have similar impacts on these two performance indicators [82,106,107]. For example, because of higher reforming activity of the $Ni_{0.9}Fe_{0.1}$ alloy for the wet methane, more syngas mixture generated will diffuse into the anode functional layer and subsequently be available for electrochemical reactions, leading to increased P_{max} of 1.01 W cm^{-2} compared to that (0.84 W cm^{-2}) of the Ni-supported cell. Besides, cell with the $Ni_{0.9}Fe_{0.1}$ anode achieved 50 hours nearly stable operation in the current sweep condition, while for Fe-free cell, the deposited carbon occupied the active sites of electrochemical and methane reforming reactions in conduction and functional layers, respectively, causing complete failure of the cell in first 8 h [106]. In the study of copper modification effects [107], twice Cu impregnation has been

proved to achieve the best power density because decreased ohmic resistance exceeds the increased polarization resistance caused by more Cu content due to the fact that Cu serves as an excellent electronic conductor but an inferior oxidation catalyst [5]. However, the cell with Cu-doped Ni-YSZ anode showed contradictory tendency on electrochemical performance in another study (Fig. 8) [102], which may be attributed to the high operating temperature since because of the low melting point of Cu metal, high temperature may result in the sintering of Cu and thus loss of corresponding role [108]. In general, Cu basically shows high carbon tolerance as it does not catalyse carbon fibre formation [108]. Therefore, addition of Cu into the Ni-based anode will achieve better stability [102,107].

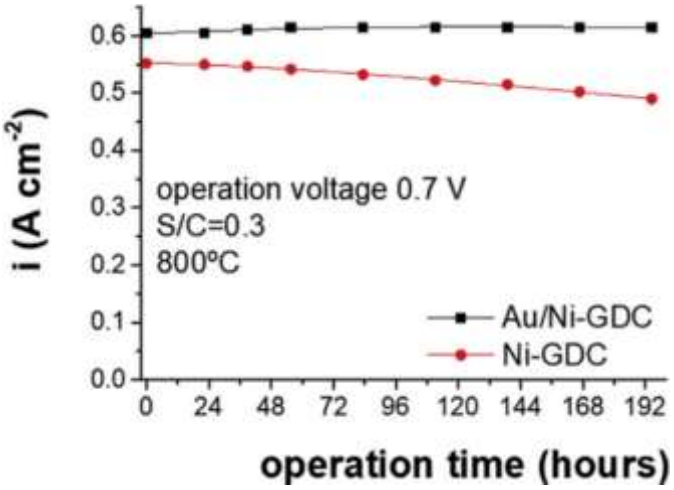

Fig. 7. *I-t* behaviour for Ni-GDC and Au/Ni-GDC porous anodes operated at 0.7 V polarization voltage, 800 °C and steam to carbon ratio S/C = 0.3. Figure reproduced from ref. [99] with permission from Elsevier.

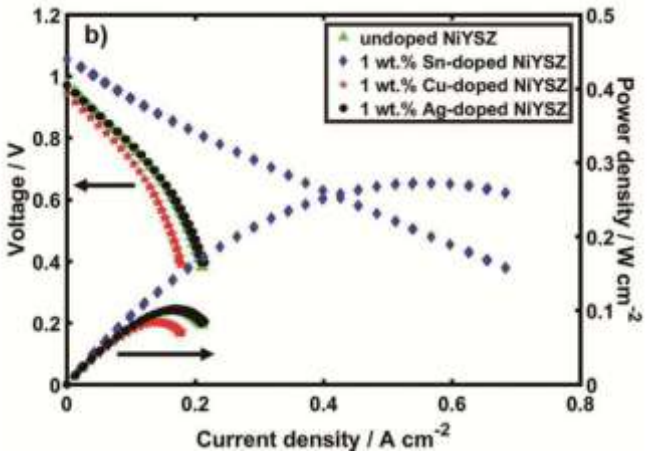

Fig. 8. *I-V* characterization measured at 750 °C for undoped Ni-YSZ, 1wt% Sn-doped Ni-YSZ, 1 wt% Cu-doped Ni-YSZ, 1 wt% Ag-doped Ni-YSZ anode single cells fuelled by dry biogas. Figure reproduced from ref. [102] by permission of The Electrochemical Society.

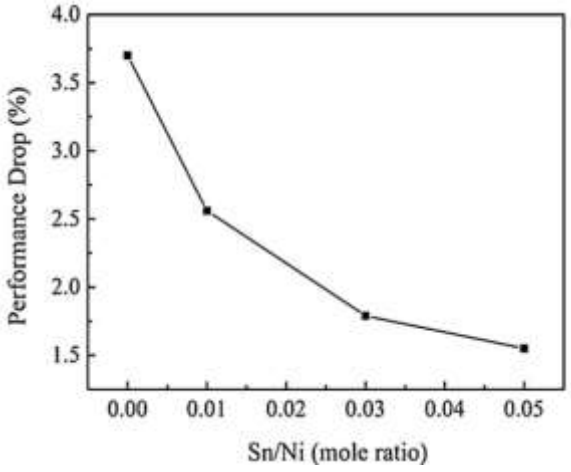

Fig. 9. Drop of performance of the cells after 72 h discharge. Figure reproduced from ref. [105] with permission from Elsevier.

Incorporation of alkaline earth metal oxides (e.g., BaO, MgO and CaO) to conventional Ni cermet anode can be another kinetic method to alleviate coking problem when methane is used as fuel. This is because small amount of basic oxide additives could help increase the local basicity [100] and thereby improve the chemisorption capability of steam and carbon dioxide, which can contribute to the reduction of deposited carbon through chemical reactions [109]. CaO and BaO decorations showed the best carbon resistance compared to other incorporations for pristine Ni-SDC anode in oxygen temperature-programmed oxidation (O_2-TPO) test, while due to unreduced phase of $Ni_{0.938}Mg_{0.062}O$, the coke formation rate of Mg modification was 6 times that of Ni-SDC [100]. Besides, because the process of CaO decoration could bring many nanoparticles onto the anode surface, which considerably reshaped the cermet morphology without compromise electrical conductivity, highest P_{max} among various anodes has been achieved in both hydrogen and humidified methane fuels [100]. The stability of cell with the CaO-modified anode has been conducted with the comparison of pristine Ni-SDC at 300 mA cm^{-2} and 650 ℃ when SOFC was operating on wet methane fuel. As expected, basic CaO improved the operational durability with a slight decay in 70 hours, while cell composed of the pristine anode degraded completely in less than 2 hours. The research work investigated by Qu et al. [100] indicated that CaO could be an promising basic oxide with consideration of both coking tolerance and electrochemical performance. Similar effect of CaO on the coking mitigation was also observed in the study conducted by Mishina et al. [51], and improved carbon suppression was concluded through carbon balance. However, there was no further information about long-term stability operation to directly exhibit the better carbon tolerance. Different from the work conducted by Qu et al. [100], Yang et al. [109] prepared the nickel-

based anode promoted by 2.5 wt% MgO via impregnant method without occupying Ni active sites, leading to more uniform MgO distribution in interstitial nickel sites. The existence of MgO played a significant role in the stable operation and enable the SOFC to present a moderate P_{max} of 714 mW cm^{-2} at 800 ℃ when 3% H_2O humidified methane was fed. Contrasting effects of MgO on the coking issue are mainly due to different fabrication procedures or methods, so only proper modification treatments can the anode benefit from the merits of additives. Recently, the MgO nanolayer-decorated anode was fabricated by *in-situ* reduction which greatly improve the homogeneity of sample and economical aspects compared to the complex evaporation and impregnation [110]. Because of the presence of MgO, smaller catalyst particles could be found since this oxide with higher melting point is likely to prevent the growth of NiCu particles. Therefore, under wet methane fuel, better electrochemical performance (670 mW cm^{-2}) for the anode of $Ni_{0.875}Cu_{0.1}Mg_{0.025}O$-SDC was obtained, which is approximately 10% higher than that of unmodified counterpart as a result of possible better catalytic activity of smaller NiCu particles or intrinsic characteristics of MgO. Besides, after stable 100 hours power output with the current density of 300 mA cm^{-2} at 700 ℃, the SEM images on the cross-sectional of aged anode showed well structural integrity and no evidence of deposited carbon. In contrast, operating voltage of the NiCu-SDC-based cell gradually decayed 34% in less than two days [110].

CeO_2-based materials have attracted considerable attentions due to their high OSC (oxygen storage capacity) characteristic and the chemical release or uptake of oxygen under a reductive or oxidative atmosphere, respectively [111]. Incorporating CeO_2 or doped-CeO_2 into Ni-based anode or replacing the ionic phase is likely to improve the carbon tolerance since local high O/C ratio help to oxidize carbonaceous adsorbates on Ni partials [56,112]. Ideris et al. [113] found that deposited carbon was detected only on the outer surface of Ni-SDC ($Ce_{0.8}Sm_{0.2}O_{1.9}$) anode, and no carbon was formed in the middle and inner surface of the anode (Fig. 10) after the 100 h operation accompanied with the degradation rate of 1.33 mV h^{-1} at a constant current density of 0.35 A cm^{-2} when dry methane was used as the fuel at 700 ℃. Besides, the carbon distribution in this work was completely different from the results from Sumi et al. [114] and Buccheri et al. [90] in which the carbon nearly deposited throughout entire Ni-YSZ anode. The author tended to attribute this discrepancy to the reason that within the anode, additional oxygen vacancies can be formed under reductive atmosphere, which contributes to the oxidation of carbon. However, although doped-CeO_2 materials are known for their higher oxygen exchange/storage capacities, this explanation seems not plausible since experimental conditions of these studies [90,113,114] were not identical, especially for the temperature and

current density which have considered as the essential thermodynamic strategies for carbon prevention. Therefore, further investigation needs to be carried out for the thorough explanation of different deposited carbon distributions. The utilization of GDC in the ionic phase could also mitigate the re-oxidation of nickel metal when there is higher concentration of oxygen in the anode, showing higher redox activity. For example, in the long-term stability test, the oxidation of Ni in YSZ-based anode evidenced by the *ex-situ* surface analysis leaded to the drastic decline of power density. On the contrary, thanks to the intact metallic form of Ni after 530 hours' operation of CPOX (catalytic partial oxidation), voltage degradation of 0.91% at 650 ℃ was observed for the anode fabricated by GDC material at the OCV state that is also thought as the most favourable condition for the carbon formation, which is mainly because distinguished feature of doped-CeO_2 enables the anode to be excluded the poisoning of Ni by carbon and oxygen [56]. In addition to the samarium and gadolinium, much cheaper calcium could also be doped into ceria to enhance electronic conductivity and oxygen ionic mobility. In the investigation of the optimum amount of calcium content in compositions of $Ce_{1-x}Ca_xO_{2-\delta}$, 10 mol% calcium-doped ceria ceramic ($Ce_{0.9}Ca_{0.1}O_{2-\delta}$) showed highest conductivity (0.102 S cm^{-1}), which is comparable to those of SDC and GDC [115]. Besides, the improved oxygen ionic mobility could further suppress carbon formation. Therefore, the Ni-$Ce_{0.9}Ca_{0.1}O_{2-\delta}$ anode-supported SOFC running on methane fuel achieved lowest degradation rate of 1.1 mV h^{-1} among different calcium-doped ceria compositions.

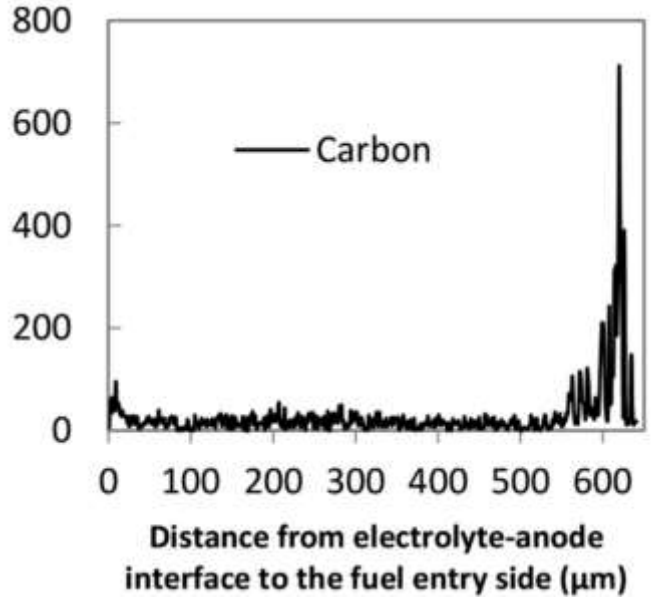

Fig. 10. EDX scan of carbon content over the labelled line from the electrolyte-anode interface to the fuel entry side of Ni-SDC anode-supported cell after 100 h operation with dry CH_4. Figure reproduced from ref. [113] with permission from Elsevier.

Although Ni exhibits high electronic conductivity and excellent catalytic effect towards electrochemical/chemical reactions, performance degradation due to carbon formation seems to still be unavoidable, especially for anode-supported cells. One straightforward approach is to replace the nickel metal with Ni-free materials which are inert for methane cracking, leading to the improvement of stability related to coking issue. Considering essential requirements of the anode and also durability, electronically conductive materials with low reforming catalytic effect could be regards as promising alternatives. Therefore, copper-based anode has been successfully utilized by Gorte et al. [5] when hydrocarbon was used because of various benefits of Cu metal such as low cost, abundance in nature, inertia for carbon formation and distinguished electronic conductivity. However, due to relatively low melting points of copper metal and its oxides [116], conventional high-temperature ceramic processing methods for Ni-YSZ might not be suitable for the fabrication of Cu-based anode. Instead, wet or vacuum-assisted impregnation, infiltration and deposition of Cu mixture into the porous electrolyte scaffold, followed by relatively low temperature calcination, are frequently-used techniques for the corresponding anode preparation, which could be one possible reason that thick electrolyte was generally fabricated for Cu-based fuel cells [116–119]. Although ceria which is generally another constituent for Cu cermet anode, provides the catalytic activity for electrochemical/chemical reactions, lower electrochemical performances of Cu-CeO_2 compared to traditional Ni-YSZ were often observed in lots of studies. For example, SOFCs with electrolyte thicknesses of 110 [117], 180 [119] and 150 μm [118] approximately exhibited P_{max}s of 70, 110 and 34.2 mW cm^{-2} when methane was used as the fuel at 800, 800 and 850 ℃, respectively. The low catalytic activity of Cu-CeO_2 for the fuel reforming or oxidation might be the dominating cause of low power output at high operating temperatures, though various factors such as the electrolyte thickness, metal loading content and scaffold materials could determine the maximum power density. Besides, although coking may not be a serious concern for copper-based anodes, long-term high-temperature operation could lead to coarser particles because of easy agglomeration of Cu metal, causing conductivity loss and thus power output decrease [118]. Fortunately, sintering as well as poor catalytic effect could be partially solved by adding transition metals (e.g., Co and Fe). For example, higher P_{max} (446.4 mW cm^{-2}) was achieved for the CoCu-CeO_2 anode when SOFC was operating on anhydrous methane at 850 ℃, and experiments showed well-kept particle distribution after 100 hour operation in hydrogen fuel due to much difficult inter-diffusion between cobalt and copper and no evidence of carbon formation after 24 hours operation in carbonaceous fuel [118]. Furthermore, it was found that copper-iron-ceria-YSZ anode presented higher maximum power density compared to

monometallic one. However, after 46 h operation in methane fuel at 0.6 V and 800 ℃, both sintering and coking were observed, resulting in increased total resistance and thereby slight decline of the current density [117].

In addition to Cu metal, MIEC materials with the perovskite or double perovskite structure have been extensively and successfully explored, e.g., $La_{0.75}Sr_{0.25}Cr_{0.5}Mn_{0.5}O_3$ (LSCM) [120], doped $SrTiO_3$ [121,122], $Sr_2MgMoO_{6-\delta}$ [123] and $Sr_2Fe_{1-x}Mo_xO_{6-\delta}$ (SFM) [124,125]. Due to the numerous advantages of perovskite oxides, such as intrinsic carbon and sulfur tolerances, higher catalytic activity compared to ceria for the fuel oxidation, mixed ionic and electronic conductive property, and redox stability in wider range of oxygen partial pressure, some studied perovskite materials could represent the most promising and effective choices for the anode. However, although these oxides have been considered as the most important alternatives, some of them basically suffer from several limitations compared to Ni-based state-of-the-art anode, involving relatively weak catalytic activity and inadequate electronic conductivity, especially at reduced operating temperature. Insufficient electronic conductivity of the anode may cause low efficiency of current conduction, higher ohmic overpotential and thus decreased cell performance. Therefore, electrolytes with the thickness from 70 to 500 μm were normally fabricated as the mechanical support to decrease the anode thickness and alleviate the negative influence of this drawback. However, despite the mitigation of perovskite electrical conductivity deficiency, thick electrolyte with moderate ionic conductivity will definitely lead to considerable ohmic resistance and thereby poor power density compared to anode-supported SOFCs with sufficient electronic conductivity, which could be one of reasons of low power density of fuel cells with perovskite-based anodes. Fortunately, as demonstrated previously, electrolyte-supported SOFCs could possess intrinsic structurally carbon tolerance in the current sweep condition, which can be one of minor merits of this configuration. In addition, catalytic activity as well as electronic conductivity could be enhanced by the partially replacement of A or B site with substitutional transition metals with the similar radius since appropriate partial elements doping could tailor or modulate the perovskite crystal structure to achieve desired properties for the anode [5,126]. For example, titanium-doped lanthanum ferrite perovskite ($La_{0.3}Sr_{0.7}Fe_{0.7}Ti_{0.3}O_3$, LSFT) has been successfully developed [127] and it was reported that Ti and Fe cations in LSFT would deliver enhanced synergistic effects on the durability and electrocatalytic activity which originate from the titanium-based perovskite and ferrite-based perovskite, respectively. The moderate P_{max} of 0.121 W cm^{-2} at 850 ℃ was achieved when wet methane was fed into the SOFC with LSFT anode considering that 8YSZ electrolyte with the thickness of 500 μm was fabricated. Besides, stable operations were observed in 24 h durability

tests conducted under humidified methane fuel and hydrogen fuel with 750 ppm H_2S, and *ex-situ* characterization techniques subsequently showed that there was no evidence of carbon deposition and nickel sulfide, indicating reasonable coking and sulfur tolerances, respectively. A new redox-stable double perovskite $Sr_2FeNb_{0.2}Mo_{0.8}O_{6-\delta}$ (SFNM20) partially doped by Nb at cationic Mo site, was synthesized to exhibit higher conductivity (5.3 S cm^{-1} in 5% hydrogen at 800 ℃) than other common perovskite materials [128]. Besides, exceptional performance (P_{max}: 380 mW cm^{-2} at 800 ℃) presented in wet methane fuel demonstrated much excellent catalytic effect towards fuel electro-oxidation. In addition, long-term capacity of 200 h stable performance showed that SFNM20 was equipped with impressive carbon endurance due to the rigid crystal structure in anodic atmosphere when methane was used as the fuel at 600 mA cm^{-2} and 700 ℃. Most recently, Ding et al. [129] developed another novel A-site deficient double perovskite oxide $(PrBa)_{0.95}(Fe_{0.9}Nb_{0.1})_2O_{5+\delta}$ (PBFN) with the layered structure as anode material. Nb element was successfully doped into the B site of the parent ceramic oxide $PrBaFe_2O_{5+\delta}$ to achieve promising anode properties in terms of the chemical stability and catalytic activity. High electrochemical performances with P_{max}s of 0.64 W cm^{-2} in humidified methane and 0.577 W cm^{-2} in dry methane at 800 ℃ were attained, which could be attributable to small anode polarization resistance due to outstanding activity of the PBFN anode. It was found that even slight increase in the current density was observed after 300 h stability test under there different power outputs in dry methane fuel at 700 ℃ (Fig. 11), and no carbon was deposited in the whole anode layer which was evidenced by the SEM images afterwards. Superior performance and stable operation in methane fuel indicated that PBFN could be a reliable carbon-tolerant anode material with the high-performing catalytic effect.

In addition to the partial doping, other efforts have also been conducted to further develop more suitable perovskite anode materials with lower electrode polarization to achieve better performance comparable to Ni-based anodes, involving forming the composite anode with high ionic conducting phase (doped CeO_2) and decorating the anode surface with nanoparticles (metals or oxides) by infiltration, impregnation or deposition techniques [130–133]. For example, when 3 wt% NiO was incorporated with $La_{0.9}Ca_{0.1}Fe_{0.9}Nb_{0.1}O_{3-\delta}$-$Sm_{0.2}Ce_{0.8}O_{1.9}$ (LCFNb-SDC) into the porous $Sc_{0.2}Zr_{0.8}O_{2-\delta}$ (SSZ) anode skeleton, remarkable enhancement of the electrochemical performance was observed. P_{max} of the SOFC operating on methane fuel was increased to 507 and 729 mW cm^{-2} from 73 and 174 mW cm^{-2} for unmodified anode at 800 and 850 ℃, respectively, which could be owing to the sufficient activity of Ni metal reduced from NiO oxide. Furthermore, both EIS (electrochemical impedance spectrum) and EDS (energy-dispersive X-ray spectroscopy) measurements subsequently confirmed the

negligible coking problem [133]. However, although infiltration methods (e.g., chemical or physical vapor deposition and wet impregnation) are widely used to decorate the perovskite anode skeleton surface by using nanostructured particles with high reaction activity and high specific surface area, the fabrication process could be time-consuming and costly since the deposition-calcination procedure generally need to be performed multiple times to obtain expected weight increments required for the better performance. In addition, nonuniform spatial distribution as well as the finite controllable grain size of nano-catalysts may have a negative effect on the long-term operation stability and electricity output due to the easy tendency of metal agglomeration. Therefore, proper preparation of the perovskite oxide anode microstructure with an even particle distribution through one effective strategy is certainly of great significance for the improvement of electrochemical performance and stable operation related to typical issues like metal sintering or coking, since the morphology of decorated porous perovskite could definitely determine the modification effect. In order to settle these deficiencies of conventional approaches mentioned-above, an alternative innovative method have been proposed and successfully carried out by many research groups. The active catalyst metals doped into the perovskite lattice (generally at B site) in the oxidizing atmosphere, will be partly exsolved from the porous perovskite precursor through *in-situ* reduction and uniformly dispersed on the backbone surface in the form of nanoscale particles. Different from traditional methods, homogenous size, uniform distribution, and well-controlled morphology of catalysts on the porous scaffold provided by the exsolution technology could exhibit excellent activity for anodic reactions and resistances for coking as well as metallic particles growth. Up to now, various nanoparticle-incorporated perovskite oxides have been used as the anode, and corresponding active mono-metals or alloys involving Cu, Fe, Co-Fe, Fe-Ru as well as Cu-Fe, were attained by *in-situ* exsolution from their parent perovskites $La_{0.5}Sr_{0.5}Fe_{0.8}Cu_{0.15}Nb_{0.05}O_{3-\delta}$ [134], $Ba_{0.3}Sr_{0.7}Fe_{0.9}Mn_{0.1}O_{3-\delta}$ [135], $Sr_2CoMo_{1-x}Fe_xO_{6-\delta}$ [136], $(Pr_{0.5}Sr_{0.5})_{0.9}Fe_{0.9}Ru_{0.1}O_{3-\delta}$ [126], $(La_{0.75}Sr_{0.25})_{0.9}(Cr_{0.5}Mn_{0.5})_{0.9}(Cu_{1-x}Fe_x)_{0.1}O_{3-\delta}$ [137], respectively. For example, Wang et al. found that $Cu_{1-x}Fe_x$ nanoparticles with the average diameter of 30 nm exsolved from $(La_{0.75}Sr_{0.25})_{0.9}(Cr_{0.5}Mn_{0.5})_{0.9}(Cu_{1-x}Fe_x)_{0.1}O_{3-\delta}$ were deeply embedded in the porous LSCM skeleton with the uniform distribution (Fig. 12a), which not only provide sufficient active sites and catalytic activity for the fuel electro-oxidation but also enhance the performance stability because of strong interaction at heterojunction interfaces between metals and ceramic oxide (Fig. 12b) [137]. Subsequent electrochemical performance of the electrolyte (300μm) supporting SOFC with proposed $(La_{0.75}Sr_{0.25})_{0.9}(Cr_{0.5}Mn_{0.5})_{0.9}(Cu_{0.5}Fe_{0.5})_{0.1}O_{3-\delta}$ anode operating on dry methane exhibited

highest power density with the P_{max} of 0.64 W cm^{-2} at 850 ℃ (Fig. 13), which was much higher than that (0.26 W cm^{-2}) of pristine LSCM. Sulfur poisoning (24 hours) and coking (100 hours) durability tests were conducted afterwards under 0.4 A cm^{-2} and 850 ℃, showing moderate resistance capacities. In addition to the single perovskite oxide (ABO_3), double perovskites could also be used for exsolution precursors. Co-Fe alloy nanoparticles with multiple-twinned defects formed from the reduced Fe-doping $Sr_2CoMo_{1-x}Fe_xO_{6-\delta}$ (x = 0, 0.05, 0.1) presented exceptional coking resistance and also active activity for fuel oxidation reactions [136]. It was reported that deposition amounts of the amorphous and graphite carbon decreased considerably for the reduced $Sr_2CoMo_{0.95}Fe_{0.05}O_{6-\delta}$ anode with exsolved bimetallic alloy compared to undoped $Sr_2CoMoO_{6-\delta}$ anode after the 50 h durability test in wet methane fuel under 200 mA cm^{-2} and 700 ℃, which was evidenced by Raman spectra of fresh and aged anodes (Fig. 14). Besides, the electrochemical testing was investigated in wet methane fuel with same anode, and much higher power densities were achieved (652.3 mW cm^{-2} at 850 ℃ and 532.9 mW cm^{-2} at 800 ℃) compared to undoped $Sr_2CoMoO_{6-\delta}$ anode (486.5 mW cm^{-2} at 850 ℃ and 350.6 mW cm^{-2} at 800 ℃) when $La_{0.9}Sr_{0.1}Ga_{0.8}Mg_{0.2}O_{3-\delta}$ (LSGM) electrolyte with the thickness of 300 μm was fabricated as the support.

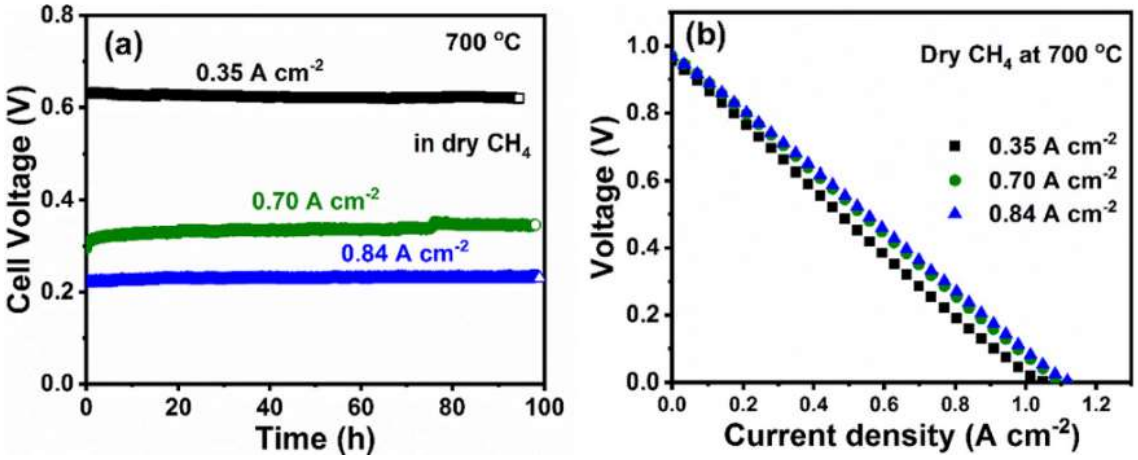

Fig. 11. The durability test of the cell discharged at different constant current densities at 700 ℃ in dry methane: (a) the observation of cell terminal voltage changes at 0.35, 0.7 and 0.84 A cm^{-2}; (b) the current-voltage curves after each test. Figure reproduced from ref. [129] with permission from Elsevier.

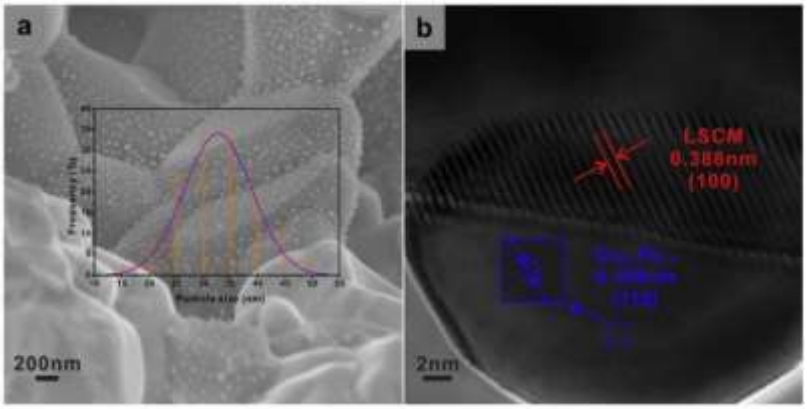

Fig. 12. (a) *In situ* grown $Cu_{1-x}Fe_x$ nanoparticles anchored on the porous LSCM skeleton with particle size distribution; (b) HRTEM image of LSCMCF50 sample heated in 5% H_2/Ar at 950 °C for 20 h. Figure reproduced from ref. [137] with permission from Elsevier.

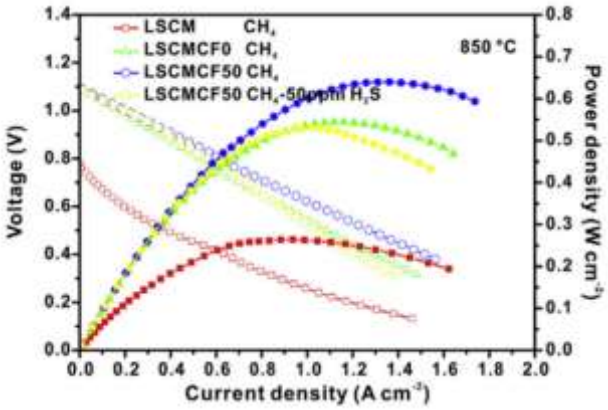

Fig. 13. *I-V/P* curves of different anodes at 850 °C in dry CH_4 and CH_4-50 ppm H_2S. Figure reproduced from ref. [137] with permission from Elsevier.

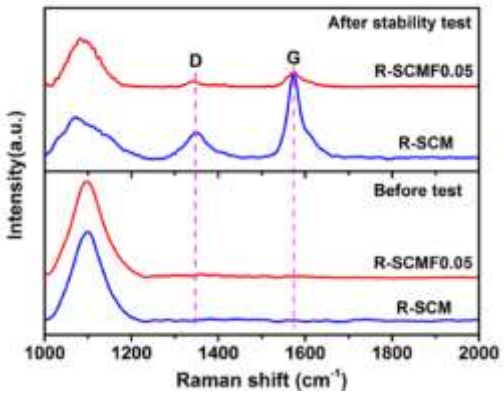

Fig. 14. Raman spectra of reduced SCM and SCMF0.05 samples before and after stability test in wet CH_4. Figure reproduced from ref. [136] with permission from American Chemical Society.

Structure

In the perspective of the SOFC structure, coking mitigation strategies include the development of symmetric SOFCs because of the excellent redox stability of electrode materials; material individually optimizations of functional and support or current conduction layers due to different functions; addition of the buffer layer as barrier or catalyst layer; micro-structure optimization benefiting the facile mass transport and fuel conversion.

Symmetric solid oxide fuel cells (S-SOFCs), as the name indicates, refer to fuel cells fabricated by the same material for both anode and cathode electrodes at the same time. Special structure of S-SOFCs shows various merits, such as reversible operation ability, the less incompatibility problem because of less material varieties used, simplified processing procedure, and thus reduced cost [138]. Considering gas conditions in both fuel and air electrodes, the materials with excellent chemical stability are required in reducing and oxidising atmospheres simultaneously. It is found that many perovskite material anodes that possess superior redox capacities performed stable in several redox cycling without property degradation [128,129,136,137]. Most importantly, even though carbon is eventually deposited or sulfide species is formed on the anode when S-SOFCs are running on carbon-containing fuels, oxygen rich gas could be flowed to the anode and easily oxidise the carbon or sulfide without sacrificing the anode ability, exhibiting high coking or sulfur tolerance. Therefore, perovskite-based electrodes are widely used for S-SOFCs, which shows promising potentials in mitigation of poisoning issues for the methane-fuelled SOFC. A-site deficient layered perovskite oxide, $(PrBa)_{0.95}(Fe_{0.9}Mo_{0.1})_2O_{5+\delta}$ (PBFM) has been successfully fabricated as electrodes for the symmetric SOFC with the configuration of PBFM (25 μm) / LSGM (200 μm) / PBFM (25 μm) [139]. As the cathode and anode simultaneously, PBFM not only showed comparable electrode polarization resistance to other cobalt-containing perovskite cathodes in the air, but also exhibited lower activation polarization in hydrogen and wet methane than other common perovskite materials [120]. Superior performance in anodic and cathodic conditions enable this S-SOFC to show a high-performing P_{max} of 0.34 W cm^{-2} at 800 ℃ in humidified methane fuel, and subsequent 280 hours operation with a slight decay under 1.0 A cm^{-2} at 800 ℃ manifested the outstanding thermal stability and coking tolerance of the symmetric SOFC with PBFM electrodes. The electrochemical performance could be further improved to 0.39 W cm^{-2} in dry methane fuel at 800 ℃ by impregnating PBFM nanoparticles with the size of 20 nm onto both fuel and air electrodes. Besides, slight increase of the cell performance was also observed after 1060 hours stability test with the current density of 1.0 A cm^{-2} when dry methane was used as fuel at 800 ℃ [139]. Holding the stable structure of electrode PBFM under the

reducing and oxidising conditions was the key factor for the stable operation of the symmetric SOFC. Currently, the reversibility of exsolution process provides another possibility for the promising durable symmetric SOFC development. Developed double perovskite $Sr_2Co_{0.4}Fe_{1.2}Mo_{0.4}O_{6-\delta}$ (SCFM) could be converted into the Co-Fe nanoparticles-decorated $Sr_3Co_{0.1}Fe_{1.3}Mo_{0.6}O_{7-\delta}$ with the Ruddlesden−Popper structure (RP-SCFM) by exsolution process in the anodic atmosphere, and RP-SCFM with the mixed ionic and electronic conductivity and uniform Co-Fe nano-alloy (CFA) with the reported high coking tolerance are likely to serve as an eligible anode material for methane fuel. Then the converted RP-SCFM with Co-Fe nanoparticles will be transformed back to SCFM with the double perovskite structure under oxidising condition, and because of Co element in the cathode, SCFM is expected to possess sufficient ORR catalytic activity [140]. Fabricated symmetric SOFC with the configuration of RP-SCFM-CFA (20 μm) / LSGM (300μm) / SCFM (20 μm) presented reasonable electrochemical performance with P_{max}s of 0.401 and 0.271 W cm^{-2} at 850 and 800 ℃, respectively, in methane fuel. In addition, this symmetric SOFC also exhibited carbon resistance in the stability test of 130 h operation without any voltage decline at 400 mA cm^{-2} and 800 ℃ when methane was used as fuel.

As discussed earlier, anode layer could be divided into two distinct layers according to the presence or absence of oxygen cation transferred from the cathode in the anode-supported SOFC [3,5,86–89]. Due to considerable oxygen ions, electrochemical reactions will be largely performed in the narrow layer near the anode/electrolyte interface which is called functional layer. Although coking issue could be a serious concern for the methane-fuelled anode-supported SOFC with conventional Ni-based anode, carbon will not deposit on the anode functional layer as long as the fuel cell is on the current output mode despite the presence of nickel. This is because oxygen ions migrated from the cathode could oxidise possible deposited carbon or higher concentrations of electrochemical products could promote reforming processes of methane (Eqs. (4) and (5)), reversed Boudouard reaction (Eq. (9)) and H_2O gasification reaction (Eq. (10)), thereby eliminating deposited carbon or preventing the cracking reaction in the anode functional layer. Despite the combined effect of the decreased concentration of methane and increased concentrations of electrochemical products along the depth of the anode as results of chemical/electrochemical reactions as well as diffusion resistance, carbon may be formed via three possible reactions (Eqs. (8), (9) and (10)) under the catalytic activity of nickel metal in the anode support or current conduction layer since the little oxygen will be available beyond functional layer. Accordingly, for conventional Ni-based anode-supported SOFCs, functional and support layers are both based on the Ni metal, which

may lead to the carbon deposition mainly on the current conduction layer. In this respect, materials optimization independently of these two separate layers could provide a promising way for the coking mitigation, involving material (e.g., Ni cermet) in the functional layer optimized for the active electrocatalytic activity and catalytically inert material in the support layer optimized for sufficient electronic conductivity [89]. Lanthanum-doped strontium titanate perovskite of $Sr_{0.8}La_{0.2}TiO_3$ (SLT) with low catalytic property which exhibits reasonable conductivity in typical anodic condition of the SOFC was successfully fabricated as the anode support, accompanied with Ni-YSZ as the active layer and Ni-SDC as the adhesive layer [88]. Stable operation of the SLT-supported fuel cell running on synthetic natural gas was observed more than 80 hours without noticeable degradation under several current densities at 800 ℃, while for the Ni-YSZ-supported cell, significant carbon deposition detected by the SEM-EDS spectra caused a dramatic voltage decline despite high current density of 1.4 A cm^{-2}, which demonstrating the much improved coking tolerance of the proposed fuel cell. Meanwhile, compared to the Ni-YSZ-supported cell, the redox durability of the SLT-supported SOFC could be correspondingly enhanced because of less amount of Ni in the anode and thus less volume expansion induced by Ni oxidation. In addition, because of inactive activity, good mechanical and chemical stability properties, Alumina was also considered for the anode support [87]. Al_2O_3-supported SOFC with Ni-SDC as the functional layer achieved excellent performance with a P_{max} of 0.79 W cm^{-2} in dry methane fuel at 700 ℃, which was slight lower compared to the Ni-SDC anode-supported counterpart. Besides, coking stability of fabricated fuel cells was tested under OCV (Fig. 15) and current density (1 A cm^{-2}) conditions in dry methane fuel at 700 ℃, and the results of both conditions demonstrated that the Al_2O_3-supported SOFC possessed best carbon tolerance. For the post-test fuel cell under output condition, SEM micrographs showed that for the Ni-SDC anode-supported fuel cell, considerable carbon and carbon whiskers were found on the bulk and inner surface of the anode, respectively, while no carbon was deposited in the entire anode of Al_2O_3-supported SOFC. Besides, even for the Ni-SDC anode-supported SOFC, there was no carbon deposition in the anode functional layer after current sweep, which basically proved intrinsic tolerance of the functional layer towards carbon deposition under current density condition.

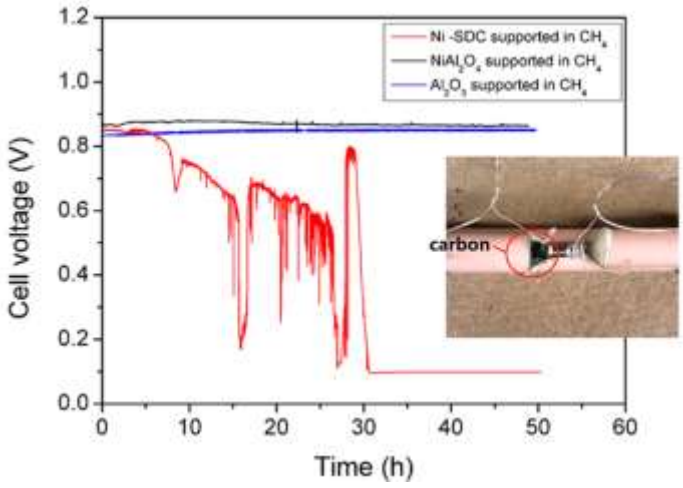

Fig. 15. Time history of open circuit voltages of the three type of cells in direct dry methane at 700 ℃ in a short-term stability test. The insert is the image of post-test anode-supported cell NiO-SDC/SDC/PBCO damaged by carbon deposited near inlet of anode electrode. Figure reproduced from ref. [87] with permission from American Chemical Society.

Although electrochemical reaction products play a significant role in the removal of deposited carbon on current output mode for the conventional Ni-based SOFC operating on methane rich fuel, the anode support layer still faces more serious coking issue since methane partial pressure nearly linearly increases from the electrolyte to anode surface based on the analysis from Lin et al. [85]. In order to further reduce the methane concentration and maintain high reaction products throughout the anode, attachment of a porous buffer or barrier layer with no catalytic activity onto the outside surface of anode support layer (Fig. 16) was proposed and successfully fabricated [141]. The long-term stability test showed that the voltage of modified SOFC with CeO_2 and stabilized-ZrO_2 buffer layer remained stable for about 155 hours under 0.6 A cm^{-2} when wet methane was fed at 750 ℃, and no noticeable carbon or structure damage was observed in the SEM-EDX measurement test afterwards, while for the pristine SOFC with Ni-YSZ as the anode, continuous drop of the electrochemical performance was detected with time, demonstrating much improved carbon resistance of the SOFC with the addition of buffer layer. In addition, composite layer of $Sr_{0.8}La_{0.2}TiO_3$ (SLT) and YSZ was also considered to serve as the barrier because both are chemically inert towards methane fuel [142]. Stable operation was achieved over 280 hours in humidified biogas fuel at 850 ℃ when current density was as low as 0.1 A cm^{-2}, which indicated that the integration of tubular SOFC with SLT barrier layer could improve coking capacity. However, the negative influence of adding a separated layer to the anode is that electrochemical performance will be sacrificed due to the increased fuel/gas diffusion resistance and thus larger concentration polarization caused by

longer transport pathway [141,142]. In order to address this deficiency, the adhesion of reforming or catalyst layer rather than catalytic inert layer to the anode was proposed [143]. With the introduction of active catalytic sites, more syngas could be generated through methane reforming reactions, which could provide more direct fuels for electrochemical reactions and less coking threatening atmosphere (carbon monoxide rich instead of methane rich gas mixture) for nickel-based anode, leading to improved carbon tolerance as well as power density. For example, $Ce_{0.8}Ni_{0.2}O_{2-\delta}$ (CNO) was employed as the internal reforming layer for Ni-SDC anode-supported SOFC, and it was found that stability and P_{max} were both enhanced when wet methane was used as the fuel [144]. Because of dispersed metallic Ni reduced from NiO and generated oxygen vacancies in the CNO layer, the voltage degradation rate declined from 1.36×10^{-2} V h^{-1} for the pristine SOFC to 4.38×10^{-4} V h^{-1} for the modified counterpart under 0.2 A cm^{-2} at 650 ℃, and at the same operating temperature fuel cell with this reforming layer exhibited increased performance with a P_{max} of 664 mW cm^{-2}. In addition to the oxide, bimetallic or alloy such as Cu-Ni [145] and even proton-conducting oxide like $La_2Ce_2O_7$ and $La_{1.95}Sm_{0.05}Ce_2O_7$ [146] have also been successfully utilized as the reforming or catalyst layer due to their respective outstanding properties. Besides, exsolution technology with more advantages compared to traditional preparation methods could also be used to improve the catalytic performance of the reforming layer. Under the reducing condition, $Fe_{0.64}Ni_{0.36}$ alloy nanoparticles exsolved from perovskite precursor $La_{0.7}Sr_{0.3}Fe_{0.8}Ni_{0.2}O_{3-\delta}$ (LSFN) were evenly distributed on the oxide backbone layer [147]. With the exsolved catalyst layer, maximum power densities increased by 26.01% and 24.48% at 850 ℃ compared to the unmodified fuel cell under methane-steam and methane-air fuels, respectively. Then, stability tests were conducted to investigate coking resistance, and the comparison of long-term operations at different fuel compositions (Fig. 17) showed stable operations with slight decay were achieved when the reforming layer was attached, while fuel cells without the reforming layer completely failed due to considerable carbon deposition in the anode at the initial stage of long-term durability test. More recently, a low-temperature SOFC with the Ni-$BaZr_{0.1}Ce_{0.7}Y_{0.1}Yb_{0.1}O_{3-\delta}$ (Ni-BZCYYb) multifunctional anode and $Ce_{0.90}Ni_{0.05}Ru_{0.05}O_2$ (CNR) catalyst layer was reported to exhibit more than 550 hours stable operation with no evidence of coking when wet methane was fed at 500 ℃ [148]. Besides, due to the synergistic effect of single-atom Ru and Ni, high performance with a P_{max} of 0.37 W cm^{-2} was achieved under the same condition, demonstrating improved catalytic activity of the CNR reforming layer especially at such low operating temperature. The investigations mentioned-above are all based on the same configuration that the barrier or reforming layer was directly coated on the outside surface of

anode support. However, this kind of configuration could lead to some undesired consequences, involving current conduction inefficiency if the catalyst layer is electrically insulating, and the possible cell fracture due to the thermal expansion coefficients (TECs) mismatch of components and nonuniform temperature distribution [149]. In this respect, other structure configurations of the addition of reforming layers were proposed and investigated, such as the placement of current collector directly between anode and reforming layers [150–152], placement of the independent catalyst layer without direct contact to the anode surface (Fig. 18) [153] and the addition of catalyst tube to the fuel gas inlet of tubular SOFC without integration into the structure [154]. The independent reforming layer from study conducted by Chang et al. [153] was composed of perovskite catalyst $La_{0.6}Sr_{0.4}Co_{0.2}Fe_{0.8}O_{3-\delta}$ (LSCF) and thick Al_2O_3 substrate, and with the feeding of hydrogen, CoFe alloy with uniform dispersion exsolved from LSCF was capable of providing the remarkable catalytic activity for methane reforming. Accordingly, cell with the reforming layer exhibited a higher P_{max} (0.66 W cm^{-2} at 850 °C) compared to the unmodified counterpart (0.50 W cm^{-2} at 850 °C), but the improvement was not obvious at low operating temperature. In addition, stability test subsequently presented that the modified fuel cell with separated reforming layer possessed the best coking tolerance. It was found that under humidified methane fuel at 800 °C, cell with this layer maintained stable power output for about 116 hours at 333 mA cm^{-2}, while the pristine conventional Ni-YSZ-based SOFC completely failed within few minutes due to the structure crack caused by serious carbon deposition (Fig. 19).

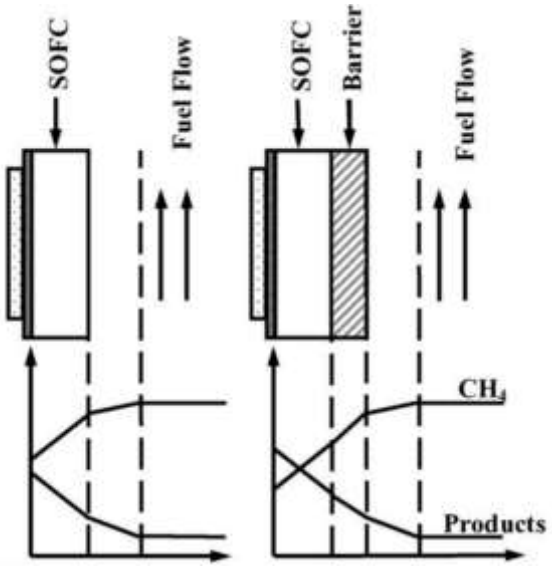

Fig. 16. Simplified schematic illustrations of how reactant and product gas concentrations are expected to vary with position during SOFC operation without (left) and with (right) barrier layers. Figure reproduced from ref. [141] with permission from Elsevier.

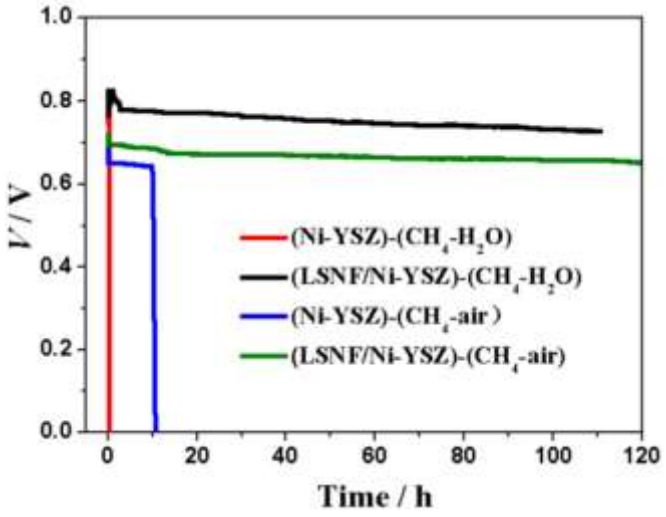

Fig. 17. Durability of Ni-YSZ and LSFN-Ni-YSZ using CH_4-H_2O fuel and CH_4-air fuel at a current of 335 mA cm^{-2} at 800 °C. Figure reproduced from ref. [147] with permission from Elsevier.

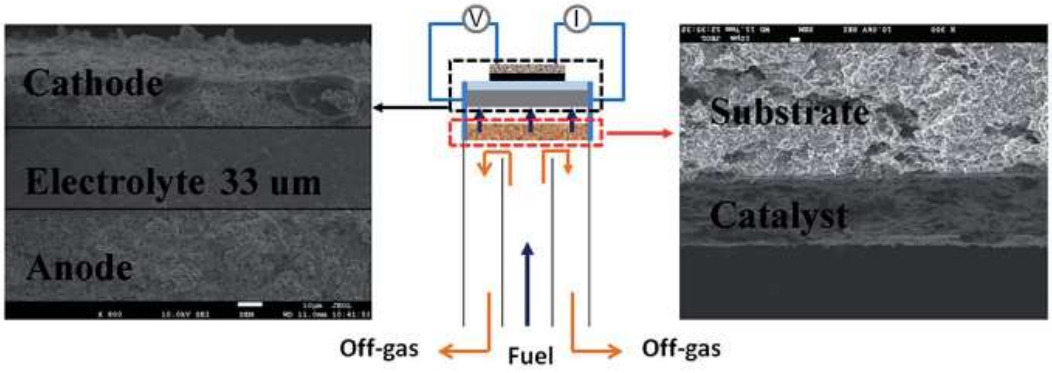

Fig. 18. Illustration of the cell with an independent catalyst layer. Figure reproduced from ref. [153] with permission from the Royal Society of Chemistry.

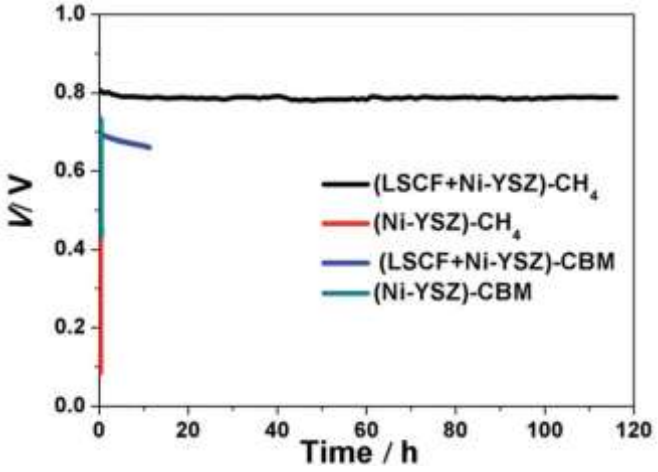

Fig. 19. Time-dependent voltage of cells with and without a catalyst layer at a current density of 333 mA cm^{-2} at 800 °C using 3% H_2O-97% CH_4 and 3% H_2O-97% CBM fuels. Figure

reproduced from ref. [153] with permission from the Royal Society of Chemistry.

Construction of micro-channels in the thick anode support could be an effective strategy to improve the cell electrochemical performance by promoting fuel diffusion to eliminate concentration overpotential which will be considerable especially when SOFC is operating at high current density. It was also found that the introduction of micro-channels by phase inversion technique could effectively reduce the anode tortuosity several times compared to conventional design [155]. Besides, numerical model developed by Chen et al. [156] reported finger-like channels could facilitate gas transport and thereby improve the SOFC performance. In addition to the transport convenience, micro-channels also plays a role in the carbon mitigation [116,157,158]. The stabilities test conducted by Wang et al. [157] demonstrated that the button-shaped fuel cell with micro-channels in anode showed the best coking durability compared to fuel cells with half-channels and no channel in the anodes at 600 ℃ when the 30%, 60% and 80% CH_4/Ar mixture were used as the fuel (Fig. 20), respectively. The improved carbon tolerance of the micro-channelled anode was due to well infiltrated catalyst into the depth, which promoted methane reforming. Therefore, the efficient catalyst coating not only enhance the power output but coking durability in methane fuel [157]. Rabuni et al. [116] has drawn the same conclusion that micro-channels of YSZ micro-tubes in the tubular SOFC benefited the delivery of anode materials (Cu-CeO_2), which enhanced both electrochemical performance and carbon resistance in dry methane fuel. Recently, the tubular Ni-YSZ micro-monolithic anode incorporating 6 droplet-shaped sub-channels was fabricated through phase inversion process, and anode supports were distributed between sub-channels [158]. Besides, due to the presence of sub-channels, the anode thickness in unsupported area was decreased to less than 50 μm. Because of the particular geometrical structure as well as developed micro-channels, SOFC with this unique anode exhibited excellent power output with P_{max}s of 1.77, 2.03 and 2.22 W cm^{-2} at 750 ℃ when simulated LCVGs (low calorific value gas) with methane concentrations of 10%, 15% and 20% (reminder: carbon dioxide) were fed into SOFC, respectively. In addition, stable operation with negligible degradation was achieved for more than 500 hours when cell was operating on methane and carbon dioxide mixture with the ratio of 1:1 at 0.7 V and 700 ℃. Although the current density as well as carbon dioxide could help to hinder the carbon deposition, decreased anode thickness in unsupported area could be one of reasons for carbon mitigation.

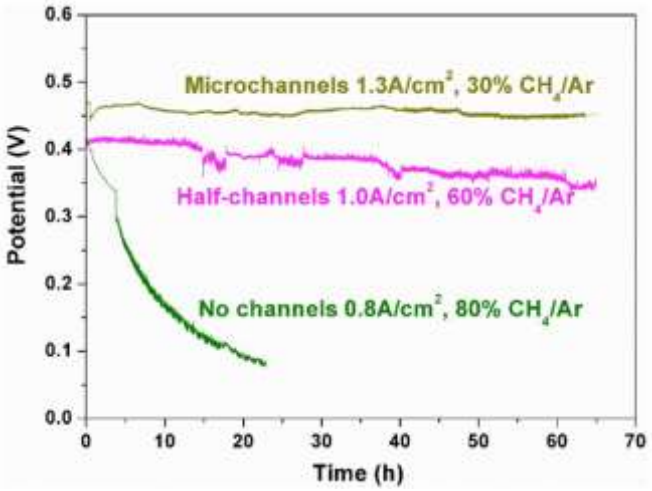

Fig. 20. Stability test of methane-fueled SOFCs with different anode microstructure. Figure reproduced from ref. [157] with permission from Elsevier.

Remaining challenges and future perspectives for methane-fuelled SOFCs

Although thermodynamic strategies, involving addition of oxygen agents, higher polarization current and typical operating temperature as well as the utilization of deposited carbon as a fuel, might be effective for preventing coking, some drawbacks will inevitably be introduced to SOFC systems, such as: the dilution effect and thereby lower overall efficiency caused by the externally supplied oxygen content; increased complexity and cost because of supply units (e.g., steam generator); faster degradation rate due to higher current density [159]. Meanwhile, it seems impractical for the SOFC to operate below the certain temperature region, since temperature will be highly enhanced due to improved exothermic processes during full load operation, which could be catastrophic to the cell stable operation [5]. As for the IFS mode, the intermittent supply time interval needs to be well controlled at different operation conditions, since less consumption of carbon and thus quick carbon accumulation could lead to some adverse situations.

Thanks to the significant efforts devoted by many researchers, kinetic methods related to material science offer numerous strategies to solve coking issue which is inevitable problem for the Ni-based SOFC fed by methane rich fuel. However, most of them are not yet ready to be used in mature level. Incorporation of metals or oxides could bring about enhanced coking tolerance as well as the increased electrochemical performance to some extent but suffered from one or several disadvantages depending on the particular material, such as the high cost or easy agglomeration of noble metals, or complicated anode fabrication procedure. Besides, different fabrication processes could lead to inverse effect on the fuel cell performance. Therefore, although the prolonged lifespan and improved power density might partially

compensate the cost as demonstrated earlier, more investigations need to be conducted to explore effective and reasonable manufacturing technological process in order to simplify the complex fabrication procedure and thus reduce processing cost, which could enable this approach to be easily manufacturable and used in a commercial scale. The biggest obstacles for Cu-based anode are the low power density due to sluggish activity of copper or ionic phase (e.g., doped Ceria), and easy sintering at elevated operating temperature, which could hinder its direct practical utilization. Perovskite- or double perovskite-based anodes with intrinsic resistant benefits present remarkable properties in terms of the activity and conductivity after the optimization of infiltration, doping or surface exsolution. However, relatively high temperature (higher than 800 ℃) must be maintained to achieve reasonable power output for perovskite-based anode, which may be conflicting to developments of intermediate and low temperature SOFCs because it is significant for the commercialization of SOFC to lower its operating temperature. Therefore, most oxides including perovskite are not likely to serve as a suitable anode for the methane-fuelled SOFC due to their sluggish kinetics when operating temperature is not sufficiently high. Besides, it is known that in order to alleviate the inadequate electronic conductivity of perovskite anode, electrolyte-supported structure is extensively employed in the fabrication of SOFC. However, due to the good structurally intrinsic carbon tolerance of electrolyte-supported structure especially under high current density, it is difficult to recognize the actual coking resistance capacity of the perovskite anode in long-term durability tests since high current density has been considered as one of thermodynamic strategies to mitigate coking problem. Therefore, standard requirements for durability tests related to carbon deposition need to be proposed, such as OCV (zero current density) condition, high operating temperature (higher than 700 ℃) as well as specific dimensions of the cell structure.

Although those structural strategies, involving the development of symmetric SOFC, optimizations individually of functional and support layers, additions of the barrier or catalyst layer and the construction of micro-channels in the anode support, will inevitably complicate the anode fabrication, greater flexibility of electrode design could also be provided, which correspondingly offers enhanced carbon tolerance to the SOFC system. However, several drawbacks will be caused by the specific method. For symmetric SOFCs which rely on the redox-stable perovskite material, most of these oxide materials still suffer from the low electronic conductivity and catalytic activity especially at low or intermediate temperature. Optimizations individually of functional and support layers could be a promising approach to address coking issue, but appropriate material selections of different layers are vitally important

for the long-term performance since mechanical/chemical stabilities, conductivity and the material compatibility in reducing atmosphere should be considered. Although the direct contact of methane gas and anode support could be largely prevented because of the attachment of barrier layer, which could definitely improve carbon resistance, some negative influences such as higher concentration overpotential and thereby decreased performance, will be unavoidable. In addition to the barrier effect, reforming layer acting as catalyst could convert methane to syngas, which is less prone to carbon deposition, and more direct fuels generated for electrochemical reactions will compensate the performance loss due to concentration polarization caused by the thick gas diffusion layer. However, for fuel cells with the reforming or barrier layer must be operating on the substantial current density mode since oxygen ion from the cathode side is the only oxygen source and carbon mitigation is achieved by using electrochemical products to consume methane to a less coking level. Moreover, these two strategies are more likely to slow the process of the carbon deposition, some post-mortem analysis indicated that carbon was still observed in the bulk anode after the stability test in methane fuel [144,146,153]. Therefore, thickness and material optimizations of the reforming layer can be important factors for the stable operation of direct methane-fuelled SOFCs. The development of finger-like or micro channels constructed in the anode has turned out to be a facile way of promoting the gas transport and methane conversion and reducing carbon formation, though the fabrication process could be slightly time-consuming and complicated.

3.1.3. The development of higher hydrocarbon-fuelled SOFCs

Higher hydrocarbons, such as ethane (C_2H_6), propane (C_3H_8), butane (C_4H_{10}) and octane (C_8H_{18}) have also been used as the fuel for SOFC due to their special characteristics, especially liquid state or easier liquefaction property compared to methane, which could be beneficial to the application of portable SOFCs. Besides, the conversion of hydrocarbon to syngas through reforming reactions could be more straightforward because of weaker C-H bond strength (CH_4: 435 kJ mol^{-1}, C_3H_8: 412 kJ mol^{-1} and C_4H_{10}: 409 kJ mol^{-1}) with increasing hydrocarbon chain length [160]. However, SOFCs running on higher hydrocarbons thermodynamically suffer from more severe coking problem as a result of higher carbon ratio in comparison with methane fuel. Therefore, according to the literature, stable operations of SOFCs running on the higher hydrocarbon in terms of carbon mitigation were still achieved through three perspectives of thermodynamics, kinetics as well as structure. There is one exception for the utilization of ethane: the cogeneration of high-value product (ethene) and electricity could be possible when ethane is fed to SOFC, which provides new strategy for carbon mitigation since the dehydrogenation reaction of ethane (Eq. (14)) avoids the crack of C-C bond and thus the

formations of amorphous and graphite carbons. Table 2 and Table 3 list the developments of higher hydrocarbon-fuelled SOFCs in recent years.

Strategies to suppress degradation issues of propane or butane-fuelled SOFCs

Propane and butane are the main constituents of liquefied petroleum gas (LPG), which has been considered as clean, low-carbon and most suitable power source especially in some emergency situation since LPG could be portable by cylinders or cartridges [161]. Although propane and butane are gas state at ambient temperature and atmospheric pressure, they could be more easily liquefied at relatively lower pressure compared to the methane, which are practically available for portable SOFC systems since the storage, transportation or distribution of these liquefied hydrocarbon fuels could be based on existing gasoline infrastructure systems.

As demonstrated previously, requirements for portable SOFC power generators, such as rapid response, start-up capacity and simple compact system design enable the partial oxidation of hydrocarbon to be the most desired operation modes [150,161–166] for carbon mitigation because of not only increased O/C ratio but the greater heat generated from propane or butane partial oxidation which is several times compared to methane fuel [164], while few investigations were focusing on steam or dry reforming reactions [167,168] despite the higher efficiency of these reforming processes. Zhan et al. [164] found that the anode-supported SOFC with configuration of Ni-YSZ/YSZ/LSCF-GDC approximately exhibited a P_{max} of 0.7 W cm^{-2} at 790 ℃ when fuel with the composition of 10.7% propane, 18.7% oxygen and 70.6% argon was fed and stable operation without coking was achieved for more than 100 hours though detailed conditions for the stability test were not provided. Similarly, improved durability of the SOFC operating on butane could be achieved in the same thermodynamic method for the research conducted by Sumi et al. [161]. The fuel gas mixture with O/C ratio of 1.5 achieved by fuel feeding composition of 10 mL min^{-1} *n*-butane, 30 mL min^{-1} oxygen and 112.9 mL min^{-1} nitrogen showed enhanced stability in comparison to the less oxygen feeding gas (O/C: 1.0) when microtubular SOFC with the fabrication of Ni-GDC (640 μm) / YSZ (10 μm) / GDC (interlayer: 1 μm) / LSCF-GDC (20 μm) was operated at 0.1 A cm^{-2} and 650 ℃ (Fig. 21).

In addition, stable operations on higher hydrocarbon could also be achieved based on the material science via kinetic approach. For example, It was reported that the infiltration of doped ceria into the Ni-based anode or the replacement of anode ionic phase with the doped barium zirconate-cerate or doped ceria could improve coking tolerance capacity when wet propane or butane was directed used as the fuel for SOFC [169–172]. For example, the mixed ion conductor of BZCYYb ($BaZr_{0.1}Ce_{0.7}Y_{0.1}Yb_{0.1}O_{3-\delta}$) with the higher ionic conductivity compared to frequently used electrolyte materials involving YSZ, GDC and BCZY especially at

intermediate temperature, was successfully fabricated as the ionic phase of Ni-based anode [169]. With YSZ as the electrolyte, cell with supporting Ni-BZCYYb anode achieved more than 100 h stable operation without performance degradation in wet propane fuel under 0.3 A cm^{-2} at 750 ℃. The excellent coking resistance was predominately attributed to the enhanced water adsorption capability of BZCYYb since when dry propane was used as the fuel, OCV decreased rapidly within 1 h because of carbon deposition while voltage could be maintained for 24 hours in wet propane (3 vol% steam) at OCV condition [169]. Besides, the stable operation period was increasing with the increase of $(Ce_{0.9}Gd_{0.1})O_{1.95}$ (GDC) molar ratio in the ionic phase of the anode, when microtubular SOFC was directly running on wet butane (10% *n*-C_4H_{10}, 4% H_2O and 86% N_2) [171]. Meanwhile, decreased peak intensities of the G band and D band indicated that the amount of carbon deposition could be gradually mitigated by the replacement of YSZ phase with GDC phase. One interesting phenomenon is that slight increase of voltage was observed for the Ni-25YSZ75GDC (the molecular ratio of YSZ to GDC is 25:75) anode, which could be ascribed to the high electronic conductivity of small amount of deposited carbon in the corresponding anode. Furthermore, Adding or alloying other metal, such as palladium (Pd) could be an effective way to improve the catalytic effect and carbon resistance capacity of the conventional Ni-based anode towards butane fuel [168,173]. It was found impregnating Pd into the Ni-YSZ anode support enhance the activity of butane steam reforming reaction, achieving a higher P_{max} of 946 mW cm^{-2} compared to unmodified Ni-YSZ (≈ 800 mW cm^{-2}) for butane fuel with S/C of 3 and no obvious performance difference was observed for hydrogen fuel at 600 ℃ [168]. It should be noted that excellent electrochemical performance at such low operating temperature was attributed to the fabricated thin YSZ/GDC bi-layer electrolyte with thicknesses of 1 μm and 200 nm, respectively. As indicated earlier, thickness reduction of the electrolyte is an essential method to lower the operating temperature of SOFC without compromising power output. In addition, incorporation of nanostructured barium oxide (BaO) into the conventional Ni cermet anode can also effectively maintain the stable power output without carbon deposition [174]. This is because the water adsorption capacity of nanostructured BaO/Ni interfaces facilitated water-mediated carbon removal reactions, which contributed to the stable operation for over 100 hours at 500 mA cm^{-2} and 750 ℃ when dry propane was used as the fuel. For comparison, voltage of the fuel cell with traditional Ni-YSZ dropped rapidly within one hour due to heavy carbon formation.

Besides, Ni-free materials with necessary anode requirements could also exhibit higher durability towards higher hydrocarbon fuels [126,175]. For example, Silver, which has been considered as an outstanding electronic conductor and electrocatalyst, was successfully

fabricated as the anode with GDC phase for the electrolyte-based SOFC [175]. The fuel cell with Ag-GDC anode exhibited 160 hours stable operation without any noticeable degradation in stability test when dry propane was fed (Fig. 22a). However, although the degradation rate of fuel cell with Ni-GDC anode under 103 mA cm^{-2} was much slower in comparison to OCV condition because of good structurally intrinsic carbon tolerance of the electrolyte-based construction in current output mode, cell with the conventional Ni-GDC gradually failed after about 60 hours due to the pulverization of anode which was observed form the SEM image of aged anode, showing much more serious coking risk of dry propane fuel towards Ni-GDC structure integrity. Besides, although the thin carbon layer (3-8 μm) and amount of carbon were found in the top surface and inside of Ag-GDC anode, respectively, after the exposure to dry propane, the type of carbon was mostly amorphous (Fig. 22b) due to the reduced mobility and/or solubility of carbon in Ag metal [57,175]. In addition, as said previously, different from the carbon catalytically formed on Ni metal, amorphous carbon has less deactivating effect towards the anode structure since this kind of carbon formed by gas-phase barely cause anode mechanical failure. Perovskite materials also provide alternatives for the anode of SOFCs operating on higher hydrocarbons [126,176,177]. The *in-situ* exsolution technology could serve as an important method for well decorated anode with uniformly distributed nanoparticles which provide active catalytic effect towards chemical/electrochemical reactions. FeRu alloy (FRA) was successfully prepared from $(Pr_{0.5}Sr_{0.5})_{0.9}Fe_{0.9}Ru_{0.1}O_{3-\delta}$ in reducing atmosphere and evenly coated on porous RP type layered perovskite $PrSrFe_{1-x}Ru_xO_{4-\delta}$ (RP-PSFR). It was found that fuel cell with the configuration of RP-PSFR-FRA-GDC/LSGM/LSCF-GDC showed constant voltage up to 50 hours in 40 ml min^{-1} wet propane/nitrogen fuel mixture (50% C_3H_8 and 50% N_2) at 0.15 A cm^{-2} and 750 ℃, indicating excellent carbon tolerance of the fabricated alternative anode [126]. Under the same fuel composition, single fuel cell delivered a P_{max} of 0.50 W cm^{-2} at 800 ℃ which was slightly higher compared to the methane fuel (P_{max} of 0.49 W cm^{-2} in the 50 ml min^{-1} wet methane fuel), demonstrating that C-H bond strength decreases with the increase of hydrocarbon chains [160]. Similar results could be found in the study of Xu et al. [176]. The symmetric SOFC with same fuel/air composite electrodes, $La_{0.4}Sr_{0.6}Co_{0.2}Fe_{0.7}Nb_{0.1}O_{3-\delta}$-$Gd_{0.1}Ce_{0.9}O_{2-\delta}$ (LSCFN-GDC) fabricated by one step co-synthesis method, presented a P_{max} of 324 mW cm^{-2} in humidified propane fuel which was nearly twice higher than that in wet methane fuel at 850 ℃, indicating simpler cleavage of C-H for higher hydrocarbon though flow rate details for each fuel were not provided. Meanwhile, developed symmetric SOFC showed comparable long-term performance stabilities with slight decay possibly due to the metal evolution in more than 100 hours operation tests for both wet propane

and hydrogen under 0.42 A cm^{-2} and 0.4 A cm^{-2}, respectively, at 850 ℃, showing reasonable carbon tolerance capacity [176].

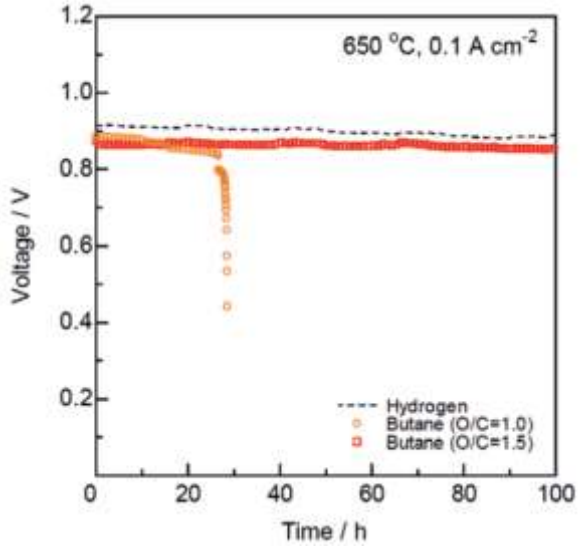

Fig. 21. Time courses of cell voltage at 0.1 A cm^{-2} with internal partial oxidation reforming of butane at 650 ℃. Figure reproduced from ref. [161] with permission from John Wiley and Sons.

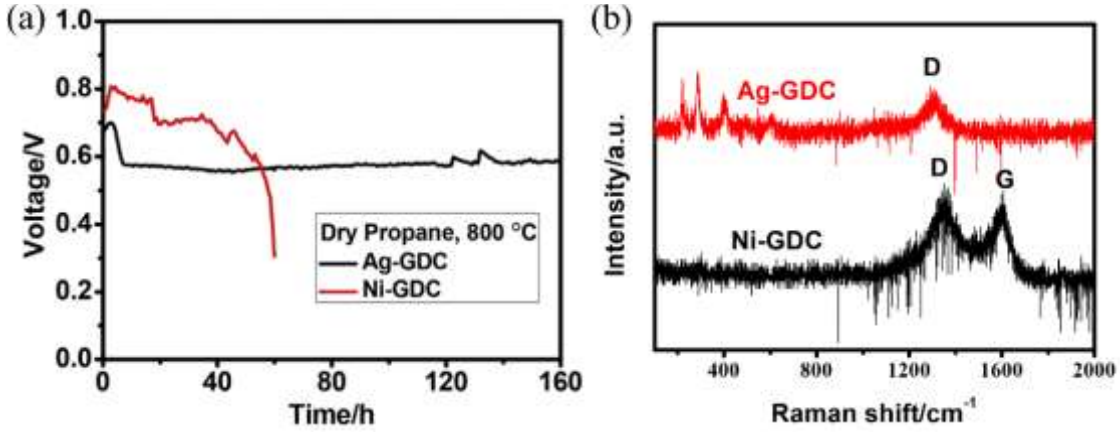

Fig. 22. (a) Durability of SOFCs with different anode (Ag-GDC or Ni-GDC) operated on propane (flow rate: 20 ml min^{-1}) at a constant current density of 103 mA cm^{-2}, at 800 ℃. (b) Raman spectra of the carbon collected in the anode chamber of Ni-GDC cell (black line) and the carbon layer deposited on the anode surface of Ag-GDC cell (red). Figure reproduced from ref. [175] with permission from Elsevier.

Strategies to suppress degradation issues of octane-fuelled SOFCs

Octane (C_8H_{18}), main component of gasoline, has also been investigated as the fuel for SOFCs in several studies [143,178–180]. Due to high boiling point (higher than 100 ℃) of octane, it is relatively easy for transportation and storage especially in the hot weather since

there is no need for the new refuelling infrastructure system which has always been the biggest obstacle for hydrogen.

In order to prevent carbon formation, a large amount of oxygen-containing gas (carbon dioxide or oxygen) was co-fed with octane fuel because of more coking risk due to the high carbon ratio in the molecule. Despite these, an catalyst layer based on Ru-CeO_2 was still needed to be attached onto the anode to improve carbon tolerance [143,178,179]. It was found that the Ni-based anode-supported SOFC operating on octane/carbon dioxide [143] or octane/air [179] mixture achieved 50 hours operation when the catalyst layer was placed. Without the catalyst layer, gradual degradation of the performance was observed not only for Ni-YSZ but Ni-GDC anode because of severe carbon build-up [178]. Besides, although the efficiency for partial oxidation of hydrocarbon was substantially lower than that of dry reforming, dry reforming may pose more severe degradation risk to the anode or catalyst layer. For example, slight carbon was deposited on the Ru-CeO_2 catalyst layer after 50 hours operation of SOFC with the catalyst layer at 0.6 A cm^{-2} and 770 °C when fuel mixture of 6% octane and 94% carbon dioxide was fed [143], while for the SOFC running on the mixture of 6% octane and 94% air, both anode and catalyst layer maintained clean and were free of carbon after stability test [179]. In addition to the attachment of reforming layer, another carbon mitigation method in terms of structure, individually material optimizations of anode support and functional layers, could also be used for the stable operation of the octane-fuelled SOFC. For example, SOFC with the configuration of Ni-YSZ-$BaZr_{1-x}Y_xO_{3-\delta}$ (800 μm) / Ni-YSZ (15 μm) / YSZ (15 μm) / LSCF (50 μm) achieved a stable power output more than 100 hours, and subsequent observation indicated that there was no microstructure change or any carbon deposition in the entire anode, while cell with conventional Ni-YSZ anode degraded within 1 hour when wet iso-octane (6.5% in Argon) fuel was fed at 0.56 A cm^{-2} and 770 °C (Fig. 23) [180]. Authors attributed the reasons of enhanced coking resistance of the Ni-YSZ-BZY anode to the characteristic of water uptake by discrete nano particles of BaO on Ni surface and a conformal BZY coating on YSZ surface, which is why 3 v% water vapor was necessary for stable power output. Therefore, the optimization of Ni-YSZ by BZY enabled fabricated SOFC to stably operate on less humidified octane fuel, avoiding co-feeding of excess carbon dioxide or air and thereby reducing the complexity of system as well as safety concerns such as flammability.

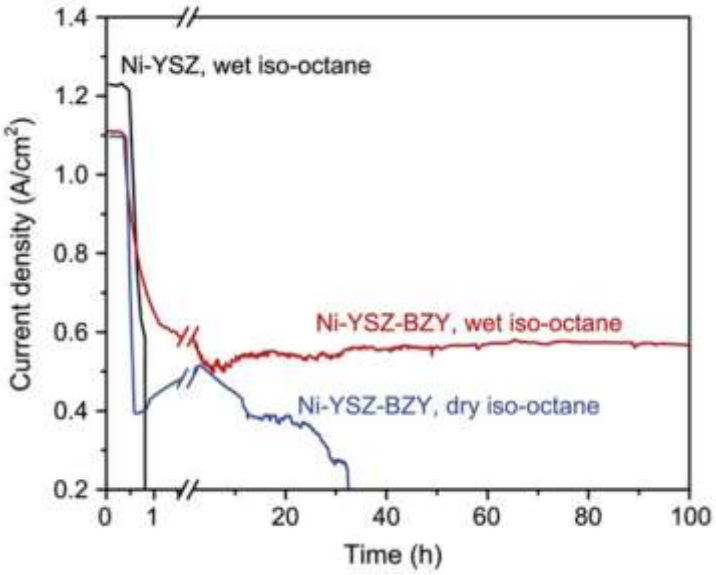

Fig. 23. Fuel cell performance in different fuels. Current density as a function of time for the Ni-YSZ and Ni-YSZ-BZY supported cells operated at 750 ℃ at a constant cell voltage of 0.7 V as the fuel was switched from humidified H_2 to dry or wet iso-Octane (6.5% in Ar) (wet gas contained 3 v% water vapor as humidified at 25 ℃). Figure reproduced from ref. [180] with permission from Elsevier.

Operation of SOFCs on ethane for power and chemical

Direct utilization of ethane fuel on the SOFC with the conventional Ni-based anode has been studied experimentally [181]. It was found that stable operation could be maintained at 823 K for more than one week when gas mixture of ethane and steam with a low S/C ratio was used as the fuel, which was mainly because electrochemical reaction products at high current density (operating voltage: 0.5 V) helped to eliminate carbon formation. Meanwhile, relatively low operating temperature was likely to play a role in the mitigation of deposited carbon since anode was deposited a large amount of carbon rapidly after the feeding of ethane fuel at 973-873 K [181]. However, different from methane fuel, temperature control may not be considered as a principal thermodynamic strategy for carbon mitigation since carbon formation from ethane fuel will be shifted to the relatively low temperature [5].

Cogeneration of ethene (C_2H_4) and electricity power can provide a particular way for the prevention of carbon formation when ethane fuel is used as the fuel for SOFCs, because the dehydrogenation process of ethane (Eq. (14)) avoids the cleave of C-C bond and thereby the formation of deposited carbon. In this respect, SOFC not only serve as the energy conversion device for electricity power but also the ceramic membrane reactor for ethene production. Actually, ethene is the most important chemical intermediate for the production of

petrochemicals and polymers and has been considered as the building block of chemical industry [182]. Presently, the industrial ethene production is mainly based on the energy-intensive steam cracking of hydrocarbon which requires significant energy input, and this highly endothermic process is also severely limited by thermodynamic equilibrium due to reversible nature. Alternatively, although the oxidative dehydrogenation of ethane to ethene tends to lower the energy requirement since it is an exothermic reaction, the presence of oxygen is likely to deeply oxidise ethane, causing large emission of carbon dioxide and thereby less ethene selectivity. Therefore, based on the mechanism of ethane dehydrogenation, the electrochemical device, SOFC, could give an efficient option for ethene production since hydrogen from selective dehydrogenation process in the anode will be electrochemical consumed, which will overcome the thermodynamic equilibrium limitation and thus promote ethane conversion according to the Le Chatelier's principle. Meanwhile, ethene production parameters such as the conversion or selectivity could be easily controlled or tuned by adjustment of current density or operating voltage. Although the oxygen ion conducting SOFC tends to have a great advantage in carbon mitigation aspect during the operation mode, direct contact between ethene or ethane and oxygen ion in the anode may lead to undesired deep oxidization of hydrocarbon feeding. Accordingly, electrochemical conversion of ethane using proton conducting SOFC is more suitable since there is no greenhouse gas emission due to the physical separation of oxygen and fuel or ethene by the proton membrane electrolyte. Besides, compared to the oxygen ion conducting electrolyte, proton conducting oxide could achieve higher ionic conductivity especially at intermediate or low temperature because of the relatively low activation energy, which benefits the reduction of SOFC operating temperature. Based on the mass conservation, the conversion of ethane ($X_{C_2H_6}$), selectivity of ethene ($S_{C_2H_4}$) as well as ethene yield ($Y_{C_2H_4}$) are described by Eqs. (16), (17) and (18), respectively [183,184], where *F* represents the flow rate or velocity of gas species.

$$C_2H_6 \leftrightarrow C_2H_4 + H_2 \quad (14)$$

$$H_2 \rightarrow 2H^+ + 2e^- \quad (15)$$

$$X_{C_2H_6} = \frac{F_{C_2H_6(in)} - F_{C_2H_6(out)}}{F_{C_2H_6(in)}} \quad (16)$$

$$S_{C_2H_4} = \frac{F_{C_2H_4}}{F_{C_2H_6(in)} - F_{C_2H_6(out)}} \quad (17)$$

$$Y_{C_2H_4} = X_{C_2H_6} \times S_{C_2H_4} \times 100\% \quad (18)$$

In order to achieve efficient and stable cogeneration of ethene and electricity in proton conducting SOFC, anode material need to be equipped with catalytic effects for

electrochemical and selective dehydrogenation reactions required for outstanding cell performance and high ethene yield, respectively. However, conventional Ni cermet seems not suitable for dehydrogenation reaction since nickel still suffer from coking problem due to its sensitivity of carbon formation [185,186]. It was found that platinum (Pt) metal could serve as the preferred catalyst fo light alkane dehydrogenation and show high selectivity at short reaction time [187]. Although SOFC with the Pt-based anode achieved reasonable power output as well as ethene yield from the electrochemical dehydrogenation of ethane [188], the prohibitively expensive cost of Pt material hinders its commercial scale application. Chromium oxide (Cr_2O_3) is also a good alkane dehydrogenation catalyst in the absence of oxygen [189] and a proton conducting oxide in the hydrogen atmosphere [190]. In this respect, copper (Cu), Cobalt (Co) and iron (Fe) were successfully fabricated as the anode material with Cr_2O_3 due to intrinsic insufficient electronic conductivity of oxide [191–194]. For example, proton conducting SOFC with the Cu-Cr_2O_3 composite anode achieved 10 days stable cogeneration operation under a constant power load of 125 mW cm^{-2} and ethene yield of 22% at 700 ℃, which indicated excellent resistance of the anode material towards carbon formation as well as Cu sintering. Meanwhile, the P_{max} and ethene yield were 170 mW cm^{-2} and 39%, respectively, when ethane was fed with the fuel flow rate of 150 mL min^{-1} at 750 ℃, and relatively low power density was because of thick electrolyte (800 μm) [192]. Recently, perovskite materials with excellent chemical catalytic effect and coking resistance have been utilized as the anode material for the cogeneration of ethane-fuelled SOFCs [185,186]. Due to the exsolution effect of metal from perovskite framework in the reductive atmosphere, uniformly distributed catalytically active metallic nanoparticles are likely to improve the ethane conversion and thus ethene yield. With evenly dispersed Co-Fe alloy (CFA) nanoparticles with the diameter of about 20 nm on double-layered perovskite $(Pr_{0.4}Sr_{0.6})_3(Fe_{0.85}Mo0.15)_2O_7$ (PSFM), the $BaCe_{0.7}Zr_{0.1}Y_{0.2}O_{3-\delta}$ (BCZY) electrolyte-supported SOFC achieved outstanding ethene yield of 41.5 % and P_{max} of 348.84 mW cm^{-2} at 750 ℃ when dry ethane as the fuel was fed at 100 mL min^{-1}. In addition, 100 hours cogeneration operation without performance degradation under 0.65 A cm^{-2} demonstrated the superior tolerance of fabricated anode (CFA-PSFM-BCZY) in terms of carbon deposition since the current density could not help to prohibit the formation of carbon in proton conducting SOFC configuration, while for the comparison, two notable carbon peaks in the Raman spectra were observed for reference anode (Ni-BCZY) after the stability test [185]. Furthermore, the symmetric protonic SOFC with enhanced carbon tolerance ability have also been tested for the cogeneration of ethene and electricity [184]. With $La_{0.6}Sr_{0.4}Fe_{0.8}Nb_{0.1}Cu_{0.1}O_{3-\delta}$ as the electrode, ethene yield in the S-SOFC reached 40.4% at

750 ℃, which exhibited exceptional chemical catalytic effect towards dehydrogenation rection of ethane. Besides, ethane conversion was improved to 43.4% at 200 mA cm^{-2} from 41.5% at OCV condition, indicating that fuel dehydrogenation process could be promoted by hydrogen consumption. However, relatively low electrochemical performances in hydrogen (P_{max}: 182 mW cm^{-2}) and ethane (P_{max}: 90 mW cm^{-2}) at 750 ℃ were mainly because of the low electrocatalytic effect of perovskite oxide [184]. Accordingly, the idea of material optimizations of the outer layer with high catalytic effect for ethane dehydrogenation reaction and functional layer only for electrochemical oxidation of hydrogen (Eq. (15)) has been proposed by Yang et al. [183]. However, to the best of author's knowledge, there is no relevant research study conducted based on this structure strategy to simultaneously enhance the electrochemical performance as well as value-added chemical yield.

Remaining challenges and future perspectives for higher hydrocarbon-fuelled SOFCs

Due to easier liquefaction characteristic and lower temperature required for reforming reaction, the utilization of higher gas alkanes, including ethane, propane, and butane, in the SOFC has received many attentions, especially for portable SOFCs. Besides, although carbon deposition is more threatening in comparison to methane fuel, stable operation can be achieved with traditional Ni-based or Ni-free anode through there perspectives similar to those used for methane-fuelled SOFCs. However, for octane fuel, in addition to the reforming layer, large amount of oxygen-containing gas needs to be co-fed into the fuel stream due to extreme high carbon ratio of liquid octane fuel in molecule structure, which could negatively affect the overall efficiency. Ba-based oxides (BZCYYb [169] ,BaO [174] and $BaZr_{1-x}Y_xO_{3-\delta}$ [180]) as the additive or ionic phase in the anode showed promising effects in the mitigation of deposited carbon because of their enhanced carbon removal properties due to high water-uptake capacity [160], which enables SOFCs with conventional Ni-based anodes to operate on dry propane or even nearly dry octane fuel. In addition, anode-supported proton-conducting SOFC with the configuration of Ni-$BaZr_{0.8}Y_{0.2}O_{3-\delta}$/$BaZr_{0.8}Y_{0.2}O_{3-\delta}$/$BaCo_{0.4}Fe_{0.4}Zr_{0.1}Y_{0.1}O_{3-\delta}$ achieved stable operations for thousands of hours with negligible performance degradation (less than 1.5% per 1000 hour) when various carbon-containing fuels with the O/C ratio of about 2.5/1 were used as the fuel, exhibiting outstanding performance and excellent durability of proposed anode [160]. Those research studies indicated that Ba-based oxides could be an effective material for SOFCs when hydrocarbon is used as the fuel.

Due to some specific reasons such as the low electronic conductivity of perovskite anode, most cells were using electrolyte as the cell support, which will cause less contact time between ethane and anode catalyst due to the thin anode and much low cell performance because of

high ohmic resistance induced by the thick electrolyte. Therefore, searching the possibility of anode-supported SOFC would be desired to achieve higher ethene yield or ethane conversion and the improved co-generated electricity power output.

3.2. Alcohol

The physical state of fuel at atmospheric condition is an important factor for the fuel suitability and applicability of SOFCs since liquid fuel could be conveniently stored, transported, and distributed. Therefore, the direct utilization of oxygenated liquid hydrocarbon, such as alcohols primarily including methanol and ethanol fuels, in SOFCs have received much attention of researchers. Unlike liquid higher hydrocarbons (e.g., octane), alcohols exhibit less coking risk due to less carbon atoms and the intrinsic relatively high oxygen/carbon ratio in their chemical structures. However, carbon formation is still an deteriorative cause for SOFCs directly running on alcohol fuels, especially for ethanol [24–26]. For example, the delamination of the Ni-YSZ anode caused by severe carbon deposits was observed for both OCV and current load (0.6 V) conditions after 12 h operation when pure methanol was used as the fuel at 800 ℃ [195]. Besides, electrolyte-supported SOFC with the thin Ni-YSZ anode completely failed after 10 h in the fuel mixture of ethanol and steam with the S/C ratio of 3.1 under 20 mA at 800 ℃ [196]. Despite these, promising characteristics of methanol and ethanol fuels, involving complete miscible nature with water, relatively higher volumetric energy density, liquid state at normal condition and less coking threatening [3,22], have enable researchers to develop more durable and powerful alcohol-fuelled SOFCs. More importantly, both methanol and ethanol could be generated from biomass sources [12,26,197,198], which indicates that integrating direct alcohol SOFCs with renewable bio-fuels productions could provide an efficient and carbon dioxide neutral power production technology to the SOFC community, benefiting both environment and economy. Table 4 summarizes the configurations and electrochemical performances of SOFCs operating on methanol and ethanol fuels.

3.2.1. The development of methanol-fuelled SOFCs

The methanol has been considered as convenient carrier for syngas because methanol is primarily generated based on the reforming of natural gas in the current industry [197]. Besides, thanks to the absence of C-C bond in the molecular structure since methanol is simplest alcohol, methanol can be conveniently decomposed back to the hydrogen rich gas mixture at typical operating temperature of SOFCs, because the frequently used anode metal phase of Ni metal could predominantly catalyse methanol decomposition process (Eq. (19)), followed by the kinetically slower water gas shift reaction (Eq. (7)) in the case of the presence of steam [199]. Besides, based on experimental observations, the mixture of carbon monoxide and hydrogen

with approximate ratio of 2 was the main product of Ni-based anode off-gas when pure methanol was used as the fuel [195], which was consistent with the thermodynamic analysis [200]. Therefore, because of the easy decomposition nature of methanol on the catalytic effect of nickel cermet, methanol-fuelled SOFC tends to show excellent electrochemical performance, which have been proved by various studies. For example, experimental test conducted by Sasaki et al [201] indicated that direct-methanol SOFC showed the comparable current-voltage characteristic to that of simulated complete reformed gas (the mixture of carbon monoxide and hydrogen with the molar ratio of 2:1) at the 1000 ℃ . In addition, maximum power densities of 0.6 and 1.3 W cm^{-2} at 650 ℃ and 800 ℃, respectively, were achieved when the Ni-YSZ anode-supported SOFC operated on pure methanol [202]. Besides, with more effective low-temperature electrolyte material of SDC, more excellent performance with a P_{max} of 698 mW cm^{-2} at 650 ℃ was obtained with pure methanol fuel [203]. Moreover, methanol-fuelled SOFC presented a P_{max} of 0.82 W cm^{-2} at 600 ℃ mainly because of the fabricated thinner electrolyte (6 μm) of SDC and more efficient cathode material of LSCF ($La_{0.6}Sr_{0.4}Co_{0.2}Fe_{0.8}O_3$) [204]. Based on the analyses of experimental studies mentioned-above, methanol could be thought as the promising alternative fuel to SOFCs.

$$CH_3OH \leftrightarrow CO + 2H_2 \quad (19)$$

Carbon formation mechanism of methanol-fuelled SOFCs

However, commonly used Ni-based anode likely suffers from severe graphitic carbon deposition when carbon-containing fuels, including methanol, are fed, which could rapidly deteriorate the cell performance and even irreversibly destroy the cell structure. One interesting phenomenon related to carbon formation comparison between methanol and methane fuels on Ni-YSZ anodes is worth noting that according to the investigation of coke formation rates on Ni-YSZ anodes after exposure to various carbon-containing fuels at 750 ℃ conducted by Qu et al. [205], feeding methane fuel was the most susceptible condition to cause carbon deposition compared to methanol fuel, while based on observations of thermal imaging and vibrational Raman spectroscopy measurements [206], carbon formation induced by methanol fuel was more significant than that of methane fuel when electrolyte-supported SOFC with the Ni-YSZ anode was operated at 715 ℃ under OCV condition. The possible underlying reason for these two contrasting comparisons might be the difference of carbon formation mechanisms for these two C1 fuels. Different from methane that carbon formation is largely due to methane cracking reaction, deposited carbon in methanol-fuelled SOFCs is primarily generated from the decomposed carbon monoxide via Boudouard reaction (Eq. (9)) [207]. As demonstrated previously, forward Boudouard reaction is favourable thermodynamically at lower temperature,

which indicates that carbon deposition would take place at relatively lower temperature (below 700 ℃ [92]). Besides, results of equilibrium calculations and experimental tests also showed that the amounts of deposited carbon would increase with the decrease of operating temperature [200,208], which poses more serious degradation threat to low or intermediate temperature methanol-fed SOFCs. Therefore, at relatively higher temperature of 750 ℃, the methane cracking reaction could be promoted, leading to the highest coke formation rate in comparison to methanol fuel, while for relatively lower operating temperature of 715 ℃, the deposited carbon from Boudouard reaction will be thermodynamically favoured and methane cracking reaction will be limited [85,92], leading to opposite carbon deposition phenomena for methane and methanol fuels at different operating temperatures. Therefore, various strategies from the perspectives of thermodynamics and kinetics were reported to tackle the coking issue which has been experimentally observed in various research works to improve the durability of methanol-fed SOFCs with Ni-based anodes [195,203,204,207,209,210].

Strategies to suppress carbon formation for methanol-fuelled SOFCs

Similar to other hydrocarbons, addition of steam to methanol stream could be the straightforward and effective way to suppress the phenomenon of carbon deposition in methanol-fed SOFCs because of the increased O/C. With the addition of sufficient steam in methanol fuel, the partial pressure of carbon monoxide could be decreased since added water will promote water gas shift reaction to move forward (Eq. (7)). Besides, H_2O gasification reaction (Eq. (10)) could also be proceeded to remove the possible generated carbon, thereby preventing the formation of carbon in the anode. It was reported that there was no carbon deposition on Ni-YSZ catalyst at 1000 ℃ when the mixture of methanol and steam with molar ratio of 1.0/3.0 was supplied [84]. Besides, at least 2 mole steam per mole methanol was needed to guarantee the stable operation of anode-supported SOFC with Ni-YSZ as the anode for more than 120 h under 0.221 A cm^{-2} at 750 ℃ [210]. The discrepancy between these two steam to carbon ratios can possibly be attributed to the fact that current density could also play a role in carbon mitigation because high concentrations of electrochemical products tend to consume carbon monoxide. In light of equilibrium calculations [200], the minimum fuel utilization for methanol fuel was about 2.1% at 800 ℃ to avoid coking issue, and higher current density or fuel utilization is required for lower temperature. For example, low fuel utilization of 0.4% estimated by the methanol flow rate and current led to the substantial performance decrease from 100 to about 50 mW cm^{-2} at 800 ℃ within 12 hours for the SOFC with Ni-YSZ anode, while for the cell with modified Ni-YSZ anode by ZDC ($Zr_{0.35}Ce_{0.65}O_{2-\delta}$), the improved performance of 240 mW cm^{-2} due to mixed conducting properties of ZDC could be maintained

for 12 h at same operating temperature because of enhanced fuel utilization (about 2.2%), though small amount of carbon was detected by EDX measurement [195]. In addition to the improved fuel utilization or performance, adding the coking resistance material doped-CeO_2 could also help to improve carbon tolerance, which was evidenced by less carbon deposition on the modified anode than that of the Ni-YSZ anode at OCV condition [195]. Similarly, with the high current density condition and SDC as ionic phase of the anode, long-term operations of consecutive 160 hours at three operating temperatures (550 ℃, 600 ℃ and 650 ℃) and 60 hours at 600 ℃ for the methanol-fuelled SOFC were achieved at 0.5 V and 0.8 A cm^{-2}, respectively [203,204]. Carbon deposition could also be mitigated by incorporating or alloying other metals to modify the coking tolerance ability as well as catalytic activity of the Ni-based cermet anode. Cu is chemically inert to carbon deposition and was also reported to be active catalyst to provide the desired fast kinetics for methanol decomposition process especially at low temperature [199]. In addition, Cu shows higher promotion effect for water gas shift reaction compared to Ni so high production of hydrogen and less carbon monoxide could be achieved through the combination of Ni and Cu [12]. Therefore, with the copper infiltrated Ni-GDC ($Gd_{0.1}Ce_{0.9}O_{1.95}$) anode, both electrochemical performance and durability of the methanol-fed SOFC were enhanced significantly at low temperature of 550 ℃ [207]. The P_{max} of cell in methanol fuel was increased to 0.42 W cm^{-2} for the infiltrated anode from 0.18 W cm^{-2} for pristine anode, which was mainly due to the improvement of methanol conversion and thus increased yields of direct fuels. Cell with the pristine anode experienced immediate degradation after 15 h because of severe filamentous graphitic carbon distinguished by SEM image, while stable performance was maintained for over 50 hours for the modified counterpart when methanol was fed at 550 ℃, which demonstrated higher carbon tolerance capacity of the proposed SOFC [207]. Further, less expensive noble metal of Pd nanoparticles were successfully deposited into the porous Ni scaffold of electrolyte-supported SOFC by sputtering through ALD (atomic layer deposition) technique [209]. The power output and stability against carbon were both considerately enhanced with the fabricated heterogeneous Ni-Pd bimetallic anode due to higher kinetics towards the chemical/electrochemical reactions and intrinsic high coking resistance of Pd metal. In addition, other coke tolerant materials such as basic oxides (Pr_4O_7 and Pr_6O_{11} [211], NbO_x [212], and La_2O_3 or Sm_2O_3 [213]) and metals (Mo [214], and Co [215]) were reported to added into the Ni-SDC ($Ce_{0.8}Sm_{0.2}O_{1.9}$) anode to reasonably improve carbon tolerance of composite SDC-carbonate electrolyte-supported SOFCs.

3.2.2. The development of ethanol-fuelled SOFCs

More research works related the utilization of ethanol fuel in SOFCs have been conducted

compared to methanol fuel because global bio-fuel production capacity is currently dominated by renewable bioethanol which is the ethanol produced from biomass sources such as forestry residues and agricultural wastes [216,217]. Besides, different from methanol, no toxicity and easy biodegradability of ethanol does not pose a risk for the environment. In addition, bioethanol generated from the fermentation of biomass contains high amount of water and no sulfur, which could be directly fed into the SOFC with the Ni-based anode to precede steam reforming reaction and thus provide direct fuels for electrooxidation reactions, which eliminating distillation requirements for pure ethanol [218]. Nickel has been considered as the best transition metal catalyst for ethanol steam reforming with considering the ethanol conversion and hydrogen selectivity since Ni not only shows high activity for cleaves of O-H bond and C-C bond and also exhibits high catalytic effect for the formation of molecular H_2 from H atoms [12]. Therefore, the promising prospect of ethanol-fuelled SOFCs has received much more attention of researchers.

Carbon formation mechanism of ethanol-fuelled SOFCs

In comparison to methanol, due to the presence of C-C bond in the molecular structure of ethanol, higher temperature and higher S/C ratio are required for the best hydrogen production via steam reforming of ethanol [160,218], which was also evidenced by several experimental observations that relatively lower electrochemical performance was achieved for ethanol fuel than that of methanol fuel [160,202,203,219]. The steam reforming processes of ethanol with sufficient water (Eq. (20)) or insufficient water (Eq. (21)) are desired for SOFC operation. However, main by-products such as methane the ethene produced through the ethanol decomposition reaction (Eq. (22)) or acetaldehyde decarbonylation reaction (Eq. (24)) and ethanol dehydration reaction (Eq. (25)) during ethanol steam reforming process could cause serious carbon deposition through decomposition reactions of methane and ethene (Eq. (8)), especially at relatively higher temperature [220], which was also well explained why higher temperature facilitated carbon formation under Ni catalyst [221]. Whereas, at lower temperature, due to the presence of carbon monoxide, Boudouard (Eq. (9)), and reversed H_2O gasification (Eq. (10)) reactions will be favourable for carbon deposition. Therefore, because of severe deactivation risk on the Ni-based anode of ethanol-fed SOFCs, hybrid strategies for carbon mitigation were frequently investigated for the cell long-term stability. For example, despite with high carbon resistant electrolyte material of GDC ($Ce_{0.9}Gd_{0.1}O_{1.95}$) as the anode ionic phase, large amount of steam (S/C = 2.0) was still needed to co-fed into ethanol stream to maintain the stable operation for more than 100 h at 650 ℃ and 0.1 A cm^{-2}, while for less steam-added cases, the performance of anode-supported microtubular SOFCs deteriorated after

8 h and 79 h at S/C = 1.0 and 1.5, respectively, due to broken Ni-GDC anodes mainly caused by graphitic carbon [161]. For most experimental studies in the literature, adding steam or high current density seems to be an indispensable method when the carbon suppression strategy from the perspective of the kinetics or structure was adopted.

$$C_2H_5OH + 3H_2O \leftrightarrow 2CO_2 + 6H_2 \quad (20)$$

$$C_2H_5OH + H_2O \leftrightarrow 2CO + 4H_2 \quad (21)$$

$$C_2H_5OH \leftrightarrow CO + CH_4 + H_2 \quad (22)$$

$$C_2H_5OH \leftrightarrow C_2H_4O + H_2 \quad (23)$$

$$C_2H_4O \leftrightarrow CH_4 + CO \quad (24)$$

$$C_2H_5OH \leftrightarrow C_2H_4 + 4H_2O \quad (25)$$

Strategies to suppress carbon formation for ethanol-fuelled SOFCs

In addition to few investigations related to the carbon suppression method of alloying other transition metals involving Fe [222] and Sn [223] with commonly used Ni, most studied strategies were mainly focusing on alternative Ni-free anodes or adoption of the catalyst layer to improve the durability of ethanol-fuelled SOFCs. Inspired by Cu-based anode used in direct hydrocarbon-fuelled SOFC, Cu-CeO_2-ScSZ anode was successfully fabricated as the support for the SOFC operating on ethanol-steam mixture (with the volume ratio of 2:1) [224]. The proposed SOFC achieved 50 hours stable operation under 0.5 V at 800 ℃ primarily due to the fact that Cu does not catalyse carbon formation in the way that Ni does [108]. However, although it was reported that Cu catalyst is active for the water gas shift reaction and ethanol dehydrogenation process [12], principal role for Cu in the composite anode is electronic conductor [108]. Besides, relatively lower catalytic effects of the catalytic phase, ceria, in the Cu-based anode for both electrochemical and chemical reactions led to lower electrochemical performance of the SOFC in both fuels of hydrogen and ethanol-steam mixture [224]. In order to improve the electrocatalytic activity of anode and thus the electrochemical performance of direct ethanol SOFC, thin Ni-ScSZ anode functional layer was added into the interface of electrolyte and Cu-based anode to enhance electrooxidation activities of hydrogen and carbon monoxide [225]. In addition, a new composite anode fabrication method was used to provide a porous YSZ scaffold with the proper porosity and microstructure which was fabricated by caid leaching of nickel from the traditional Ni-YSZ matrix, for the wet impregnation of Cu and CeO_2, which could benefit the processes of fuel diffusion as well as charge transfer. With promotions of the well-developed microstructure of Cu-CeO_2-YSZ and the Ni-based anode functional layer with high activity, the SOFC with ScSZ as the electrolyte exhibited P_{max}s of

604 and 438 mW cm^{-2} at 800 ℃ for hydrogen and ethanol rich fuels (the mixture of ethanol and steam with volume ratio of 2:1), respectively. Meanwhile, under the same ethanol fuel composition, the developed SOFC achieved 50 h stable operation at 0.7 V and 800 ℃ with negligible performance degradation, indicating high coking resistance of the Cu-based anode [225]. Furthermore, the perovskite alternative anode of LSCM ($La_{0.75}Sr_{0.25}Cr_{0.5}Mn_{0.5}O_{3-\delta}$) was attempted to use as the anode material for the ethanol-fed SOFC [226]. The electrolyte-supported SOFC with the LSCM anode achieved over 60 hours stable operation with negligible carbon detected on the anode, demonstrating reasonable carbon resistance towards ethanol-steam fuel. However, although the electrolyte material of LSGM ($La_{0.8}Sr_{0.2}Ga_{0.8}Mg_{0.2}O_3$) with relatively high ionic conductivity at low-temperature was used as the support because of intrinsic low electronic conductivity of the oxide anode compared to metal, thick electrolyte (600 μm) and low catalytic activity of the perovskite anode resulted in low power output for both hydrogen and ethanol-steam fuel even at 850 ℃ [226]. Therefore, researchers tried to solve these two drawbacks of low electronic conductivity and low catalytic activity for LSCM anode by impregnating Ru [227], Pd [228] and Cu [229], respectively. With palladium nanoparticles, cell with the impregnated LSCM-YSZ composite anode significantly decreased electrode polarization resistance and thus considerably improved the power density in ethanol fuel in comparison to the pristine anode, while little enhancement of the performance was observed under hydrogen fuel [228], which shows that the addition of Pd metal could promote the hydrogen production from ethanol fuel. In addition, Cu with high electronic conductivity was also impregnated into the LSCM-ScSZ anode matrix, followed by low temperature calcination [229]. Despite this, SOFC with the developed Cu-LSCM-ScSZ composite anode as the support presented low electrochemical performance for both ethanol-steam and hydrogen fuels primarily because of low conductivity of the anode.

Due to the low performance of both anode- and electrolyte-supported SOFCs with the LSCM-based anode, Ye et al. [229] also tried to use Cu-LSCM-YSZ as the catalyst layer for the Ni-YSZ anode-supported SOFC to improve carbon tolerance capacity and mitigate deficiency of low conductivity mentioned-above at the same time. With assistances of the additional catalyst layer and Ni-ScSZ functional layer, proposed cell exhibited the increased P_{max}s of 584 and 384 mW cm^{-2} at 800 ℃ for hydrogen as well as the mixture of ethanol and steam (volume ratio of 2:1) fuels, respectively. Meanwhile, no carbon deposition in the presence of nickel was detected in the anode after 120 h operation under 300 mW cm^{-2} at 800 ℃ when ethanol-rich fuel was fed, showing beneficial effects of the catalyst layer for ethanol conversion and thus carbon suppression [229]. Moreover, the composition of catalyst layer also

shows important significance in both electrochemical performance as well as stability of the ethanol-fuelled SOFC. It was found that with the increase of CeO_2 content in the LSCM-CeO_2 catalyst layer, electricity powers for both hydrogen and ethanol-rich fuels were enhanced probably because of the better conducting network as well as enhanced ethanol steam reforming activity [230]. Besides, under about 200 hours OCV condition in ethanol-rich fuel, polarization resistance was found to decrease initially because of the connection of isolated nickel by moderate carbon, and then to increase due to negative effects caused by excess deposited carbon. With the help of current density (0.6 V), there was no carbon formation in the Ni-ScSZ anode after the stable operation of 216 h in the fuel mixture of ethanol and steam at 700 ℃ [230]. Similar promotion effect by the higher CeO_2 content could also be found in results of experiment using Cu-CeO_2 as the reforming layer [149,231]. However, inappropriate composition of the catalyst layer could result in undesired situation. For example, delamination between anode and reforming layer could be easily observed from SEM images (Fig. 24b) of the aged anode with high amount of CeO_2 content after 80 h operation in ethanol-rich fuel due to the steep temperature gradient caused by endothermic chemical reforming reaction in the catalyst layer (Cu-CeO_2) and exothermic electrochemical reactions in the anode layer (Ni-YSZ) as well as TECs mismatch between these two layers because TECs of copper and ceria are both higher than those of nickel and YSZ, respectively, at typical operating temperature of SOFC [232–235], causing the gradual performance drop at 0.6 V and 800 ℃ [149]. In order to tackle this issue, an Ni-CeO_2 interlayer possessing a compatible TEC was added into the interface of Cu-CeO_2 and Ni-YSZ layers [231]. With additions of the catalyst layer and thermal compatible interlayer, although the cell electrochemical performance experienced a slight drop due to the increased ohmic and concentration overpotential caused by thicker anode and possible formation of solid solution, the cell fed by ethanol-steam fuel showed no performance decline for more than 200 h operation under a constant power density of about 250 mW cm^{-2} at 750 ℃ because of high carbon resistance capacity as well as the well-adhesion of these layers (Fig. 25). Besides the composition of catalyst layer, calcination temperature could influence the performance of cell due to the fact that the well adhesion at relatively high heat-treatment temperature between reforming and anode layers is significant for the charge transfer and structure integrity [149].

In addition to CeO_2 or LSCM as catalytic phase, various metals involving Ni [151,152,236,237], Pd [238], Rh [196] and Ir [239,240] were successfully fabricated as catalysts of the reforming layer to enhance coking tolerance capacity of ethanol-fuelled SOFCs. For example, with exsolved core-shell nanoparticles of metallic Ni-Co-Fe ternary alloy

encircled by Fe-oxide on Co-Fe depleted perovskite support from the Ni-modified $La_{0.6}Sr_{0.4}Fe_{0.8}Co_{0.2}O_3$-$Gd_{0.1}Ce_{0.9}O_{2-\delta}$ composite catalyst layer, SOFC with the Ni-YSZ supporting anode exhibited a 400 h stable operation in dry ethanol fuel under 0.8 V at 800 ℃ and no carbon was detected since carbon was hindered due to the modified surface basicity and the absence of Ni on the outer surface of nanoparticles [237]. In addition, Ir-based catalyst showed higher stability capacity of catalytic performance without any deactivation in ethanol steam reforming compared to Co and Ni due to highly distributed Ir particles via strong interaction with the CeO_2 support [241]. Recently, the Ir-GDC reforming layer was successfully deposited onto the surface of the supporting Ni-YSZ anode [240]. Under high catalytic activity of nanostructured Ir particles in this reforming layer, the cell fed by dry ethanol achieved total 700 h operation with little degradation at 0.6 V and 850 ℃ since hydrogen production was promoted by the generated water from electrochemical reaction through steam reforming process, eliminating the deposition of carbon.

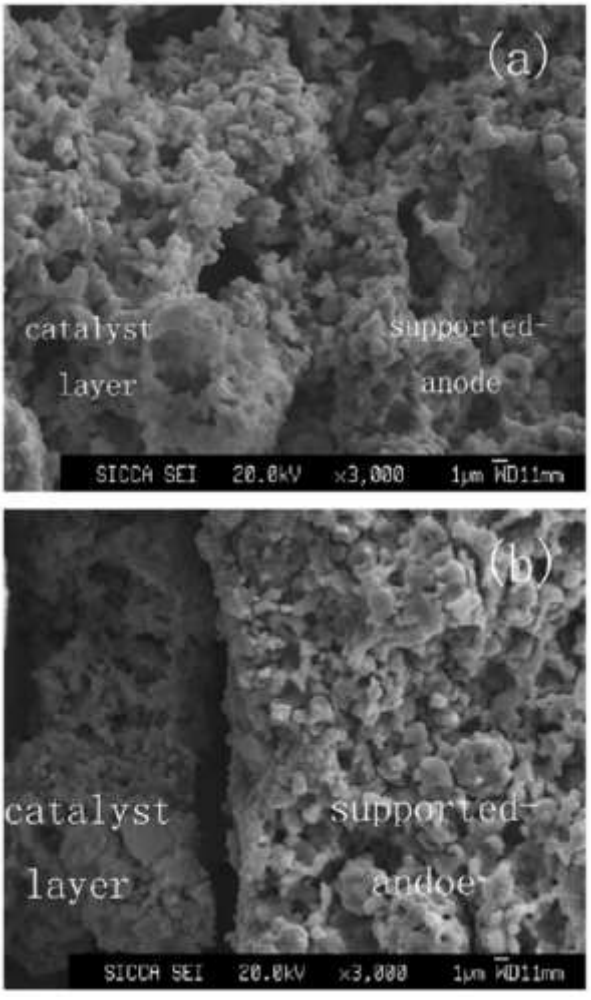

Fig. 24. SEM images of the interface between the catalyst layer and the supported anode of cell121100 (a) and cell131100 (b) after 80 h operation in ethanol steam. Figure

reproduced from ref. [149] with permission from Elsevier.

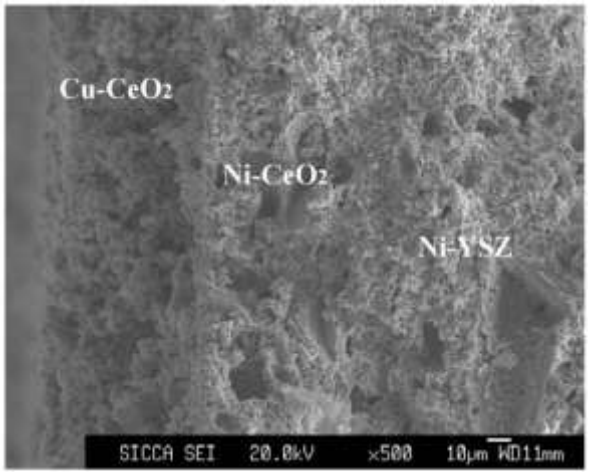

Fig. 25. The cross-sectional SEM image of cell 3 showing interfaces of three layers in the anode after operation in ethanol for 250 h. Figure reproduced from ref. [231] with permission from Elsevier.

3.2.3. Remaining challenges and future perspectives for alcohol-fuelled SOFCs

Alcohols have attracted lots of attentions in the fuel cell community because of liquid state at normal condition. Relatively easy reforming or decomposition of alcohol fuels under the effect of nickel metal enables these promising fuels to be directly fed into SOFCs. However, potential deactivation of the Ni-based anode caused by carbon deposition is an intrinsic issue for SOFCs running on carbon-containing fuels. In this respect, numerous achievements related to the improvement of durability for alcohol-fuelled SOFCs were reported.

Methanol-fed SOFC suffers from less coking risk compared to ethanol fuel because of the absence of C-C bond, so long-term stable operation for cells with the Ni-based anode could be conveniently achieved even through thermodynamical methods involving the high current density and the addition of steam. However, as indicated previously, high current density could not serve as the dominating strategy for carbon suppression since SOFC system needs to be practically working under various operating conditions including zero or low load situation which are the most favourable conditions for carbon formation [195]. Temperature control could also be another thermodynamical strategy to suppress carbon formation because based on the mechanism of carbon formation in methanol-fed SOFCs, carbon could be partially hindered at high temperature (more than 700 ℃). Therefore, it is essential for direct methanol SOFC to conduct further investigations especially at relatively high temperature. However, for the partible SOFC, low operating temperature is desired. Copper metal shows higher kinetics for methanol reforming reaction, or methanol decomposition followed by water gas shift

reaction, especially at low temperature. Besides, with Ce-based oxide as the support, the catalytic effect of Cu-based catalysts could be further promoted due to higher dispersion of Cu particles and the strong interaction between metal and oxide support [199]. Therefore, Cu-doped ceria composite cermet could be a promising anode for the direct methanol SOFC with considering high carbon resistance as well as chemical kinetics for hydrogen production. Besides, similar to the configuration used in the ethanol-fuelled SOFC [225], Ni-based anode functional layer could also be considered to be added into the interface of electrolyte and Cu-based anode support layer to further enhance electrochemical kinetics. Several challenges such as sintering problem of copper and the TECs mismatch of different components need to be paid attention to.

Most research studies of ethanol-fuelled SOFCs were focusing on alternative Ni-free anodes or utilization of the additional catalyst layer since Ni-based anode of the cell fed by ethanol is more susceptible to coking. Although Cu-based and LSCM-based materials could be utilized in both anodes and catalyst layers since they are chemically inert to the formation of graphitic carbon, the amount of steam was essentially necessary to be co-fed to enhance the cell durability despite the fact that cell was operated at the current mode. For example, the gradual performance drop of the SOFC with Cu-Co(Ru)-$Zr_{0.35}Ce_{0.65}O_2$-YSZ composite anode was observed due to the deposition of amorphous carbon after the initial rapid increase of power density when the pure ethanol was fed at 0.6 V and 800 ℃, though the degraded performance could be recovered by refuelling hydrogen fuel and Cu-based anodes were not irreversibly deactivated by coking [219]. Besides, the low catalytic activities of electrochemical/chemical reactions for both Cu-based and LSCM-based anode as well as the low electronic conductivity or thick electrolyte for anode or electrolyte supporting structure respectively while using the LSCM as the anode still limit the electrochemical performance of ethanol-fed SOFCs.

Active metals have also been used as catalyst in the reforming layer for SOFCs operating on ethanol fuel to enhance the stability. Due to their high catalytic effect for ethanol reforming or decomposition process, electrochemical performances were not significantly compromised or even slightly enhanced at specific condition. For example, when the cell with the catalyst layer of Ni-$Ce_{0.8}Zr_{0.2}O_2$ synthesized by a better fabrication procedure of glycine nitrate process on the Ni-YSZ anode yielded a P_{max} of 536 mW cm^{-2} at 700 ℃ in ethanol-steam gas mixture (molar ratio of 2.3:1), which was slightly lower than that of the cell without this reforming layer (P_{max} of 626 mW cm^{-2} at 700 ℃), while when the temperature was decreased to 600 ℃, the cell with this catalyst layer showed higher catalytic activity for ethanol steam reforming, delivering a P_{max} of 126 mW cm^{-2} which was considerably higher compared to the cell without

reforming layer (20 mW cm^{-2}) [236]. In addition, it seems that amounts of additional steam required for stable operations of direct ethanol cells with the active metals-based catalyst layer were less compared to those with Cu-based and LSCM-based catalyst layers. For example, dry ethanol fuel was used for stability tests of SOFCs in few studies [237,239,240]. Well-developed microstructure and strong interaction between metal and support could play an important role in carbon resistance. However, although nanosized active metal catalysts in the catalyst layer show promising prospects in direct ethanol SOFCs without adding any amount of steam, current sweep states were adopted to maintain the continuous generation of electrochemical products [237,240], and stability of these SOFCs fey by dry ethanol fuel on the OCV condition remains unknow. Therefore, more research works from carbon suppression strategy of additional reforming layer should be conducted to investigate the stability test on the OCV situation in the future.

Proton conducting oxides involving $BaZr_{0.4}Ce_{0.4}Y_{0.2}O_3$ (BZCY) [242] and $BaZr_{0.1}Ce_{0.7}Y_{0.1}Yb_{0.1}O_{3-\delta}$ (BZCYYb) [243] with the mixed conductivities shows excellent resistance for carbon formation due to outstanding water storage capacity as well as high catalytic activity. For example, the anode-supported SOFC with the configuration of Ni-BZCY/SDC/SSC ($Sm_{0.5}Sr_{0.5}CoO_{3-\delta}$) achieved 180 h stable operation at 0.3 A cm^{-2} and 600 ℃ in the fuel mixture with equal molar amounts of steam and ethanol, while for the cells with anodes of Ni-YSZ and Ni-SDC failed completely within 1 h and 2 h, respectively [242]. Besides, it was reported that the enhancement of both oxide ion and proton conductivities in the doped barium zirconate-cerate oxide is expected to further benefit the water-uptake capacity and thus coking tolerance [169]. In this respect, BZCYYb with higher ionic conductivity was fabricated as the ionic phase of supporting anode [243]. With SDC and BSCF as the electrolyte and cathode, respectively, the excellent P_{max} of 953 mW cm^{-2} at 750 ℃ was obtained in pure ethanol fuel, and less carbon was on the outer surface of Ni-BZCYYb after the 100 h operation in pure ethanol fuel under a constant current density of 0.3 A cm^{-2} and 600 ℃ with more stable cathode material of SSC, showing enhanced reforming catalytic activity and superior coking suppression capacity of the fabricated anode [243]. The Ba-based mixed ion conductor could be an effective ionic phase material due to its specific characteristics especially at relatively low temperature when alcohols are used as the fuel. Besides, under practical consideration, easy and mature fabrication procedure of Ni-based anode would still be the best choice since other carbon suppression strategies such as incorporation of oxides or metals as well as the addition of catalyst or functional layer, could not be commercially practical due to several challenges like chemical or thermal instability of different components, complicated

manufacturing procedures and thus increased cost. Therefore, composite anodes of nickel and Ba-based ionic phase show promising prospects in the direct utilization of ethanol fuel.

3.3. Solid carbon fuel

Solid carbon fuels with relatively higher volumetric density, involving the commercial activated carbon, coal and biomass-based carbon could be used as the fuel for SOFCs to electrochemically produce electricity power. Compared to cells using liquid or gaseous fuels, carbon-fuelled SOFCs naturally possess various advantages, such as superior overall electric efficiency and thus low emission of carbon dioxide per unit electricity, and no further vessel, tank or other equipment for the storage and pump of gases [66,93,244]. However, several challenges including sluggish kinetics of direct carbon electrooxidation, limited physical contact of the carbon particle and TPB sites, and refilling issue of solid carbon, faced by carbon fuel still inhibit the application of carbon-fuelled SOFCs.

In order to solve problems mentioned-above, especially for the poor electrochemical contact barrier, fuel cells using molten metal anode or fuel mixture of solid carbon and molten carbonate could improve mass transportation between anode and solid carbon and thereby enhance electrochemical performances. Despite the effective boost of the power density by introductions of molten carbonate and molten metal to carbon-fed SOFCs [245,246], potential leakage and corrosion issues due to aggressive molten nature could pose a severe risk to cell components and jeopardize the cell life time [27,93]. Fortunately, carbon monoxide which could be one direct fuel for SOFCs (Eq. (2)) is the favourable product in the presence of excess carbon at typical operating temperature of high temperature SOFC since reverse Boudouard reaction (Eq. (9)) will be thermodynamically favoured at more than 750 ℃ [244,247]. Therefore, the operation mechanism, involving the electrochemical oxidation of carbon monoxide at active TPB sites and reverse Boudouard reaction at the solid carbonaceous fuel, of carbon-fuelled SOFCs was firstly proposed by Nakagawa and Ishida [248] at earlier time, which was subsequently verified by the experimental observation of almost identical performances obtained from SOFCs operated on solid carbon and pure carbon monoxide at 850 ℃ [249]. Therefore, the effective coupling of these two reactions enable all-solid-state carbon-fuelled SOFC to be fabricated without any purging gas or liquid medium, simplifying the system deployment, and thereby reducing the cost. It is worth noting that the reduction of NiO could also be possible under the anodic atmosphere of carbon-fuelled SOFC when Ni-based anode is used [250]. Although the theoretical thermodynamic efficiency for carbon monoxide (61%) is much lower compared to solid carbon (101%) at 980 ℃ [244], the carbon monoxide without contributing to Faradaic process could be an essential chemical feed stock

for industry, which will make it possible for the cogeneration of carbon monoxide and electricity when carbon-fuelled SOFCs operate on appropriate operation condition. For example, taking the chemical energy of carbon monoxide as the part of performance output, overall efficiencies of more than 70% were experimentally achieved for both fuels of 5wt% Fe-loaded activated carbon and biochar derived from camellia oleifera shells [251,252]. Besides, the results of simulation conducted by Xu et al. [253] indicated that smaller distance between the anode and carbon fuel as well as higher operation potential were both desired to achieve relatively higher production of carbon monoxide if the generation of carbon monoxide was the main target.

The counter diffusion of carbon monoxide and carbon dioxide between carbon fuel and anode is essential important for the performance of carbon-fed SOFCs since the gasification of solid carbon tackles the difficult mass transport issue of carbon particles. Besides, although no direct physical contact between carbon fuel and anode could cause concentration overpotential, which might negatively affect the electrochemical performance [253,254], it will be beneficial to the integrity of anode structure since the cell structure is susceptible to the movement of solid carbon fuel due to the fragile nature of cell while refilling fuel. Consequently, based on the working mechanism, strategies to improve the performance of carbon-fuelled SOFCs are primarily focusing on the development of more durable anodes with high electrocatalytic activity for carbon monoxide as well as the design of effective catalyst material with the promotion effect on the rate-determining step of Boudouard reaction. Several excellent review papers available in the literature have discussed the developments of anode materials and novel catalysts loaded on the solid carbon in carbon-fuelled SOFCs [27,28,66,93]. In this respect, we just briefly introduce the latest anode progress and new loaded catalysts, and then the focus is given to the effects of chemical and physical properties of different types of solid carbon, involving the activated carbon, coal and char derived from biomass, on the performance and output power durability of carbon-fuelled SOFCs.

3.3.1. The development of solid carbon-fuelled SOFCs

In addition to basic requirements of anode material, higher coking and sulfur poisoning resistances are also significant for anode materials of SOFCs operating on solid carbon fuels. Accordingly, Ag-based cermet is the most frequently used electrode material for carbon-fuelled SOFCs since Ag metal not only serves as the excellent electrocatalyst for carbon monoxide [255] but also shows good electrocatalytic activity for oxygen reduction reaction [256]. Besides, in comparison to Ni metal, carbon deposition could not be a serious issue to Ag-based anode due to the reduced solubility of carbon in Ag metal [57,175]. However, limited by the expensive

cost, cell configuration of the electrolyte-supported structure is the most commonly used for carbon-fuelled SOFCs with the Ag-based anode, which leads to relatively lower electrochemical performance (less than 400 mW cm^{-2} [28]) due to the high ionic resistance of thick electrolyte. Based on the investigation theoretically conducted by Xu et al. [253], it was found that the anode-supported carbon-fuelled SOFC with Ag-$Ce_{0.8}Gd_{0.2}O_{1.9}$ as both electrodes showed better performance compared to the electrolyte-supported counterpart since decreased ohmic loss by the reduction of electrolyte thickness was much higher than the increased carbon monoxide concentration overpotential led by anode-supported cell structure. Therefore, anode-supported structure is still desired for the carbon-fuelled SOFC, which was also evidenced by several experimental observations. For example, anode-supported SOFC button cell with the configuration of Ni-YSZ (680 μm) /Ni-ScSZ (15 μm) / ScSZ (20 μm) / LSM-ScSZ (20 μm) delivered an excellent P_{max} of 1477 mW cm^{-2} when K-loaded carbon black was used as the fuel at 750 ℃ [257]. However, although serious performance degradation and even failure of the cell structure were not observed during experimental stability tests due to the limited operation duration restricted by the amount of carbon fuel and the assistances of high current density as well as the necessary high operating temperature which serve as important thermodynamical carbon suppression strategies for carbon-fuelled SOFCs, the post-mortem analyses indicated that coking and sulfur poisoning issues are still the severe threats to Ni-based anodes in carbon-fuelled SOFCs [258,259]. Therefore, considerable efforts are still needed to be devoted into the developments of novel composite Ag-based with more commercially practical consideration and the Ni-based anode with higher tolerances towards degradation issues.

Alternative anode materials especially perovskite-based anodes, also show a promising prospect in carbon-fuelled SOFCs since some MIEC oxide materials naturally exhibit outstanding sulfur poisoning and coking resistances. Recently, remarkable P_{max}s of 302.8 and 218.5 mW cm^{-2} were achieved at 850 ℃ when electrolyte-supported cells with novel perovskite $La_{0.8}Sr_{0.2}Fe_{0.9}Nb_{0.1}O_{3-\delta}$ (LSFNb) anode operated on activated carbon and char derived from corn straw, respectively [260]. In addition, modified perovskite material with some transition metals could further enhance the conductivity as well as electrocatalytic activity. For example, anode material of $La_{0.3}Sr_{0.7}Fe_{0.1}Ti_{0.9}O_3$ (LSFT) was obtained by small substitution of Ti with Fe, which exhibited improved ionic conductivity and lower polarization resistance compared to the pristine material of $La_{0.3}Sr_{0.7}TiO_3$ (LST) at the CO-CO_2 gases atmosphere [261]. Besides, under the Ca-catalysed activated carbon fuel, SOFC with the LSFT anode presented a P_{max} of 292 mW cm^{-2} at 850 ℃, which was higher than the cell with the LST anode (207 mW cm^{-2}). In addition, a much more stable discharging operation was observed with the modified anode,

followed by the rapid cease of output due to the exhaustion of carbon fuel (Fig. 26a). Furthermore, the stable voltage with negligible decline demonstrated remarkable coking and sulfur tolerances when the long-term stability of the proposed anode was assessed by carbon monoxide gas fuel with 1000 ppm H_2S because of the limited amount of solid carbon fuel (Fig. 26b), showing promising perspective of this anode candidate for SOFC running on carbon fuel, especially coal-based carbon fuels. In addition, *in-situ* exsolution technique have been reported to further optimize the electrocatalytic activity of anode material due to decorated nanoscale metal particles on the perovskite scaffold for carbon-fed SOFCs [262,263]. With uniformly distributed Ni nanoparticles on the porous perovskite skeleton surface, carbon monoxide electrochemical oxidation activity was enhanced since dispersed Ni metals with the average diameter of 30 nm could provide more active sites for the electrochemical reaction, leading to the enhanced performance (153 mW cm^{-2} at 850 ℃) of the electrolyte-supported SOFC fuelled by Fe-loaded activated carbon compared to the cell with the unmodified anode material of $La_{0.7}Sr_{0.3}Cr_{0.5}Mn_{0.5}O_{3-\delta}$ (114 mW cm^{-2}) [262]. Actually, metal dopant content could be further optimized to enhance the performance. For example, the optimal composition of Cu-doped $YST_{1-x}Cu_x$ is $Y_{0.08}Sr_{0.92}Ti_{0.9}Cu_{0.1}$ since the highest P_{max} of 366 mW cm^{-2} at 800 ℃ was achieved by the cell with this alternative anode material when mixture of activated carbon and carbonate was used as the fuel [263].

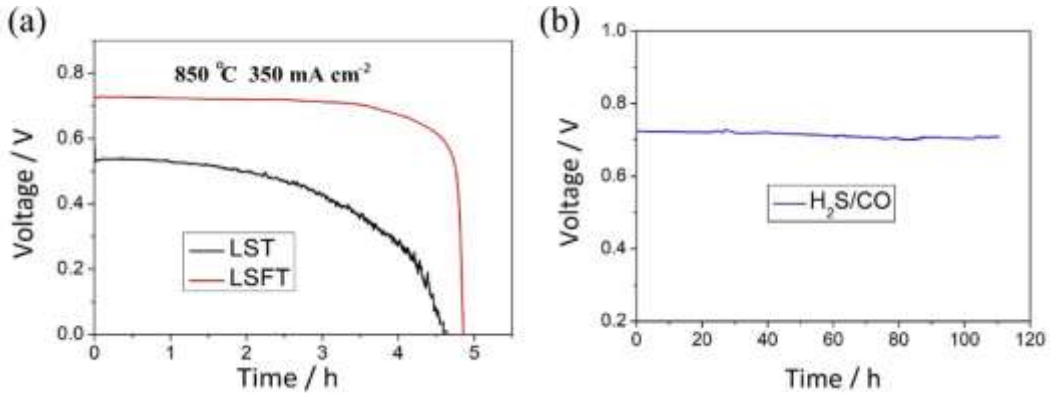

Fig. 26. The discharging curves (a) of LST and LSFT anode DC-SOFCs powered by 0.4 g of Ca-loaded activated carbon, and the long-term stability (b) of LSFT anode cell operated on CO with high contents of H_2S (1000 ppm) at 850 ℃. Figure reproduced from ref. [261] with permission from Elsevier.

Reverse Boudouard reaction is significant for the overall performance of the carbon-fuelled SOFC since it provides carbon monoxide for electrochemical process. In addition to the increase of operating temperature as well as the optimization of carbon fuel microstructure, catalytically boosting reverse Boudouard reaction by suitable catalysts has been proven to be a

simple and effective approach to enhance electric output. Various catalysts involving alkali, alkaline earth and transitions metals have been loaded on solid carbon fuels through impregnation or wet agglomeration technique to assess their catalytic activity. The transition metal of Fe is one of efficient catalysts with high promotion effect for carbon gasification [255], and Fe-loaded activated carbon is frequently used as the benchmark fuel for comparison to evaluate the effectiveness of other catalysts. Recently, several alkaline earth metals including Ba, Ca, and Sr have been tested for the suitability of catalysts for reverse Boudouard reaction. It was found that 5 wt% loading content was the most effective ratio for these proposed catalysts with considering the power density and discharging time of carbon-fuelled SOFCs [264–266]. In addition, these catalysts performed better in these indicators compared to 5 wt% Fe loaded on the same carbon fuels. As for the degradation or low fuel utilization of carbon-fuelled SOFCs, the potential reasons are summarised as the carbon consumption as well as agglomeration of catalysts at high working temperature [264,265]. Different from Ba and Ca-loaded carbon fuels, there was no observation of Sr agglomeration based on SEM/EDX results of the aged active charcoal after long-term stability test, which could be the reason for high fuel utilization of 18.3% [266] that is higher compared to Ba and Ca-loaded carbon fuels [264,265]. Steel slag, as the by-product of steelmaking process, could also be adopted as the catalyst material for reverse Boudouard reaction since steel slag is full of CaO and Fe_mO_n which have been proved to be good catalyst to accelerate this chemical reaction [267].

Considerable efforts have been devoted into developments of anode and carbon gasification catalyst materials, leading to improved power density and stability of carbon-fuelled SOFCs. Carbons used in studies mentioned-above are mainly focusing on the commercial activated carbon with relatively high price, so other carbon-rich resources featured by low price or environmental-friendly nature such as coal or biomass from agriculture, forestry and even marine have also been tested as alternative fuels for power generation via SOFC technology. Table 5 outlines the latest developments of SOFCs fuelled by various solid carbon fuels, but electrochemical characteristics involving power density, operation duration and fuel utilization show differently for different carbon fuels. Therefore, considering the complexity of structure as well as composition of alternative solid carbons, understanding the effects of physical and chemical characteristics of these carbon resources, in terms of crystal structure, impurities, carbon content as well as microstructure, is essentially important for the electrochemical performance as well as lifetime of fuel cells. The latest research works related to the influences of various properties on the performance are discussed from two fuel resources of coal and biomass-based carbons since in addition to activated carbon, carbon fuels from these two

sources are frequently examined.

Coal

Because of the abundant reserve and thus low cost, the second greatest main energy source of coal plays a primary role in global energy consumption. With the gradual depletion of high-quality coal stock, the efficient utilization of low-rank coal containing a variety of organic and inorganic impurities show important prospects from economic and environmental perspectives.

Purification process is necessary procedure when high-sulfur coal (HSC) is used as the fuel for SOFC since for Ni-based anode, sulfur contaminant is also a serious degradation issue among volatile impurities of the coal. In addition, carbon content will be correspondingly improved due to the fact that purification process could remove not only sulfur but also other minerals and volatile matters, which benefiting the performance and fuel utilization. After the effective purification method of molten caustic leaching, sulfur and ash contents decreased by the 80% and 60%, respectively [258]. Meanwhile, enhanced specific surface areas and pore volume as well as reduced average pore size were observed for purified-HSC, leading to the superior oxidation reactivity compared to HSC based on the thermogravimetric analysis. Therefore, enhancements of both electrochemical and stability time were achieved for the Ni-YSZ anode-supported cell operated on purified-HSC, though less carbon deposition and sulfur poisoning still occurred in the used anode [258]. Pyrolysis process is another method to remove volatiles from raw coal carbon. During this process, majority of organic volatile matters can be released while most ash content consisted of inorganic impurity still remains in coal char. Ash composed of various impurities shows different effects on the cell performance. On one hand, several minerals involving Ca, Fe, Mg, and K, have been proved to have a promotion effect on the kinetics of reverse Boudouard reaction [66]. On the other hand, some such as Al or Si compound tends to negatively affect the carbon monoxide production by physically blocking pore or active sites [268]. After pyrolysis process, char derived from brown coal with better microstructures in terms of specific surface area and pore volume and richer favourable impurities exhibited the highest oxidation reactivity compared to raw brown coal and Fe-loaded activated carbon, respectively [269]. Therefore, in subsequent electrochemical tests, electrolyte-supported cell with brown coal char fuel delivered the highest P_{max} of 221 mW cm^{-2} at 850 ℃ since naturally presence of abundant Ca species could effectively accelerate reverse Boudouard reaction, though Fe-loaded activated carbon possesses the excellent microstructure. Raw brown coal gave a lowest performance of 211.4 mW cm^{-2} due to bulk fuel particles and low reactivity towards oxidation [269]. Meanwhile, the discharge time of 13.73 h and fuel utilization of 61.5% were achieved for brown coal char fuel, which demonstrated that pyrolysis

process could be an effective method to prepare coal fuel for SOFCs despite energy-consuming nature.

Biomass

Biomass, a carbon-balanced energy resource, has attracted much attention due to its renewable feature, abundance and low emission. Currently, many of them could not be used efficiently, leading to tremendous waste since it was reported that only for terrestrial plants, energy stored each year is 3-4 times higher than energy demand globally [270]. Therefore, with the efficiency of SOFCs, power generation from biomass-based energy via electrochemical conversion process could be considered as a promising option.

Biochar fuels obtained from agricultural by-products have been frequently adopted as solid carbon fuel for SOFCs. Reasonable electrochemical performances have been attained because natural porous structure as well as presence of evenly dispersed and biologically accumulated elements like Ca, Fe, and K, could benefit carbon monoxide generation. For example, EDS analysis showed that carbon content in pepper straw char was 61.59 wt%, indicating this biochar high carbon could be proper carbon fuel, and Ca, K and Mg contents were 11.73, 5.47 and 3.66 wt%, respectively [271], which have been considered as the favourable elements for carbon monoxide generation. Accordingly, electrolyte-supported microtubular SOFC with Ag-GDC as anode performed the P_{max} of 217 mW cm^{-2} at 850 ℃ with pepper straw char which was slightly lower compared to hydrogen fuel (252 mW cm^{-2}). Besides, operation discharging time and fuel utilization of 21 h and 44.4% were achieved, respectively [271]. All these indicators showed that biochar derived from pepper straw could be used as fuel for efficient power generation. However, it should be noting that different kinds of crop tend to possess totally different compositions with variable wight contents as well as microstructure, which could greatly influence cell performance as well as discharging duration when biochar fuels derived from different plants are used as solid carbon fuels. For example, study conducted by Qiu et al. [272] tested different biochar fuels derived from wheat straw, corncob and bagasse in the electrolyte-supported-SOFC with Ag-GDC as electrodes. It was found cell on bagasse char fuel presented the highest P_{max} of 260 mW cm^{-2} at 800 ℃ (204 mW cm^{-2} for corncob and 187 mW cm^{-2} for wheat straw char), which was because the lowest tap density of 0.73 g cm^{-3}, the most disordered (amorphous) form of carbon (intensity ratio of D bond to G bond: 0.98), relatively higher contents of excellent catalyst elements such as K and Ca and less undesired elements like S and Si of bagasse char led to highest carbon monoxide concentration of 71.87% emitted from the cell compared to other char fuels. In addition, discharging capacities of SOFC operated on these three biochar fuels were followed the order of corncob, bagasse and wheat

straw (from the highest to the lowest), which was consistent with the order of ash contents (from the lowest to the highest) remained after thermogravimetric analysis measurement. However, with considering the productivity of biochar via thermal pyrolysis, fuel utilization of bagasse was the best, showing that bagasse could be an excellent alternative carbon fuel for SOFCs [272]. Similarly, it was reported that although the wheat straw char contained several beneficial elements of K, Fe, Ca and Mg indicated by EDS results, less atom contents (less than 2%) of these natural catalysts caused relatively lower P_{max} of 197 mW cm^{-2} and fuel utilization of 15.7 % at 800 ℃ when pure wheat straw char was used as the fuel for electrolyte-supported cell with Ag-GDC as the anode [273]. After loading 5 wt% Ca to this biochar, peak power density as well as fuel utilization were improved to 258 mW cm^{-2} and 33.3%, respectively, due to higher carbon gasification reactivity of loaded char [273]. Similar phenomenon could also be found in the study conducted by Xie et al. [274]. With the infiltration of Fe_2O_3 into walnut shell char, maximum power density was enhanced from 147 to 205 mW cm^{-2} at 800 ℃ for tubular electrolyte-supported SOFC with Ag-GDC as electrodes since carbon monoxide was remarkably improved which could also be evidenced from the typical *I-V-P* curve (Fig. 27) that serious mass-transfer-limited phenomenon was relieved at high current density for loaded char [274].

In addition, the cell operated on biochar fuel pyrolyzed from agricultural plant was also compared with activated carbon to evaluate the effectiveness of biochar fuel. It was found that although more ratio of disorder carbon existed in corn straw char, significantly higher specific surface area and pore volume of activated carbon gave a better P_{max} of 302.8 mW cm^{-2} at 850 ℃ compared to corn straw char (218.5 mW cm^{-2}) when $La_{0.8}Sr_{0.2}Fe_{0.9}Nb_{0.1}O_{3-\delta}$ was used as the anode for electrolyte-supported SOFC. However, due to higher ash content (39.5 wt%) of activated carbon since it was derived from the coal, relatively lower fuel utilization of 25% was obtained, while for corn straw char, fuel utilization reached 30% because only 1.6% wt% of ash was contained in corn straw char, causing less weight of residue remaining and thus higher fuel utilization after stability test [260]. Differently, the electrochemical performance of electrolyte-supported SOFC on kelp biochar was highest (285 mW cm^{-2} at 850 ℃) compared to Na-loaded and unloaded activated carbons mainly because of a large amount of inherent favourable elements like Na, Ca and Mg as well as porous microstructure [275]. From the above research works on utilizations of biochar in SOFCs, obtainment of biochar from biomass via thermal pyrolysis process is a necessary procedure to provide proper solid carbon fuel, so as an important factor, the temperature of thermal pyrolysis process could have an influence on the cell performance. For example, with the increase of carbonisation temperature of walnut

shell, peak power density of the cell supplied with walnut shell biochar decreased although there was more carbon content in the biochar pyrolyzed at higher temperature [276]. The possible reason could be higher hydrogen content in biochar sample with lower treatment temperature, since gaseous products from the thermal decomposition of insufficient pyrolyzed biochar in high working temperature of carbon-fuelled SOFCs could perform electrochemical reactions [259]. Besides, with the increased carbon content, fuel utilization and discharging time of SOFC operated on the biochar from toothpick were correspondingly increased as the treatment temperature increased [277].

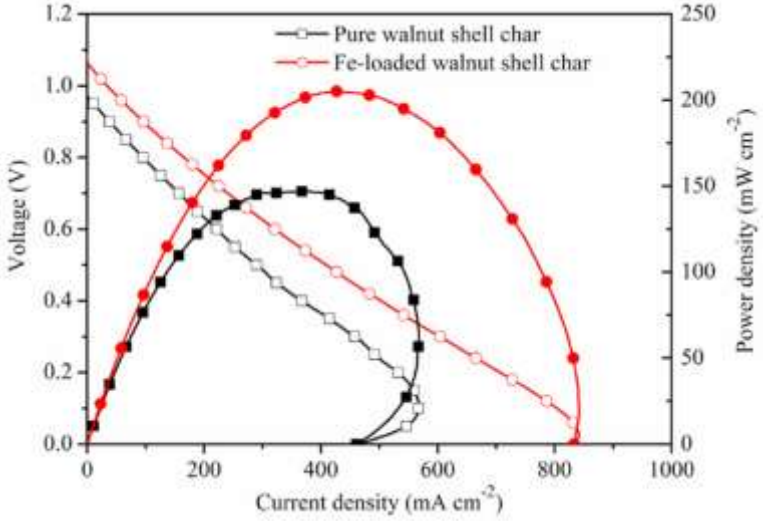

Fig. 27. Electrochemical performances of DC-SOFCs operated on walnut shell char and Fe-loaded walnut shell char at 800 ℃. Figure reproduced from ref. [274] with permission from Elsevier.

3.3.2. Remaining challenges and future perspectives for solid carbon-fuelled SOFCs

The utilizations of solid carbon fuels especially for coal and biomass carbon in SOFCs show important significance to human society because coal will still be the predominating energy source in the coming decades and biomass has always been thought as an alternative solution to pollution emission and energy crisis. However, in order to achieve the development of industrial scale of carbon-fuelled SOFCs and then contribute to the global energy economy, several obstacles need to be addressed.

The biggest issues related to carbon fuelled-SOFCs is the limited amount of solid fuel. With the continuous consumption of fuel, most SOFCs could not operate more than 30 h, though there are lots of attempts to increase the carbon loading capacity such as, the development of tubular segmented-in-series SOFC stack [274] or load of carbon outside tubular cell [271]. Therefore, the continuous supply of solid fuel is critically prerequisite for the cell with a

prolonged running process. In addition, several anode degradation issues could not be effectively evaluated due to the limited lifetime of SOFC system. For example, although discharging duration was improved with purified-HSC, anode material deactivations of carbon deposition and sulfur poisoning still occurred [258]. However, due to the complete exhaustion of solid carbon, it is difficult to assess the tolerance capacity of anode material for a longer operation. Therefore, efficient solid carbon supply and ash removal strategies are essential important not only for the cell lifetime but the evaluation of long-term stability of materials.

The ash contained in solid carbon derived from coal or biomass tends to have a complex effect on the overall performance of carbon-fuelled SOFCs. The promotion effects of inherent inorganic species on reverse Boudouard reaction could benefit the initial performance, but lower discharging duration or fuel utilization was frequently observed due to high ash content. In addition, deposit of ash components as well as corrosion of carbonate could degrade the cell performance by the blockage of anode pores or anode material deactivation [275,278]. Therefore, chemical and physical effects of specific impurity on the solid carbon fuel and anode need further investigation, and appropriate pre-treatment of solid carbon fuels from coal and biomass is still necessary to achieve long-term stable operation of SOFCs.

Another matter is the enhancement of overall cell efficiency. For carbon-fuelled SOFCs, although the direct fuel for electrochemical conversion is carbon monoxide which shows reduced theoretical electrical efficiency, thermal coupling of exothermic electrochemical reaction and endothermic reverse Boudouard reaction and the co-generation of electricity as well as carbon monoxide could result in high efficiency. Therefore, the high fuel utilization and necessary equipment for the capture of carbon monoxide or the separation of carbon dioxide is significant to guarantee the high overall efficiency of carbon-fuelled SOFCs.

3.4. Carbon-free fuel

Numerous contributions and achievements have been made to improve the electrochemical performance as well as long-term stability of SOFCs running on carbon-containing fuels including hydrocarbon, alcohols, and solid carbons etc. However, intrinsic coking issue on the state-of-the-art Ni-based anode is still likely to negatively affect anode working functions and thus hinder the development and commercialization of SOFCs. Therefore, the exploration of promising carbon-free fuel in terms of ready availability, transportation/storage conveniences, high energy density etc. has been carried out to substitute hydrogen fuel.

Ammonia (NH_3) has been thought as an excellent alternative for hydrogen carrier [279] because of various outstanding features such as high hydrogen content and no carbon in the molecular structure, ease for transportation and storage because of convenient liquification,

relatively low flammable range and penetrating odour (in case of leakage) [280], which could also be the reasons that many policymakers are strongly decided to promote the ammonia as clean or low-carbon fuel [29]. Besides, despite the fact that ammonia has been classified as the toxic substance for people's health, taking accidental explosion or combustion into account, there is similar or even lower hazard level for ammonia due to its low reactivity compared to gasoline, natural gas or LPG [281].

Lots of experimental studies have indicated that comparable cell performances could be achieved when SOFC was operating on pure ammonia and hydrogen at relatively high operating temperature, which is principally because ammonia fuel could be completely decomposed into the hydrogen rich fuel through catalytic ammonia decomposition reaction (Eq. (26)) under typical operating temperature of SOFC and the catalytic effect of anode metallic phase (nickel) since nickel shows the best catalyst activity except expensive Ru (ruthenium) [282]. Furthermore, ammonia decomposition reaction tends to be an effective cooling strategy for the cell temperature control because of endothermic nature [283], which could reduce the auxiliary energy related to cathode air flow and thus increase the overall system efficiency since active cooling of the cell is normally achieved by oversupplying the air into cathode side [4]. More importantly, toxic nitric oxides (NO_x) that are possible chemical products have been proved to be negligible in the anode off-gas under the most oxidizing condition [284]. Therefore, ammonia could be efficiently used in both oxygen-ion-conductive and proton-conductive SOFCs for electricity generation. In addition to the energy-consuming Haber-Bosch reaction (Eq. (27)) for generation of the ammonia in the industry, alternative electrochemical synthesis could also provide a promising way for the production of renewable ammonia [285], so the combination of direct operation of SOFC on ammonia fuel and the renewable ammonia production could provide an efficient and sustainable power system for the future.

$$2\mathrm{NH_3(g)} \leftrightarrow \mathrm{N_2(g)} + 3\mathrm{H_2(g)} \qquad \Delta H^0_{298} = +46\ \mathrm{kJ\ mol^{-1}} \tag{26}$$

$$\mathrm{N_2(g)} + 3\mathrm{H_2(g)} \leftrightarrow 2\mathrm{NH_3(g)} \tag{27}$$

3.4.1. The development of ammonia-fuelled SOFCs

The utilization of ammonia as a fuel for SOFC was firstly tested by Wojcik et al. [286]. However, due to the presence of oxygen ion in the anode side, possible formation of toxic NO in NH_3-fuelled SOFCs have forced SOFC to use proton conducting oxides including gadolinium-doped barium cerate (BCGO) [287–289], gadolinium and praseodymium-doped barium cerate (BCGP) [287,290] and $BaCe_{0.9}Nd_{0.1}O_{3-\delta}$ (BCNO) [291] as electrolytes. With

proton conductive electrolyte, the anode-supported NH_3-SOFC were expected to be operated on the intermediate temperature range, and presented reasonable maximum power densities of 355 mW cm^{-2} [288], or 315 mW cm^{-2} [291] at 700 ℃ and 200 mW cm^{-2} at 650 ℃ [289], showing comparable cell performance to hydrogen-fed SOFCs. Despite these accomplishments achieved by NH_3-fuelled proton-conducting SOFCs, more mature oxygen-ion electrolyte materials such as doped CeO_2 or YSZ needs more investigations on the feasible operation of SOFC on ammonia fuel [203,284,292–295] since long-term operation of doped-$BaCeO_3$ electrolytes could be much more challenging due to chemical instability problem in carbon dioxide or steam atmosphere [289]. Ma et al. [284] experimentally analysed the anode off-gas composition by gas chromatograph measurement when ammonia fuel was fed into the Ni-SDC ($Ce_{0.8}Sm_{0.2}O_{1.9}$) anode-supported SOFC using SDC as the electrolyte at various temperatures and fuel flow rates, and it was found that no NO was detected for all tests under the extreme oxidising circumstance (maximum flux of oxygen ion). Meanwhile, P_{max} of 252.8 mW cm^{-2} at 700 ℃ was attained with ammonia as the fuel and relatively low power density was probably attributed to relatively thick electrolyte (50 μm). In order to further improve the cell performance and reduce working temperature, SDC with the thickness of 10 μm was successfully fabricated by Meng et al. [292], and increased power density of 1190 mW cm^{-2} at 650 ℃ was obtained for ammonia fuel. However, significant deviation of maximum power densities (more than 35%) was observed between ammonia and hydrogen fuels (P_{max} of 1872 mW cm^{-2} at 650 ℃ for hydrogen fuel). The discrepancy was mainly due to the incomplete conversion of ammonia at relatively low temperature [292]. Besides, the decreased ionic conductivity could be another cause since actual cell temperature could be lower than that of furnace because of the endothermic characteristic of decomposition reaction (Eq. (27)), and it was indicated that temperature difference could reach 30-65 ℃ [296], which will lead to increased ohmic resistance and thus the drop of cell performance.

Actually, the main mechanism for electricity generation of ammonia-fuelled SOFCs is a two-step process that ammonia is readily to decompose into hydrogen and nitrogen under the catalytic effect of Ni metal (Eq. (26)), followed by the oxidation of hydrogen (Eq. (1)), which was evidenced by the relationship between OCV and operating temperature in numerous research studies [293,295,297–300]. The indication of main route for SOFCs running on ammonia fuel is essentially important for the cell performance improvement and stability, and will also provide useful guidance for selections of suitable anode material and operating condition.

As advised by the principle of NH_3-fed SOFC, the desired complete conversion of ammonia

is crucial for high cell performance. Therefore, the factors that affect ammonia decomposition reaction rate could definitely influence the maximum power density. In general, strategies employed to improve the chemical reaction rate could be achieved from two perspectives: thermodynamics and kinetics.

Thermodynamics

The ammonia decomposition reaction rate is likely to be affected by various thermodynamic factors under the Ni-based cermet such as partial pressures of gases including NH_3, H_2, N_2 as well as H_2O, fuel flow rate, current density and operating temperature. Therefore, the investigations of potential factors on the ammonia conversion have been experimentally conducted based on state-of-the-art Ni-YSZ anode [301,302]. It was found that the reaction rate is independent of N_2 concentration due to its inert nature. Besides, NH_3 partial pressure tends to positively influence the decomposition reaction rate, while H_2 shows an opposite trend, which was reported that H_2 could have an poisoning effect towards reaction since unreacted hydrogen would occupy active sites for decomposition reaction [299]. Therefore, the reaction rate can be described by Eq. (28), as given by:

$$r_{\mathrm{NH_3}} = -\frac{\mathrm{d}P_{\mathrm{NH_3}}}{\mathrm{d}t} = kP_{\mathrm{NH_3}}^{\alpha}P_{\mathrm{H_2}}^{\beta} \tag{28}$$

where $r_{\mathrm{NH_3}}$ denotes the reaction rate of ammonia decomposition; P_i represents the partial pressure of gas species; k is constant. However, α and β vary according to different catalysts, supports and temperatures, and positive and negative signs of α and β indicate promotion and inhibition effects of NH_3 and H_2 for the catalytic decomposition of ammonia, respectively.

The influences of steam concentration and fuel flow rate are quite complicated based on experimental observations. The effect of steam partial pressure will be different in terms of fuel flow rate and electrolyte phase used in the anode. For example, the conversion of ammonia over Ni-BCY25 ($BaCe_{0.75}Y_{0.25}O_{3-\delta}$) experienced a sharp drop from 98.6% to 55% once 0.8% of steam was co-fed with ammonia fuel, and decreased gradually as water concentration increased afterwards, while the slight declines for Ni-GDC and Ni-YSZ were observed, which indicates that Ni-GDC and Ni-YSZ exhibit reasonable higher resistance towards the inhibition effect of excess steam compared to Ni-BCY25 since stronger water adsorption capacity of the Ni-BCY25 cermet tends to influence decomposition process due to the occupation of active sites [299], and similar phenomena could be found in the study conducted by Miyazaki et al [300]. Despites this, this poisoning effect imposed by steam content could be diminished by increasing fuel flow rate [301]. In addition to the ammonia decomposition reaction rate, steam is likely to have a positive influence towards the proton conductivity of electrolyte and

electrocatalytic effect of the anode, which could benefit cell performance [299,300,303]. Therefore, optimization of steam content would be essential for cell performance due to the combined effects between ammonia decomposition rate as well as resistances of ohmic and polarization caused by steam. Actually, it should be noted that ammonia partial pressure should be kept constant by altering another inert gas (e.g., Ar) content for the effect investigations of H_2, N_2 and H_2O.

Fuel flow rate of ammonia is another critical factor that affects the decomposition rate and thus power output. In general, ammonia conversion is found to decrease because of the decreased contact time between fuel gas and catalyst metal in the anode when fuel flow rate increases [302,304–307]. However, there are two opposite tendencies for the performance of the ammonia-fed SOFC in the literature. One is that the power density increased with the increase of fuel flow rate [305], while another is that power density was found to decrease as fuel flow rate increased [301,307]. These two opposing changes might be two stages of the cell performance change towards the increase of ammonia flow rate, which is similar to methanol-fuelled SOFC [308]. At relatively low flow rate, more ammonia is supplied to catalytically generate more hydrogen, which will help to improve the power density [305]. However, a further increase of flow rate could decrease the cell performance [301,307] since fuel gas stream with high velocity could easily take away the generated hydrogen. It is worth noting that the drop of cell performance was not because of the suppression of decomposition reaction [306] or less hydrogen generation [307] because hydrogen production was correspondingly enhanced with the increased amount of converted ammonia, though the ammonia conversion percentage was found to decrease, as shown in Fig. 28, which indicates that ammonia conversion and decomposition rate are equivalent only when flow rate is fixed.

Furthermore, current density was reported to be another factor because when fuel cell was operated on the current mode, produced hydrogen is continuously consumed, which will promote ammonia conversion according to the Le Chatelier's principle and meanwhile eliminate the poisoning effect of hydrogen towards decomposition process rate [304]. Temperature shows dominating effect towards ammonia decomposition reaction, which is mainly because that catalytic activity of Ni-based anodes or catalysts will significantly be improved with the increase of temperature. Besides, for most catalytic activity tests, the conversion percentage could reach 100% when temperature was approximately 700 ℃ which is in line with that for SOFCs [298–300,305,306,309–313]. However, for nickel-based anode in the cell, the temperature required for ammonia complete decomposition will be higher because calcination temperatures used for catalyst powder in the fixed bed reactor and for

anode in the cell were different [300], indicating that the anode microstructure is optimized for electrochemical reactions but not for ammonia conversion. Besides, weaker adsorption of hydrogen on the anode active sites under higher temperature could improve the resistance of poisoning effect on ammonia conversion.

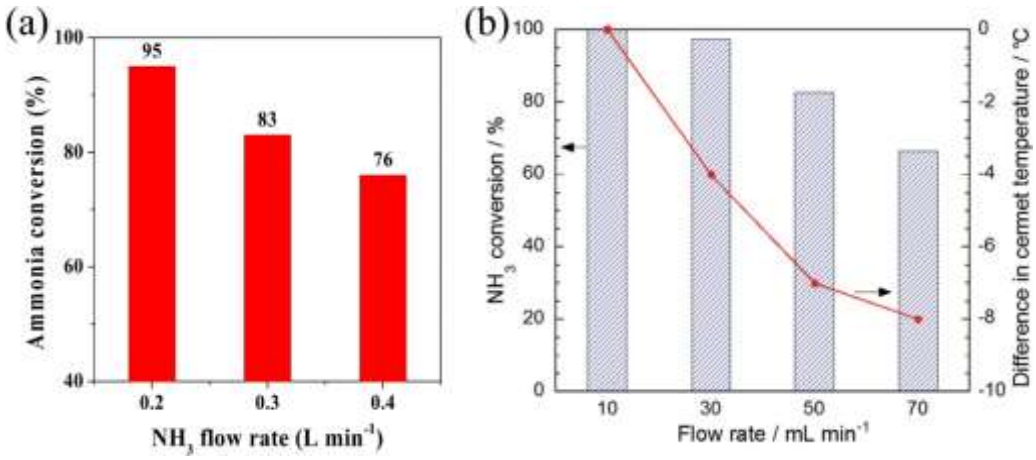

Fig. 28. (a) Ammonia conversion for the DSC with the catalyst Ba-Ni-YSZ under the NH_3 flow rate of 0.2-0.4 l min^{-1}. Anode gas: 66.7% NH_3-33.3% N_2, cathode gas: Air. Figure reproduced from ref. [307] by permission of The Electrochemical Society; (b) Ammonia conversion for ammonia decomposition over the Ni–BCZY cermet and difference in the cermet temperature compared to that at the ammonia flow rate of 10 mL min^{-1}. Reaction conditions: 100% NH_3. Furnace temperature: 600 ℃. Figure reproduced from ref. [306] with permission from the Royal Society of Chemistry.

Kinetics

Ammonia decomposition is a catalyst sensitive reaction, since the reaction cannot precede without catalyst even over 900 ℃ [305]. Due to unfortunate expensive cost of Ru, Ni-based catalyst is extensively used for ammonia decomposition due to its proper nitrogen binding energy [282], because catalytic decomposition of ammonia is related to NH_3 adsorption and N_2 desorption [314]. Actually, the catalytic effect of fabricated catalyst could be further enhanced by alloying or adding other active metals to form a bi- or even multi-metallic catalyst system because nitrogen binding energy can be adjusted to be the right range that is neither too weak nor too strong by combining Ni with the metal (Mo, Fe or Cr) with strong nitrogen binding energy [29]. In addition to metal phase, support material plays a role in the catalytic reaction process. In order to promote the effect of desired catalyst, support with larger surface area is often preferred. Therefore, the anode of NH_3-fuelled SOFC could be designed according to the principle of catalyst from material science to promote ammonia conversion, especially at intermediate or low operating temperature.

Anode ionic phase serves as the support for active metal, so selection of proper electrolyte oxide used in the composite anode is crucially important for the promotion of ammonia decomposition reaction. Frequently used electrolyte materials have been investigated comprehensively for ammonia conversion tests. It was found that as the ionic phase, BCY25 ($BaCe_{0.75}Y_{0.25}O_{3-\delta}$), BZY20 ($BaZr_{0.8}Y_{0.2}O_{3-\delta}$) and BCZY ($BaCe_{0.4}Zr_{0.4}Y_{0.2}O_{3-\delta}$) showed better catalytic effect for decomposition process in comparison to commonly used oxygen conductive electrolyte oxides GDC and YSZ when nickel was fabricated as the metal phase for composite catalyst systems [298–300,306]. Generally, complete ammonia conversion for those higher catalytic activity nickel-based catalysts can be achieved at relatively lower temperature of 600 ℃, which benefits the application of intermediate-temperature SOFCs. The reasons for the superior catalytic effect principally are larger amounts of basic sites and the exceptional tolerance towards inhibition effect of hydrogen occupation when these proton electrolytes mentioned-above were used as catalyst supports. It has been reported that the basicity of support could be an essential factor to speed up the rate-limiting step of ammonia decomposition [315] since higher surface basicity favours NH_3 adsorption and N_2 desorption [309]. Besides, the inhibition effect of hydrogen on decomposition reaction rate could be considerably mitigated for the proposed Ni-BCY25, Ni-BZY20 and Ni-BCZY cermets and nearly zero value for β in Eq. (28) could be observed based on catalytic activity tests, as indicated in Fig. 29. In addition, it was reported that Ni-GDC catalyst possess relatively higher activity compared to Ni-YSZ at intermediate temperature. Electrolyte-supported cells with Ni-GDC and Ni-YSZ anodes fed by the ammonia mixture of 0.7% NH_3-0.5% H_2O-98.8% Ar showed comparable performances at 1000 ℃ (Fig. 30a) [309], which indicated that ammonia was almost completely decomposed at this temperature and both anodes exhibited the similar electrocatalytic activity for hydrogen oxidation. However, when temperature dropped to 700 ℃, considerable difference could be observed for cells with different anodes (Fig. 30b), which was mainly because Ni-GDC showed better activity for ammonia decomposition due to more abundant basic sites on its surface. Recently, a new proton electrolyte of Pd-doped $Ba(Zr_{0.1}Ce_{0.7}Y_{0.1}Yb_{0.1})_{0.95}Pd_{0.05}O_{3-\delta}$ (BZCYYbPd) perovskite has been successfully fabricated as the electrolyte and anode ionic phase [313]. When pure ammonia was fed into these two single anode-supported fuel cells whose only difference is the anode ionic phase, the cell with Ni-BZCYYbPd anode presented relatively higher P_{max} of 600 mW cm^{-2} at 650 ℃ compared the Ni-BZCYYb counterpart due to superior features including higher proton conductivity as well as the better catalytic activity for both ammonia decomposition and hydrogen electrooxidation because Pd nanoparticles with the average diameter of 15 nm exsolved in the

reducing atmosphere were uniformly dispersed. Meanwhile, a further improved performance with excellent P_{max} of 724 mW cm^{-2} at 650 ℃ was achieved for ammonia-fed SOFC with the configuration of Ni-BZCYYbPd/BZCYYbPd/BCFZY ($BaCo_{0.4}Fe_{0.4}Zr_{0.1}Y_{0.1}O_{3-\delta}$).

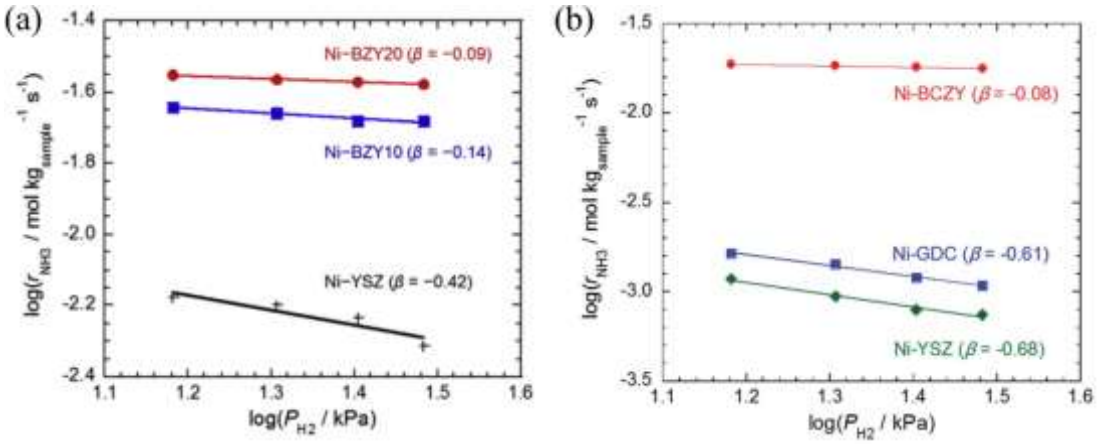

Fig. 29. (a) Ammonia decomposition rate as a function of partial pressure of hydrogen over Ni-BZY20, Ni-BZY10, and Ni-YSZ at 500 ℃, reaction condition: *x*% H_2-30% NH_3-(70-*x*)% Ar (*x* = 15, 20, 25, 30), S.V. = 10,000 L kg^{-1} h^{-1}; Figure reproduced from ref. [300] with permission from Elsevier; (b) Ammonia decomposition rate as a function of partial pressure of hydrogen over cermets at 500 ℃, reaction conditions: *x*% H_2-30% NH_3-(70-*x*)% Ar (*x* = 15, 20, 25, 30), S.V. = 10,000 L kg^{-1} h^{-1}. Figure reproduced from ref. [306] with permission from the Royal Society of Chemistry.

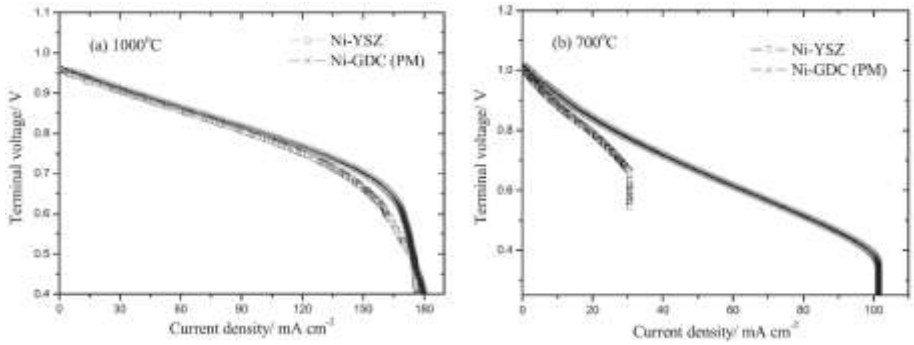

Fig. 30. *I-V* curves for the cell of Ni-YSZ|YSZ|LSM and Ni-GDC (PM)|YSZ|LSM at (a) 1000 ℃ and (b) 700 ℃. Anode gas; 0.7% NH_3-0.5% H_2O-98.8% Ar (flow rate; 100 ml min^{-1}). Cathode gas; O_2 (flow rate; 100 ml min^{-1}). Figure reproduced from ref. [309] with permission from Elsevier.

Metal phase of the anode show an extremely important significance in chemical catalytic effect and the performance of NH_3-fuelled SOFCs since it should serve as the active catalyst for both ammonia decomposition reaction as well as hydrogen electrooxidation simultaneously. For the enhancement of catalytical ammonia decomposition rate, both intrinsic catalytic effect

and large amounts of active sites play a dominate role in determining the catalyst activity [316]. As demonstrated earlier, nickel is the favourable catalyst for ammonia decomposition due to its relatively right nitrogen binding energy. However, optimal amount of Ni-loading might be different for different purposes including anode functions and decomposition reaction. Therefore, different weights of nickel metal were impregnated onto Ni-free SDC cermets to investigate the decomposition activity effect and the performance of NH_3-fuelled SOFC [311]. It was found that 10 wt% Ni-SDC presented the highest catalytic activity, but further increase of the Ni loading led to the increase of the temperature required for complete ammonia conversion because large amount of nickel metal might cause the aggregation and thus the reduction of surface area. However, for the power characteristic of NH_3-fed SOFC, fuel cells with 10 and 40 wt% Ni-SDC exhibited the comparable performances. This was because although 10 wt% Ni-SDC displayed the best decomposition activity, its electronic conductivity was less sufficient in comparison to 40 wt% Ni-SDC, which indicated that the trade-off between ammonia decomposition reaction activity and efficient electron transport is needed to be considered for the anode preparation. In addition, Ni-based anode catalyst activity could be further improved by adding or alloying another active metal since relatively weak nitrogen binding energy of nickel metal is responsible for N_2 desorption and the active metal additives with stronger nitrogen binding energy could promote NH_3 adsorption [315]. For example, specific amounts of Cr, Mo and Fe were reported to be introduced to Ni-SDC anodes to increase the catalytic activity for ammonia decomposition and thereby cell performance, which was mainly due to stronger nitrogen binding energies of Cr, Fe and Mo than that of Ni [314,317,318]. In order to enrich active sites in the catalyst, exsolution technology could also be used for the decoration of fabricated anode with uniformly distributed nanoparticles [316]. It was reported that NiCo alloy nanoparticles with an average diameter of 10-20 nm was exsolved from $La_{0.52}Sr_{0.28}Ti_{0.94}Ni_{0.03}Co_{0.03}O_{3-\delta}$ (LSTNC) perovskite precursor on $Sm_{0.2}Ce_{0.8}CoO_{1.9}$ (SDC) scaffold, and the proposed NiCo-LST-infiltrated SDC anode showed the best catalytic effect for ammonia decomposition compared to other anodes due to abundant active sites and adjusted NH_3 adsorption and N_2 desorption capabilities by introducing Co metal. Meanwhile, with this superior anode, electrolyte (350 μm) supporting cell presented an excellent power density with P_{max} of 361 mW cm^{-2} at 800 °C under dry ammonia fuel, which is much higher compared to most of NH_3-fuelled electrolyte-supported SOFCs available in the literature. Furthermore, additions of alkaline metals with electron donation property have been demonstrated to further increase the catalytic activity since additive serving as the promotor tends to donate electrons to catalyst system, leading to the electronic modification of active

sites and the reduction of ammonia decomposition activation energy [29,319]. Recently, the additive effect of alkaline earth metal of Ba on the catalytic activity of ammonia decomposition was investigated [307]. It was found that the addition of Ba with optimal loading amount of 15 wt% to the conventional Ni-YSZ catalyst could significantly promote ammonia decomposition by improving the promotion effect of NH_3 and diminishing the inhibition effect of H_2. Besides, with the Ba-modified Ni-YSZ catalyst placed in fuel channel, flat-tube SOFC with symmetric double-sided cathodes presented nearly identical performances under 60% H_2-40% N_2 at the flow rate of 0.27 l min^{-1} and 66.7% NH_3-33.3% N_2 at the flow rate of 0.2 l min^{-1} (same contents of hydrogen and nitrogen under the condition of complete ammonia conversion) even at 650 ℃, which was attributed to the improved catalytic activity caused by Ba addition.

3.4.2. Stability of ammonia-fuelled SOFCs

The feasibility of direct NH_3-fuelled SOFCs and its comparable performance to hydrogen fuel have demonstrated the promising perspective in the application of ammonia for power generation, which enables researchers to investigate the stability of SOFCs fed by ammonia since outstanding long-term durability is desired for the commercialization of SOFC technology. Different from SOFC using carbon-containing fuels, morphology and microstructural damages caused by the nitriding of Ni metals, involving the loss of metallic nickel, metal agglomeration, reduction of TPB length and even delamination, are the main degradation issues related to NH_3-fuelled SOFCs [304,305,307,312,316,318,320,321].

Degradation issue of ammonia-fuelled SOFCs

Yang et al. [320] concluded that unreacted ammonia in the anode tend to nitride Ni particles through Eq. (29), especially for lower temperature because ammonia decomposition reaction kinetics could be suppressed at low temperature and stable phase of Ni_3N (nickel nitride) could be maintained below 600 ℃ [29]. The nitriding of nickel is likely to cause agglomeration of adjacent Ni particles due to volume expansion and the weakened contact of metal and ionic phase, which may cause increase of the ohmic resistance and the reduction of TPB length [304,318,320]. Furthermore, under higher temperature condition or at reductive atmosphere, nickel nitride could convert back to metallic nickel via Eqs. (30) or (31), respectively. However, the processes of formation and decomposition or reduction of nickel nitride could lead to serious anode deformation especially for the SOFC which needs to be operating on the dynamic conditions involving rapid thermal cycling. The temperature cycling experimental test conducted by Yang et al. [320] indicated that due to repetitive volumetric change and thus induced mechanical stress, anode support layer was found to be delaminated when anode-supported SOFC was repeatedly operating at temperatures of 600 ℃ and 700 ℃ under

ammonia fuel, leading to the gradual drop of OCV (Fig. 31). One interesting phenomenon is worth noting that large amounts of microscopic pores were also observed from the SEM images of aged anode due to nickel nitriding and its subsequent decomposition or reduction [304,320]. However, although the presence of microscopic pores in Ni particles tends to deteriorate the electric contacts of metal, increased catalyst surface areas benefit ammonia decomposition, leading to the enhancement of ammonia conversion, as shown in Fig. 32 [304]. Meanwhile, as indicated by Fig. 32, cell voltages experienced two different trends for cases under 700 ℃ and 800 ℃, which was predominately due to the concentration difference of ammonia remained in anodes. As we discussed before, operating temperature shows an important effect on ammonia decomposition rate, and this is why the conversion could reach 100% at 800 ℃ (Fig. 32). However, for NH_3-fuelled SOFC under 700 ℃, relatively large quantity of unconverted ammonia accumulated in the anode was ready to deform the microstructure of Ni-YSZ anode, leading to the gradual decline of cell performance. Therefore, in this respect, high conversion or rapid decomposition reaction rate of ammonia is essentially important not only for cell performance but for the long-term operation durability of NH_3-fed SOFCs.

$$3Ni + NH_3 \rightarrow Ni_3N + H_2 \quad (29)$$

$$2Ni_3N \rightarrow N_2 + 6Ni \quad (30)$$

$$3H_2 + 2Ni_3N \rightarrow 2NH_3 + 6Ni \quad (31)$$

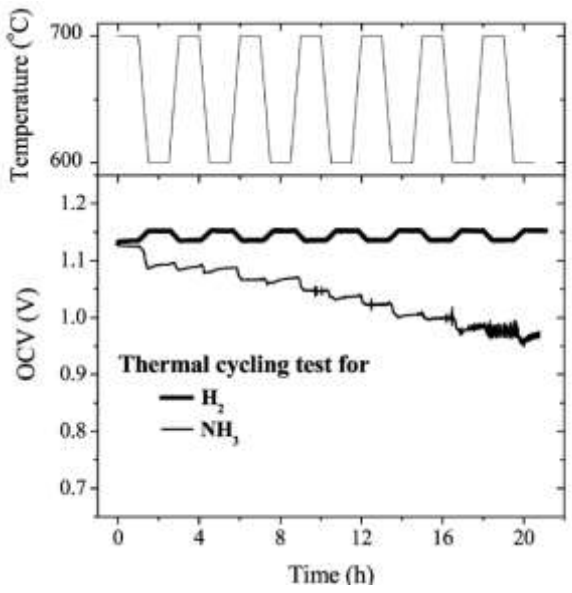

Fig. 31. Time courses of OCV of the ASC fuelled with 60.0% H_2-1.0% H_2O-39.0% N_2 and 66.7% NH_3-1.7% H_2O-31.6% N_2 during thermal cycling tests; cathode gas: O_2. Figure reproduced from ref. [320] with permission from American Chemical Society.

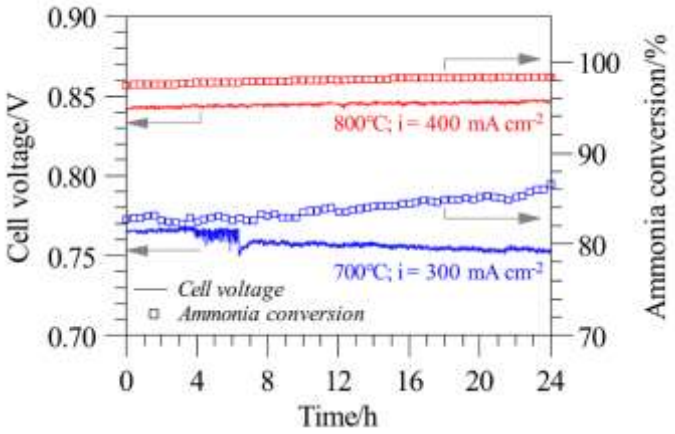

Fig. 32. cell voltage over time in 24-h tests at 800 ℃, 400 mA cm^{-2} and 700 ℃, 300 mA cm^{-2} with $A_{50\%,\ 2\ slpm}$. Figure reproduced from ref. [304] with permission from Elsevier.

Strategies to suppress degradation issue of ammonia-fuelled SOFCs

Based on the mechanism of nickel nitriding, strategies to improve the electrochemical performance of NH_3-fed SOFC could also be the approaches for the mitigation of undesired reactions, because high conversion or rapid decomposition reaction rate could help to reduce ammonia concentration in the anode, especially for anode functional layer. Substantial efforts have been devoted into the improvement of NH_3-fed SOFC stability, and according to the various long-term durability experimental tests available in the literature, approaches could also be classified into two aspects involving thermodynamics and kinetics. Details of the configurations and stabilities of ammonia-fuelled SOFCs are shown in Table 6.

High temperature could be a significant strategy to maintain the stable operation of NH_3-fuelled SOFCs [294,310,312,321,322] since the catalytic activity of Ni-based anodes will considerably be enhanced at relatively high temperature and nickel nitride could not be stable at more than 600 ℃. For example, 1500 hours stable operation with negligible degradation (2-4% per thousand hour) was achieved at 850 ℃ for anode-supported SOFC with Ni-YSZ as the anode running on ammonia fuel (Fig. 33a), and excellent stability was attributed to the nearly complete ammonia conversion which could be evidenced by almost same power output curves for ammonia fuel and the mixture of hydrogen and nitrogen with the ratio of 3/1 [322]. In addition, NH_3-fuelled 200 W-class SOFC stack comprising 10 Ni-YSZ anode-supported planar cells exhibited comparable degradation rate in comparison to the hydrogen fuel in 1000 h stability tests at 770 ℃ (Fig. 33b) [310]. However, no further post-mortem analyses for the reasons of performance degradations were conducted afterwards. Besides, Stoeckl et al. [321] performed a 1000 h durability test under wet ammonia fuel at 835 ℃ to assess the stability of MK352 electrolyte-supported SOFC stack with Ni-GDC as the anode, and an average

degradation rate of 1.1% per thousand hour was obtained (Fig. 33c) though nitriding phenomenon was found on nickel contact meshes and chromium-based interconnects in the subsequent post-mortem analyses. Similarly, after 1000 h stable operation stability test at 750 ℃ under ammonia fuel (Fig. 33d), nitridation was happened to metallic cell separators (SUS430) in the anode side though microstructure of Ni-YSZ anode remained intact and no performance decrease for SOFC stack consisting of 30 planar anode-supported cells [312]. However, although cell integrity and stack performance were not negatively influenced by the nitriding effect, for a longer operation period (e.g., more than 5000 h), nitridation happened in nickel contact meshes, chromium-based interconnects as well as the metallic cell separators could gradually deform or deteriorate the stack structure of and eventually degrade the performance. In addition to the temperature, relatively low fuel flow rate could be used for the improvement of cell stability. It was reported that no performance decay occurred during 50 h endurance capacity test for Ni-SDC anode-supported SOFC with ammonia as the fuel at 600 ℃. Although there was no detailed information about fuel flow rate for this durability test, pervious composition analysis of anode off-gas demonstrated that ammonia conversion reached more than 99% at 600 ℃ for both fuel flow rates of 30 and 5 ml min^{-1}, which indicates that relatively slow fuel velocity could help to increase ammonia conversion and thus operation period of NH_3-fuelled SOFC [284].

Lots of research studies have shown the exceptional stability of SOFCs running on ammonia fuel based on thermodynamical methods, while for kinetic strategies, few cases could be found in the literature. One example is the experimental work conducted by Wang et al. [307]: with the addition of enhanced catalytic activity catalyst, Ba-modified Ni-YSZ, into fuel channel, flat-tube SOFC with symmetric double-sided cathodes exhibited better long-term performance compared to the cell without the catalyst when ammonia was fed, which was because the complete conversion of ammonia showed less nitriding threatening for metallic nickel phase (Fig. 34), leading to almost same morphology and microstructure of the anode in comparison to fresh anode (Fig. 35). Besides, with Ni_{97}-Cr_3-SDC [318] and reduced LSTNC-infiltrated SDC [316] as anodes, NH_3-fuelled SOFCs presented better stability capacities compared to cells with Ni-SDC anodes at 600 ℃ and 700 ℃, respectively, as shown in Fig. 36. However, enhanced long-term stable operation durability was both because of superior anti-sintering ability of the proposed anodes, since conspicuous microstructure decay for both failure cases was nickel agglomeration, and complete ammonia conversions were not achieved for more durable fuel cells at their corresponding test temperature despite the improved catalytic effect towards ammonia decomposition compared to both pristine anodes [316,318].

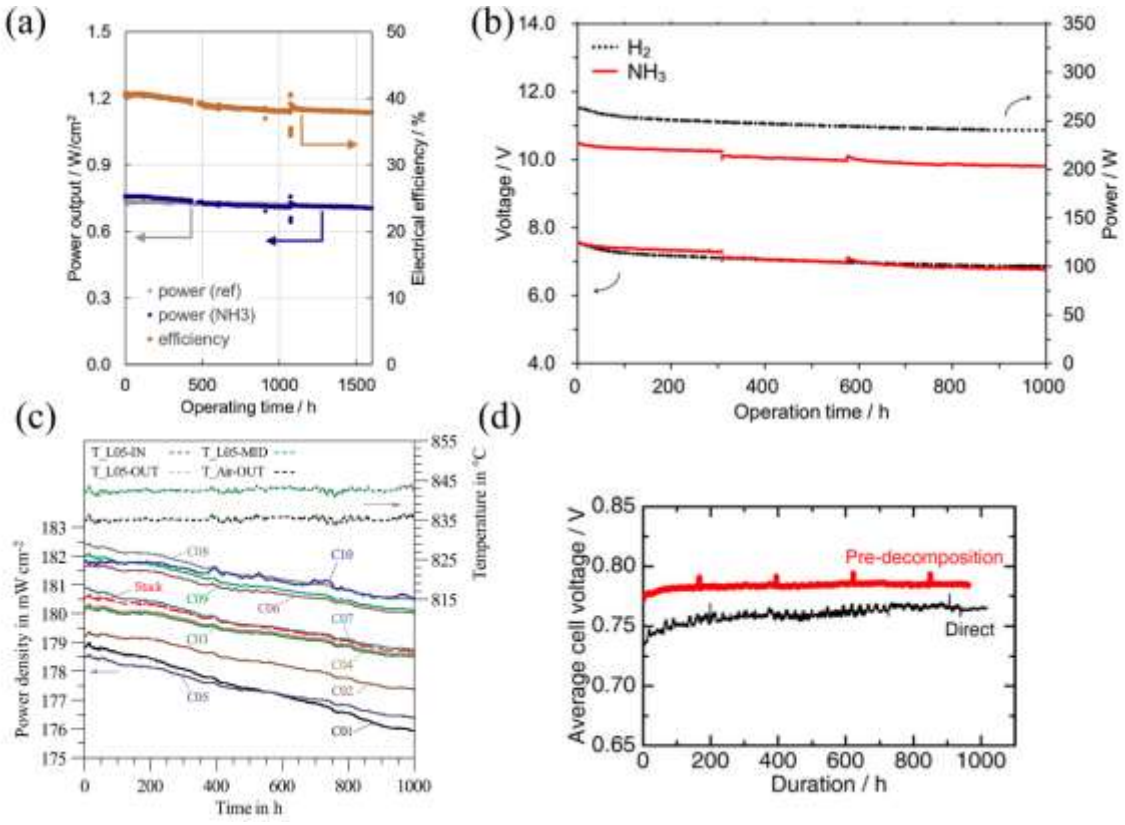

Fig. 33. (a) Power output (blue curve) and efficiency (orange curve) during long-term test with ammonia fuel at 850 °C, 1 A cm^{-2} current density. Figure reproduced from ref. [322] with permission from Elsevier; (b) Time course of the voltage and power at 770 °C for the direct NH_3-fueled (red line) and H_2-fueled (black dotted line) SOFC stacks. The current was kept at 30 and 35 A for the NH_3-fueled and the H_2-fueled ones, respectively. Figure reproduced from ref. [310] with permission from John Wiley and Sons; (c) 1000 h stability study with AS_I as fuel: Power density and temperature monitoring. Figure reproduced from ref. [321] with permission from Elsevier; (d) Average cell voltage during 1,000 h durability test. Figure reproduced from ref. [312] with permission from John Wiley and Sons.

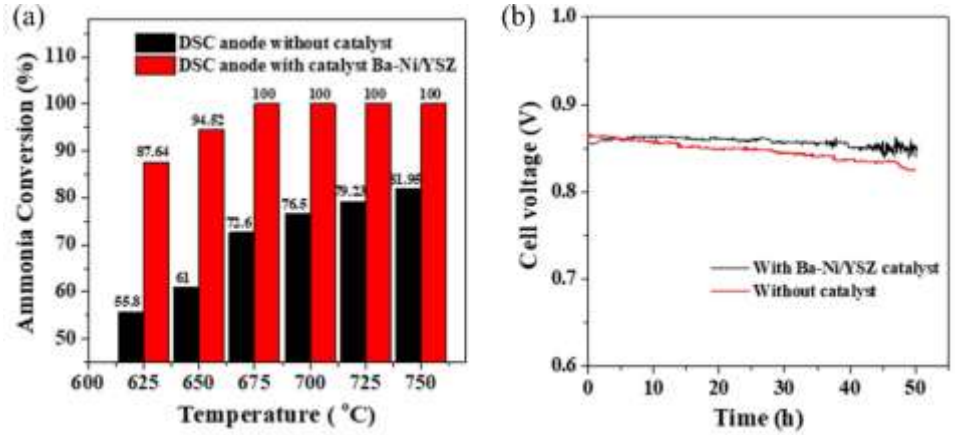

Fig. 34. (a) Ammonia conversion for ammonia decomposition on the DSC anode containing

with Ba-Ni-YSZ catalyst estimated from OCV state at 600 °C-750 °C; (b) Stability test of the DSC with the addition of Ba-Ni-YSZ catalyst into Ni-YSZ anode operated at 750 °C, 200 mA cm^{-2}. Anode gas: 66.7% NH_3-33.3% N_2, cathode gas: Air. NH_3 flow rate = 0.2 l min^{-1}. Figure reproduced from ref. [307] by permission of The Electrochemical Society.

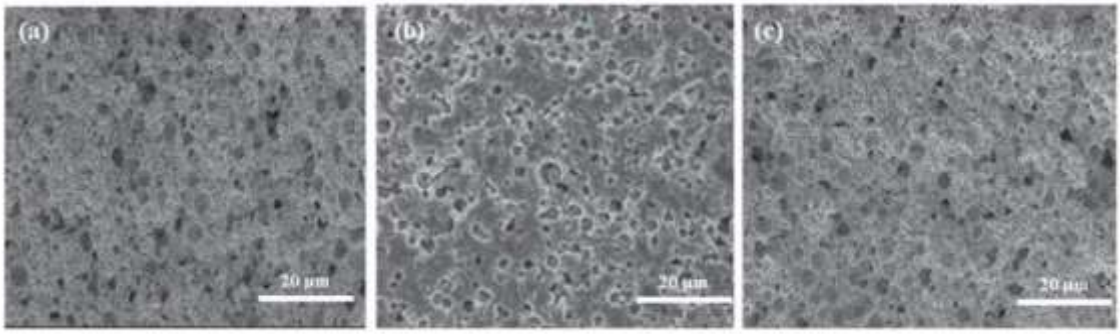

Fig. 35. SEM images of Ni-YSZ anode for DSC (a) without additional catalyst before stability tests and (b) after stability test in NH_3 fuel; (c) with Ba-Ni-YSZ catalyst after stability tests in NH_3 fuel. Figure reproduced from ref. [307] by permission of The Electrochemical Society.

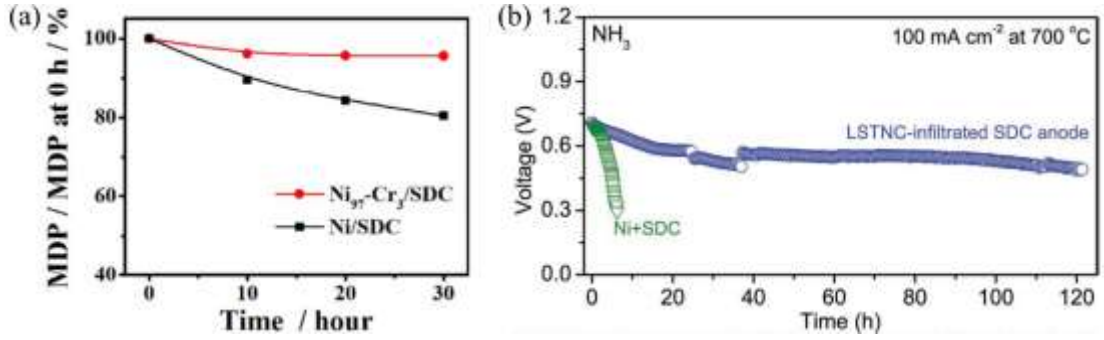

Fig. 36. (a) Variations of MPD of the Ni_{97}-Cr_3 and Ni-SDC cells as a function of NH_3 exposure time at 873 K. Figure reproduced from ref. [318] with permission from Elsevier; (b) Operational stability of the fuel cells with the reduced LSTNC-infiltrated SDC and Ni-SDC anodes operated on NH_3 fuel under a current density of 100 mA cm^{-2} at 700 °C. Figure reproduced from ref. [316] with permission from John Wiley and Sons.

3.4.3. Remaining challenges and future perspectives for ammonia-fuelled SOFCs

Ammonia shows excellent promising perspectives in the application of fuel cell especially for SOFC since ammonia as the effective hydrogen carrier could be readily decomposed back to the hydrogen rich fuel based on catalytic effect of conventional Ni-based anode under typical operating temperature of SOFC. High ammonia conversion or rapid decomposition rate is desired for both performance and stability which are equally essential for applicable

commercialization.

Operating SOFC at high temperature (more than 750 ℃) is beneficial for the development of highly durable and high-performing cells since complete ammonia conversion could be achieved and thus nickel nitriding phenomenon could be easily avoided. However, high operating temperature contradicts the future development of SOFC since reduction of temperature is a critical orientation of SOFC commercialization, especially for the transportation and portable power generations [32]. Although low-temperature SOFC possesses various merits, catalytic effect of Ni-based anodes on ammonia conversion will be greatly affected by temperature, and decreases significantly with the drop of temperature, leading to lower cell performance and potential microstructural deformations of anode due to concentrated ammonia in anode. Therefore, developing an anode equipped with the effective low-temperature catalytic effect for ammonia decomposition or high resistance towards nickel nitriding is the key for the development of NH_3-fuelled SOFCs. For example, Ni-based anode with proton electrolyte phases show better catalytic activity than frequently used oxygen conductive electrolyte GDC and YSZ, but there is limited research work done related to the durable NH_3-fuelled SOFCs with proton conducting oxide as anode ionic phase. One example is that ammonia-fed SOFC with the configuration of Ni-BZCYYbPd ($Ba(Zr_{0.1}Ce_{0.7}Y_{0.1}Yb_{0.1})_{0.95}Pd_{0.05}O_{3-\delta}$) /BZCYYbPd/BCFZY ($BaCo_{0.4}Fe_{0.4}Zr_{0.1}Y_{0.1}O_{3-\delta}$) experienced a slight voltage decline of only 0.01 V after 130 h stable operation at 550 ℃ and 0.2 A cm^{-2}, which showed good chemical stability of the proposed anode in such low temperature [313]. Besides, anodes based on the bimetallic or alloy catalyst also present enhanced catalytic effect, but again, scarce relevant study related to the durability test of NH_3-fed SOFCs could be found except the works conducted by Hashinokuchi et al. [318] and Song et al. [316].

In addition, the activity of catalyst could be enhanced through the addition of alkaline metals with electron donation characteristic, which provides new way to the durable anode design. Moreover, the preparation method also tends to affect anode microstructure and thus ammonia decomposition rate. For example, although electrolyte-supported cells with Ni-GDC anodes fabricated by physical mixing and glycine-nitrate combustion procedures showed nearly identical performance under hydrogen fuel, a reasonable enhancement of the power density was observed for the cell with anode prepared by glycine-nitrate combustion method under ammonia fuel at 600 ℃, which was because of larger surface area and small nickel particle size of the fabricated anode evidenced by SEM cross-sectional images [309]. Actually, the optimization of anode microstructure for chemical reaction kinetics is crucially significant

since currently anode microstructure is tailored to electrochemical oxidations. In this respect, more effective anodes with low-temperature catalytic effect and high metal nitriding tolerance are expected to be designed from material science and preparation methods.

Inspired by strategies of coking issue suppression, the optimization of anode support and functional layers as well as addition of a catalyst layer could also be adopted for the enhancement of ammonia conversion and cell stability. In order to achieve the complete ammonia conversion, conventional Ni-based anode-supported SOFCs are normally utilized, so functional and support layers could be designed for different duties in the power generation of NH_3-fuelled SOFCs. Accordingly, anode support layer optimized for material and microstructure based on the catalysts development for ammonia decomposition and the functional layer optimized for active electrocatalytic activity could be desired. Besides, additional catalyst layer could also be placed onto the anode support layer to additionally improve the ammonia conversion rate. It is worth noting that anodes fabricated from these two structural methods needs to be equipped with sufficient electronic conductivity as well as good chemical compatibility in order not to cause unexpected ohmic resistance.

4. Conclusion

SOFC could serve as one of the most competitive energy conversion devices because of the high intrinsic efficiency and low pollution. In addition, high working temperature enables SOFCs to effectively use readily available alternative fuels involving hydrocarbons, alcohols, solid carbons, ammonia etc., which could be significant advantage to SOFC community. Herein, we reviewed the recent developments of SOFCs operating on various promising fuels with the focus on long-term stability and power performance. In general, SOFCs with traditional Ni-based composite anode exhibit excellent performance characteristics on these fuels, showing comparable maximum power densities to hydrogen, but several degradation issues still need to be resolved to achieve the industrial commercialization of this technology. Therefore, approaches from three perspectives frequently used for improvements of stability and power output are summarised. Based on the degradation mechanisms demonstrated, suitable operating conditions related to temperature, fuel composition and current density are expected to be adopted to mitigate undesired problems. From the kinetics side, despites the fact that novel materials such as exsolved or doped perovskite materials show huge advances in carbon or sulfur tolerance, they are further from the commercialization compared to mature and well-developed Ni-based anodes especially with the modification of doped-ceria or barium-based oxides because of their promising features. Anode structure designs with separate layers which could be maximized their properties individually are likely to enhance the durability towards degradation problems or even cell performance, while the attention should be given to chemical and thermal compatibilities of various materials. Although the utilization of these alternative fuels especially renewable-featured energy resources in SOFCs shows great potential in the energy crisis and air pollution, considerable efforts are still required to be devoted into the solutions of these challenges faced by SOFC commercialization.

Acknowledgement

This work was supported by The Hong Kong Polytechnic University under the Project of Strategic Importance funding scheme [grant number P0035168]; and the National Natural Science Foundation of China [grant number 51806241].

Reference

[1] Dawood F, Anda M, Shafiullah GM. Hydrogen production for energy: An overview. Int J Hydrogen Energy 2020;45:3847–69. https://doi.org/10.1016/j.ijhydene.2019.12.059.

[2] Perera F. Pollution from fossil-fuel combustion is the leading environmental threat to global pediatric health and equity: Solutions exist. Int J Environ Res Public Health 2018;15. https://doi.org/10.3390/ijerph15010016.

[3] Cimenti M, Hill JM. Direct utilization of liquid fuels in SOFC for portable applications: Challenges for the selection of alternative anodes. Energies 2009;2:377–410. https://doi.org/10.3390/en20200377.

[4] Boldrin P, Brandon NP. Progress and outlook for solid oxide fuel cells for transportation applications. Nat Catal 2019;2:571–7. https://doi.org/10.1038/s41929-019-0310-y.

[5] McIntosh S, Gorte RJ. Direct hydrocarbon solid oxide fuel cells. Chem Rev 2004;104:4845–65. https://doi.org/10.1021/cr020725g.

[6] Shri Prakash B, Senthil Kumar S, Aruna ST. Properties and development of Ni/YSZ as an anode material in solid oxide fuel cell: A review. Renew Sustain Energy Rev 2014;36:149–79. https://doi.org/10.1016/j.rser.2014.04.043.

[7] Palomba V, Ferraro M, Frazzica A, Vasta S, Sergi F, Antonucci V. Experimental and numerical analysis of a SOFC-CHP system with adsorption and hybrid chillers for telecommunication applications. Appl Energy 2018;216:620–33. https://doi.org/10.1016/j.apenergy.2018.02.063.

[8] Hosseinpour J, Sadeghi M, Chitsaz A, Ranjbar F, Rosen MA. Exergy assessment and optimization of a cogeneration system based on a solid oxide fuel cell integrated with a Stirling engine. Energy Convers Manag 2017;143:448–58. https://doi.org/10.1016/j.enconman.2017.04.021.

[9] Garcia RF, Carril JC, Gomez JR, Gomez MR. Energy and entropy analysis of closed adiabatic expansion based trilateral cycles. Energy Convers Manag 2016;119:49–59. https://doi.org/10.1016/j.enconman.2016.04.031.

[10] Abe JO, Popoola API, Ajenifuja E, Popoola OM. Hydrogen energy, economy and storage: Review and recommendation. Int J Hydrogen Energy 2019;44:15072–86. https://doi.org/10.1016/j.ijhydene.2019.04.068.

[11] Dou Y, Sun L, Ren J, Dong L. Opportunities and Future Challenges in Hydrogen Economy for Sustainable Development. Elsevier Ltd; 2017.

https://doi.org/10.1016/B978-0-12-811132-1.00010-9.

[12] Ni M, Leung DYC, Leung MKH. A review on reforming bio-ethanol for hydrogen production. Int J Hydrogen Energy 2007;32:3238–47. https://doi.org/10.1016/j.ijhydene.2007.04.038.

[13] Jiao K, Xuan J, Du Q, Bao Z, Xie B, Wang B, et al. Designing the next generation of proton-exchange membrane fuel cells. Nature 2021;595:361–9. https://doi.org/10.1038/s41586-021-03482-7.

[14] Dincer I. Green methods for hydrogen production. Int J Hydrogen Energy 2012;37:1954–71. https://doi.org/10.1016/j.ijhydene.2011.03.173.

[15] Hosseini SE, Wahid MA. Hydrogen production from renewable and sustainable energy resources: Promising green energy carrier for clean development. Renew Sustain Energy Rev 2016;57:850–66. https://doi.org/10.1016/j.rser.2015.12.112.

[16] Nikolaidis P, Poullikkas A. A comparative overview of hydrogen production processes. Renew Sustain Energy Rev 2017;67:597–611. https://doi.org/10.1016/j.rser.2016.09.044.

[17] Akhlaghi N, Najafpour-Darzi G. A comprehensive review on biological hydrogen production. Int J Hydrogen Energy 2020;45:22492–512. https://doi.org/10.1016/j.ijhydene.2020.06.182.

[18] Abdalla AM, Hossain S, Nisfindy OB, Azad AT, Dawood M, Azad AK. Hydrogen production, storage, transportation and key challenges with applications: A review. Energy Convers Manag 2018;165:602–27. https://doi.org/10.1016/j.enconman.2018.03.088.

[19] Acar C, Dincer I. The potential role of hydrogen as a sustainable transportation fuel to combat global warming. Int J Hydrogen Energy 2020;45:3396–406. https://doi.org/10.1016/j.ijhydene.2018.10.149.

[20] Ge XM, Chan SH, Liu QL, Sun Q. Solid oxide fuel cell anode materials for direct hydrocarbon utilization. Adv Energy Mater 2012;2:1156–81. https://doi.org/10.1002/aenm.201200342.

[21] Boldrin P, Ruiz-Trejo E, Mermelstein J, Bermúdez Menéndez JM, RamÍrez Reina T, Brandon NP. Strategies for Carbon and Sulfur Tolerant Solid Oxide Fuel Cell Materials, Incorporating Lessons from Heterogeneous Catalysis. Chem Rev 2016;116:13633–84. https://doi.org/10.1021/acs.chemrev.6b00284.

[22] Wang W, Su C, Wu Y, Ran R, Shao Z. Progress in solid oxide fuel cells with nickel-based anodes operating on methane and related fuels. Chem Rev 2013;113:8104–51.

https://doi.org/10.1021/cr300491e.
[23] Su H, Hu YH. Progress in low-temperature solid oxide fuel cells with hydrocarbon fuels. Chem Eng J 2020;402:126235. https://doi.org/10.1016/j.cej.2020.126235.
[24] Wang W, Qu J, Julião PSB, Shao Z. Recent Advances in the Development of Anode Materials for Solid Oxide Fuel Cells Utilizing Liquid Oxygenated Hydrocarbon Fuels: A Mini Review. Energy Technol 2019;7:33–44. https://doi.org/10.1002/ente.201700738.
[25] Yang BC, Koo J, Shin JW, Go D, Shim JH, An J. Direct Alcohol-Fueled Low-Temperature Solid Oxide Fuel Cells: A Review. Energy Technol 2019;7:5–19. https://doi.org/10.1002/ente.201700777.
[26] Badwal SPS, Giddey S, Kulkarni A, Goel J, Basu S. Direct ethanol fuel cells for transport and stationary applications - A comprehensive review. Appl Energy 2015;145:80–103. https://doi.org/10.1016/j.apenergy.2015.02.002.
[27] Zhou W, Jiao Y, Li SD, Shao Z. Anodes for Carbon-Fueled Solid Oxide Fuel Cells. ChemElectroChem 2016;3:193–203. https://doi.org/10.1002/celc.201500420.
[28] Yu F, Han T, Wang Z, Xie Y, Wu Y, Jin Y, et al. Recent progress in direct carbon solid oxide fuel cell: Advanced anode catalysts, diversified carbon fuels, and heat management. Int J Hydrogen Energy 2021;46:4283–300. https://doi.org/10.1016/j.ijhydene.2020.10.259.
[29] Wan Z, Tao Y, Shao J, Zhang Y, You H. Ammonia as an effective hydrogen carrier and a clean fuel for solid oxide fuel cells. Energy Convers Manag 2021;228:113729. https://doi.org/10.1016/j.enconman.2020.113729.
[30] Khan MS, Lee SB, Song RH, Lee JW, Lim TH, Park SJ. Fundamental mechanisms involved in the degradation of nickel–yttria stabilized zirconia (Ni–YSZ) anode during solid oxide fuel cells operation: A review. Ceram Int 2016;42:35–48. https://doi.org/10.1016/j.ceramint.2015.09.006.
[31] da Silva FS, de Souza TM. Novel materials for solid oxide fuel cell technologies: A literature review. Int J Hydrogen Energy 2017;42:26020–36. https://doi.org/10.1016/j.ijhydene.2017.08.105.
[32] Gao Z, Mogni L V., Miller EC, Railsback JG, Barnett SA. A perspective on low-temperature solid oxide fuel cells. Energy Environ Sci 2016;9:1602–44. https://doi.org/10.1039/c5ee03858h.
[33] Dwivedi S. Solid oxide fuel cell: Materials for anode, cathode and electrolyte. Int J Hydrogen Energy 2020;45:23988–4013.

https://doi.org/10.1016/j.ijhydene.2019.11.234.

[34] Shu L, Sunarso J, Hashim SS, Mao J, Zhou W, Liang F. Advanced perovskite anodes for solid oxide fuel cells: A review. Int J Hydrogen Energy 2019;44:31275–304. https://doi.org/10.1016/j.ijhydene.2019.09.220.

[35] Abdalla AM, Hossain S, Azad AT, Petra PMI, Begum F, Eriksson SG, et al. Nanomaterials for solid oxide fuel cells: A review. Renew Sustain Energy Rev 2018;82:353–68. https://doi.org/10.1016/j.rser.2017.09.046.

[36] Fergus JW. Electrolytes for solid oxide fuel cells. J Power Sources 2006;162:30–40. https://doi.org/10.1016/j.jpowsour.2006.06.062.

[37] Ling Y, Wang X, Ma Z, Wei K, Wu Y, Khan M, et al. Review of experimental and modelling developments for ceria-based solid oxide fuel cells free from internal short circuits. J Mater Sci 2020;55:1–23. https://doi.org/10.1007/s10853-019-03876-z.

[38] Jacobson AJ. Materials for solid oxide fuel cells. Chem Mater 2010;22:660–74. https://doi.org/10.1021/cm902640j.

[39] Chen Y, Yang L, Ren F, An K. Visualizing the structural evolution of LSM/xYSZ composite cathodes for SOFC by in-situ neutron diffraction. Sci Rep 2014;4. https://doi.org/10.1038/srep05179.

[40] Wang SF, Hsu YF, Chang JH, Cheng S, Lu HC. Characteristics of Cu and Mo-doped Ca3Co4O9-δ cathode materials for use in solid oxide fuel cells. Ceram Int 2016;42:11239–47. https://doi.org/10.1016/j.ceramint.2016.04.037.

[41] Hwang HJ, Moon JW, Lee S, Lee EA. Electrochemical performance of LSCF-based composite cathodes for intermediate temperature SOFCs. J Power Sources 2005;145:243–8. https://doi.org/10.1016/j.jpowsour.2005.02.063.

[42] Shao Z, Haile SM. A high-performance cathode for the next generation of solid-oxide fuel cells. Mater Sustain Energy A Collect Peer-Reviewed Res Rev Artic from Nat Publ Gr 2010;3:255–8. https://doi.org/10.1142/9789814317665_0036.

[43] Koide H, Someya Y, Yoshida T, Maruyama T. Properties of Ni/YSZ cermet as anode for SOFC. Solid State Ionics 2000;132:253–60. https://doi.org/10.1016/s0167-2738(00)00652-4.

[44] Kawada T, Sakai N, Yokokawa H, Dokiya M, Mori M, Iwata T. Characteristics of Slurry-Coated Nickel Zirconia Cermet Anodes for Solid Oxide Fuel Cells. J Electrochem Soc 1990;137:3042–7. https://doi.org/10.1149/1.2086156.

[45] Wei K, Wang X, Budiman RA, Kang J, Lin B, Zhou F, et al. Progress in Ni-based anode materials for direct hydrocarbon solid oxide fuel cells. J Mater Sci 2018;53:8747–65.

https://doi.org/10.1007/s10853-018-2205-8.

[46] Park S, Vohs JM, Gorte RJ. Direct oxidation of hydrocarbons in a solid-oxide fuel cell. Nature 2000;404:265–7. https://doi.org/10.1038/35005040.

[47] Marina OA, Mogensen M. High-temperature conversion of methane on a composite gadolinia-doped ceria - gold electrode. Appl Catal A Gen 1999;189:117–26. https://doi.org/10.1016/S0926-860X(99)00259-8.

[48] Mogensen M, Kammer K. Conversion of Hydrocarbons in Solid Oxide Fuel Cells. Annu Rev Mater Res 2003;33:321–31. https://doi.org/10.1146/annurev.matsci.33.022802.092713.

[49] Baldinelli A, Barelli L, Bidini G, Di Michele A, Vivani R. SOFC direct fuelling with high-methane gases: Optimal strategies for fuel dilution and upgrade to avoid quick degradation. Energy Convers Manag 2016;124:492–503. https://doi.org/10.1016/j.enconman.2016.07.051.

[50] Lyu Z, Li H, Han M. Electrochemical properties and thermal neutral state of solid oxide fuel cells with direct internal reforming of methane. Int J Hydrogen Energy 2019;44:12151–62. https://doi.org/10.1016/j.ijhydene.2019.03.048.

[51] Mishina T, Fujiwara N, Tada S, Takagaki A, Kikuchi R, Oyama ST. Calcium-Modified Ni-SDC Anodes in Solid Oxide Fuel Cells for Direct Dry Reforming of Methane. J Electrochem Soc 2020;167:134512. https://doi.org/10.1149/1945-7111/abba65.

[52] Sumi H, Lee Y-H, Muroyama H, Matsui T, Eguchi K. Comparison Between Internal Steam and CO[sub 2] Reforming of Methane for Ni-YSZ and Ni-ScSZ SOFC Anodes. J Electrochem Soc 2010;157:B1118. https://doi.org/10.1149/1.3435320.

[53] Modjtahedi A, Hedayat N, Chuang SSC. Diffusion-limited electrochemical oxidation of H2/CO on Ni-anode catalyst in a CH4/CO2-solid oxide fuel cell. Catal Today 2016;278:227–36. https://doi.org/10.1016/j.cattod.2015.12.026.

[54] Gür TM. Comprehensive review of methane conversion in solid oxide fuel cells: Prospects for efficient electricity generation from natural gas. Prog Energy Combust Sci 2016;54:1–64. https://doi.org/10.1016/j.pecs.2015.10.004.

[55] Aslannejad H, Barelli L, Babaie A, Bozorgmehri S. Effect of air addition to methane on performance stability and coking over NiO-YSZ anodes of SOFC. Appl Energy 2016;177:179–86. https://doi.org/10.1016/j.apenergy.2016.05.127.

[56] Lee D, Myung J, Tan J, Hyun SH, Irvine JTS, Kim J, et al. Direct methane solid oxide fuel cells based on catalytic partial oxidation enabling complete coking tolerance of Ni-based anodes. J Power Sources 2017;345:30–40.

https://doi.org/10.1016/j.jpowsour.2017.02.003.

[57] Argyle MD, Bartholomew CH. Heterogeneous catalyst deactivation and regeneration: A review. Catalysts 2015;5:145–269. https://doi.org/10.3390/catal5010145.

[58] Gangwal SK. Desulfurization for Fuel Cells. Elsevier; 2011. https://doi.org/10.1016/B978-0-444-53563-4.10011-2.

[59] Chen D, Christensen KO, Ochoa-Fernández E, Yu Z, Tøtdal B, Latorre N, et al. Synthesis of carbon nanofibers: Effects of Ni crystal size during methane decomposition. J Catal 2005;229:82–96. https://doi.org/10.1016/j.jcat.2004.10.017.

[60] Chen Y, Zhou W, Shao Z, Xu N. Nickel catalyst prepared via glycine nitrate process for partial oxidation of methane to syngas. Catal Commun 2008;9:1418–25. https://doi.org/10.1016/j.catcom.2007.12.009.

[61] Chen L, Zhu Q, Hao Z, Zhang T, Xie Z. Development of a Co-Ni bimetallic aerogel catalyst for hydrogen production via methane oxidative CO2 reforming in a magnetic assisted fluidized bed. Int J Hydrogen Energy 2010;35:8494–502. https://doi.org/10.1016/j.ijhydene.2010.06.003.

[62] Hao Z, Zhu Q, Jiang Z, Hou B, Li H. Characterization of aerogel Ni/Al2O3 catalysts and investigation on their stability for CH4-CO2 reforming in a fluidized bed. Fuel Process Technol 2009;90:113–21. https://doi.org/10.1016/j.fuproc.2008.08.004.

[63] Guo J, Lou H, Mo L, Zheng X. The reactivity of surface active carbonaceous species with CO2 and its role on hydrocarbon conversion reactions. J Mol Catal A Chem 2009;316:1–7. https://doi.org/10.1016/j.molcata.2009.09.023.

[64] Abdel Karim Aramouni N, Zeaiter J, Kwapinski W, Ahmad MN. Thermodynamic analysis of methane dry reforming: Effect of the catalyst particle size on carbon formation. Energy Convers Manag 2017;150:614–22. https://doi.org/10.1016/j.enconman.2017.08.056.

[65] Zhang H, Liu W, Wang Y, Wang J, Yang J, Liang T, et al. Performance and long-term durability of direct-methane flat-tube solid oxide fuel cells with symmetric double-sided cathodes. Int J Hydrogen Energy 2019;44:28947–57. https://doi.org/10.1016/j.ijhydene.2019.09.126.

[66] Jiang C, Ma J, Corre G, Jain SL, Irvine JTS. Challenges in developing direct carbon fuel cells. Chem Soc Rev 2017;46:2889–912. https://doi.org/10.1039/c6cs00784h.

[67] Papurello D, Lanzini A, Fiorilli S, Smeacetto F, Singh R, Santarelli M. Sulfur poisoning in Ni-anode solid oxide fuel cells (SOFCs): Deactivation in single cells and a stack. Chem Eng J 2016;283:1224–33. https://doi.org/10.1016/j.cej.2015.08.091.

[68] Hadi AS, Ahmed OK, Ali OM. Enhancement of Gasoline Fuel Quality with Commercial Additives to Improve Engine Performance. IOP Conf. Ser. Mater. Sci. Eng., vol. 745, 2020. https://doi.org/10.1088/1757-899X/745/1/012065.

[69] Lee HS, Lee HM, Park JY, Lim HT. Degradation behavior of Ni-YSZ anode-supported solid oxide fuel cell (SOFC) as a function of H2S concentration. Int J Hydrogen Energy 2018;43:22511–8. https://doi.org/10.1016/j.ijhydene.2018.09.189.

[70] Yoshikawa M, Yamamoto T, Yasumoto K, Mugikura Y. Degradation Analysis of SOFC Stack Performance: Investigation of Cathode Sulfur Poisoning Due to Contamination in Air. ECS Trans 2017;78:2347–54. https://doi.org/10.1149/07801.2347ecst.

[71] Xiong Y, Yamaji K, Horita T, Yokokawa H, Akikusa J, Eto H, et al. Sulfur Poisoning of SOFC Cathodes. J Electrochem Soc 2009;156:B588. https://doi.org/10.1149/1.3090169.

[72] Cayan FN, Zhi M, Pakalapati SR, Celik I, Wu N, Gemmen R. Effects of coal syngas impurities on anodes of solid oxide fuel cells. J Power Sources 2008;185:595–602. https://doi.org/10.1016/j.jpowsour.2008.06.058.

[73] Cheng Z, Wang JH, Choi Y, Yang L, Lin MC, Liu M. From Ni-YSZ to sulfur-tolerant anode materials for SOFCs: Electrochemical behavior, in situ characterization, modeling, and future perspectives. Energy Environ Sci 2011;4:4380–409. https://doi.org/10.1039/c1ee01758f.

[74] Hagen A, Rasmussen JFB, Thydén K. Durability of solid oxide fuel cells using sulfur containing fuels. J. Power Sources, vol. 196, Elsevier B.V.; 2011, p. 7271–6. https://doi.org/10.1016/j.jpowsour.2011.02.053.

[75] Lohsoontorn P, Brett DJL, Brandon NP. Thermodynamic predictions of the impact of fuel composition on the propensity of sulphur to interact with Ni and ceria-based anodes for solid oxide fuel cells. J Power Sources 2008;175:60–7. https://doi.org/10.1016/j.jpowsour.2007.09.065.

[76] Brightman E, Ivey DG, Brett DJL, Brandon NP. The effect of current density on H2S-poisoning of nickel-based solid oxide fuel cell anodes. J. Power Sources, vol. 196, Elsevier B.V.; 2011, p. 7182–7. https://doi.org/10.1016/j.jpowsour.2010.09.089.

[77] Rasmussen JFB, Hagen A. The effect of H2S on the performance of Ni-YSZ anodes in solid oxide fuel cells. J Power Sources 2009;191:534–41. https://doi.org/10.1016/j.jpowsour.2009.02.001.

[78] Kishimoto H, Horita T, Yamaji K, Brito ME, Xiong Y-P, Yokokawa H. Sulfur

Poisoning on SOFC Ni Anodes: Thermodynamic Analyses within Local Equilibrium Anode Reaction Model. J Electrochem Soc 2010;157:B802. https://doi.org/10.1149/1.3362896.

[79] Pihlatie M, Kaiser A, Mogensen M. Redox stability of SOFC: Thermal analysis of Ni-YSZ composites. Solid State Ionics 2009;180:1100–12. https://doi.org/10.1016/j.ssi.2009.04.011.

[80] Hubert M, Laurencin J, Cloetens P, Morel B, Montinaro D, Lefebvre-Joud F. Impact of Nickel agglomeration on Solid Oxide Cell operated in fuel cell and electrolysis modes. J Power Sources 2018;397:240–51. https://doi.org/10.1016/j.jpowsour.2018.06.097.

[81] Lay-Grindler E, Laurencin J, Villanova J, Cloetens P, Bleuet P, Mansuy A, et al. Degradation study by 3D reconstruction of a nickel-yttria stabilized zirconia cathode after high temperature steam electrolysis operation. J Power Sources 2014;269:927–36. https://doi.org/10.1016/j.jpowsour.2014.07.066.

[82] Wongsawatgul N, Chaianansutcharit S, Yamamoto K, Nanko M, Sato K. Improved Electrochemical Properties of an Ni-Based YSZ Cermet Anode for the Direct Supply of Methane by Co Alloying with an Impregnation Method. Ceramics 2020;3:114–26. https://doi.org/10.3390/ceramics3010012.

[83] Eguchi K, Kojo H, Takeguchi T, Kikuchi R, Sasaki K. Fuel flexibility in power generation by solid oxide fuel cells. Solid State Ionics 2002;152–153:411–6. https://doi.org/10.1016/S0167-2738(02)00351-X.

[84] Laosiripojana N, Assabumrungrat S. Catalytic steam reforming of methane, methanol, and ethanol over Ni/YSZ: The possible use of these fuels in internal reforming SOFC. J Power Sources 2007;163:943–51. https://doi.org/10.1016/j.jpowsour.2006.10.006.

[85] Lin Y, Zhan Z, Liu J, Barnett SA. Direct operation of solid oxide fuel cells with methane fuel. Solid State Ionics 2005;176:1827–35. https://doi.org/10.1016/j.ssi.2005.05.008.

[86] Alzate-Restrepo V, Hill JM. Effect of anodic polarization on carbon deposition on Ni/YSZ anodes exposed to methane. Appl Catal A Gen 2008;342:49–55. https://doi.org/10.1016/j.apcata.2007.12.039.

[87] Ren C, Gan Y, Yang C, Lee M, Xue X. Fabrication and Characterization of Direct Methane Fueled Thin Film SOFCs Supported by Microchannel-Structured Microtubular Substrates. ACS Appl Energy Mater 2020;3:1831–41. https://doi.org/10.1021/acsaem.9b02271.

[88] Pillai MR, Kim I, Bierschenk DM, Barnett SA. Fuel-flexible operation of a solid oxide fuel cell with Sr0.8La0.2TiO3 support. J Power Sources 2008;185:1086–93.

https://doi.org/10.1016/j.jpowsour.2008.07.063.
[89] Gross MD, Vohs JM, Gorte RJ. A strategy for achieving high performance with SOFC ceramic anodes. Electrochem Solid-State Lett 2007;10. https://doi.org/10.1149/1.2432942.
[90] Buccheri MA, Singh A, Hill JM. Anode- versus electrolyte-supported Ni-YSZ/YSZ/Pt SOFCs: Effect of cell design on OCV, performance and carbon formation for the direct utilization of dry methane. J Power Sources 2011;196:968–76. https://doi.org/10.1016/j.jpowsour.2010.08.073.
[91] Vural Y, Ma L, Ingham DB, Pourkashanian M. Comparison of the multicomponent mass transfer models for the prediction of the concentration overpotential for solid oxide fuel cell anodes. J Power Sources 2010;195:4893–904. https://doi.org/10.1016/j.jpowsour.2010.01.033.
[92] Perry Murray E, Tsai T, Barnett SA. A direct-methane fuel cell with a ceria-based anode. Nature 1999;400:649–51. https://doi.org/10.1038/23220.
[93] Cao T, Huang K, Shi Y, Cai N. Recent advances in high-temperature carbon-air fuel cells. Energy Environ Sci 2017;10:460–90. https://doi.org/10.1039/c6ee03462d.
[94] Ihara M, Matsuda K, Sato H, Yokoyama C. Solid state fuel storage and utilization through reversible carbon deposition on an SOFC anode. Solid State Ionics 2004;175:51–4. https://doi.org/10.1016/j.ssi.2004.09.020.
[95] Saito H, Hasegawa S, Ihara M. Effective Anode Thickness in Rechargeable Direct Carbon Fuel Cells Using Fuel Charged by Methane. J Electrochem Soc 2008;155:B443. https://doi.org/10.1149/1.2840563.
[96] Hasegawa S, Ihara M. Reaction Mechanism of Solid Carbon Fuel in Rechargeable Direct Carbon SOFCs with Methane for Charging. J Electrochem Soc 2008;155:B58. https://doi.org/10.1149/1.2801399.
[97] Jiao Y, Zhang L, An W, Zhou W, Sha Y, Shao Z, et al. Controlled deposition and utilization of carbon on Ni-YSZ anodes of SOFCs operating on dry methane. Energy 2016;113:432–43. https://doi.org/10.1016/j.energy.2016.07.063.
[98] Niakolas DK, Ouweltjes JP, Rietveld G, Dracopoulos V, Neophytides SG. Au-doped Ni/GDC as a new anode for SOFCs operating under rich CH 4 internal steam reforming. Int J Hydrogen Energy 2010;35:7898–904. https://doi.org/10.1016/j.ijhydene.2010.05.038.
[99] Garcia-Garcia FJ, Yubero F, González-Elipe AR, Lambert RM. Microstructural engineering and use of efficient poison resistant Au-doped Ni-GDC ultrathin anodes in

methane-fed solid oxide fuel cells. Int J Hydrogen Energy 2018;43:885–93. https://doi.org/10.1016/j.ijhydene.2017.11.020.

[100] Qu J, Wang W, Chen Y, Deng X, Shao Z. Stable direct-methane solid oxide fuel cells with calcium-oxide-modified nickel-based anodes operating at reduced temperatures. Appl Energy 2016;164:563–71. https://doi.org/10.1016/j.apenergy.2015.12.014.

[101] Sapountzi FM, Zhao C, Boréave A, Retailleau-Mevel L, Niakolas D, Neofytidis C, et al. Sulphur tolerance of Au-modified Ni/GDC during catalytic methane steam reforming. Catal Sci Technol 2018;8:1578–88. https://doi.org/10.1039/c8cy00107c.

[102] Jiang Z, Arifin NA, Mardle P, Steinberger-Wilckens R. Electrochemical Performance and Carbon Resistance Comparison between Tin, Copper and Silver-Doped Nickel/Yttria-Stabilized Zirconia Anodes SOFCs Operated with Biogas. J Electrochem Soc 2019;166:F393–8. https://doi.org/10.1149/2.1011906jes.

[103] Babaei A, Zhang L, Liu E, Jiang SP. Performance and carbon deposition over Pd nanoparticle catalyst promoted Ni/GDC anode of SOFCs in methane, methanol and ethanol fuels. Int J Hydrogen Energy 2012;37:15301–10. https://doi.org/10.1016/j.ijhydene.2012.07.089.

[104] Babaei A, Jiang SP, Li J. Electrocatalytic Promotion of Palladium Nanoparticles on Hydrogen Oxidation on Ni/GDC Anodes of SOFCs via Spillover. J Electrochem Soc 2009;156:B1022. https://doi.org/10.1149/1.3156637.

[105] Li P, Wang Z, Yao X, Hou N, Fan L, Gan T, et al. Effect of Sn addition on improving the stability of Ni-Ce 0.8 Sm 0.2 O 1.9 anode material for solid oxide fuel cells fed with dry CH 4. Catal Today 2019;330:209–16. https://doi.org/10.1016/j.cattod.2018.04.030.

[106] Li K, Jia L, Wang X, Pu J, Chi B, Jian L. Methane on-cell reforming in nickel-iron alloy supported solid oxide fuel cells. J Power Sources 2015;284:446–51. https://doi.org/10.1016/j.jpowsour.2015.03.062.

[107] Zhao K, Lee KS, Chen M, Kim BH, Xu Q, Ahn BG. Electrochemical performance of a copper-impregnated Ni-Ce 0.8Sm0.2O1.9 anode running on methane. Int J Hydrogen Energy 2013;38:3750–6. https://doi.org/10.1016/j.ijhydene.2013.01.036.

[108] Gross MD, Vohs JM, Gorte RJ. Recent progress in SOFC anodes for direct utilization of hydrocarbons. J Mater Chem 2007;17:3071–7. https://doi.org/10.1039/b702633a.

[109] Yang Q, Chai F, Ma C, Sun C, Shi S, Chen L. Enhanced coking tolerance of a MgO-modified Ni cermet anode for hydrocarbon fueled solid oxide fuel cells. J Mater Chem A 2016;4:18031–6. https://doi.org/10.1039/c6ta08031f.

[110] Xie Y, Shi N, Hu X, Liu M, Yang Y, Huan D, et al. Novel in-situ MgO nano-layer

decorated carbon-tolerant anode for solid oxide fuel cells. Int J Hydrogen Energy 2020;45:11791–801. https://doi.org/10.1016/j.ijhydene.2020.02.117.

[111] Trovarelli A. Catalytic properties of ceria and CeO2-Containing materials. Catal Rev - Sci Eng 1996;38:439–520. https://doi.org/10.1080/01614949608006464.

[112] Zhang Y, Fan H, Han M. Stability of Ni-YSZ Anode for SOFCs in Methane Fuel: The Effects of Infiltrating La 0.8 Sr 0.2 FeO 3-δ and Gd-Doped CeO 2 Materials. J Electrochem Soc 2018;165:F756–63. https://doi.org/10.1149/2.0171810jes.

[113] Ideris A, Croiset E, Pritzker M, Amin A. Direct-methane solid oxide fuel cell (SOFC) with Ni-SDC anode-supported cell. Int J Hydrogen Energy 2017;42:23118–29. https://doi.org/10.1016/j.ijhydene.2017.07.117.

[114] Sumi H, Lee YH, Muroyama H, Matsui T, Kamijo M, Mimuro S, et al. Effect of carbon deposition by carbon monoxide disproportionation on electrochemical characteristics at low temperature operation for solid oxide fuel cells. J Power Sources 2011;196:4451–7. https://doi.org/10.1016/j.jpowsour.2011.01.061.

[115] Zhao K, Du Y. Calcium-doped ceria materials for anode of solid oxide fuel cells running on methane fuel. J Power Sources 2017;347:79–85. https://doi.org/10.1016/j.jpowsour.2017.01.113.

[116] Rabuni MF, Li T, Punmeechao P, Li K. Electrode design for direct-methane micro-tubular solid oxide fuel cell (MT-SOFC). J Power Sources 2018;384:287–94. https://doi.org/10.1016/j.jpowsour.2018.03.002.

[117] Kaur G, Basu S. Physical characterization and electrochemical performance of copper-iron-ceria-YSZ anode-based SOFCs in H2 and methane fuels. Int J Energy Res 2015;39:1345–54. https://doi.org/10.1002/er.3332.

[118] Sarruf BJM, Hong JE, Steinberger-Wilckens R, de Miranda PEV. Ceria-Co-Cu-based SOFC anode for direct utilisation of methane or ethanol as fuels. Int J Hydrogen Energy 2020;45:5297–308. https://doi.org/10.1016/j.ijhydene.2019.04.075.

[119] Sarıboğa V, Faruk Öksüzömer MA. Cu-CeO2anodes for solid oxide fuel cells: Determination of infiltration characteristics. J Alloys Compd 2016;688:323–31. https://doi.org/10.1016/j.jallcom.2016.07.217.

[120] Tao S, Irvine JTS. A redox-stable efficient anode for solid-oxide fuel cells. Nat Mater 2003;2:320–3. https://doi.org/10.1038/nmat871.

[121] Zhou X, Yan N, Chuang KT, Luo J. Progress in La-doped SrTiO3 (LST)-based anode materials for solid oxide fuel cells. RSC Adv 2014;4:118–31. https://doi.org/10.1039/c3ra42666a.

[122] Li X, Zhao H, Zhou X, Xu N, Xie Z, Chen N. Electrical conductivity and structural stability of La-doped SrTiO 3 with A-site deficiency as anode materials for solid oxide fuel cells. Int J Hydrogen Energy 2010;35:7913–8. https://doi.org/10.1016/j.ijhydene.2010.05.043.

[123] Huang Y-H, Dass RI, Xing Z-L, Goodenough JB. Double Perovskites as Anode. Science (80-) 2006;2:254–8. https://doi.org/10.1126/science.1125877.

[124] Hodges J, Huq A, Bugaris D, Zur Loye H-C, Muñoz-García A, Pavone M, et al. Unveiling Structure Property Relationships in Sr2Fe1.5Mo0.5O6 , an Electrode Material for Symmetric Solid Oxide Fuel Cells. J Am Chem Soc 2012;134:6826.

[125] Liu Q, Dong X, Xiao G, Zhao F, Chen F. A novel electrode material for symmetrical SOFCs. Adv Mater 2010;22:5478–82. https://doi.org/10.1002/adma.201001044.

[126] Qin M, Tan T, Li K, Wang Z, Yang H, Liu Z, et al. In-situ exsolved FeRu alloy nanoparticles on Ruddlesden-Popper oxides for direct hydrocarbon fuel solid oxide fuel cells. Int J Hydrogen Energy 2020;45:21464–72. https://doi.org/10.1016/j.ijhydene.2020.05.242.

[127] Cao Z, Fan L, Zhang G, Shao K, He C, Zhang Q, et al. Titanium-substituted ferrite perovskite: An excellent sulfur and coking tolerant anode catalyst for SOFCs. Catal Today 2019;330:217–21. https://doi.org/10.1016/j.cattod.2018.04.023.

[128] Ding H, Tao Z, Liu S, Yang Y. A redox-stable direct-methane solid oxide fuel cell (SOFC) with Sr2FeNb0.2Mo0.8O6−δ double perovskite as anode material. J Power Sources 2016;327:573–9. https://doi.org/10.1016/j.jpowsour.2016.07.101.

[129] Ding H, Zhou D, Liu S, Wu W, Yang Y, Yang Y, et al. Electricity generation in dry methane by a durable ceramic fuel cell with high-performing and coking-resistant layered perovskite anode. Appl Energy 2019;233–234:37–43. https://doi.org/10.1016/j.apenergy.2018.10.013.

[130] Duranti L, Luisetto I, Licoccia S, Gaudio C Del, Bartolomeo E Di. Electrochemical performance and stability of LSFMn+NiSDC anode in dry methane. Electrochim Acta 2020;362:137116. https://doi.org/10.1016/j.electacta.2020.137116.

[131] Shahid M, He C, Sankarasubramanian S, Ramani V, Basu S. Enhanced methane electrooxidation by ceria and nickel oxide impregnated perovskite anodes in solid oxide fuel cells. Int J Hydrogen Energy 2020;45:11287–96. https://doi.org/10.1016/j.ijhydene.2020.02.040.

[132] Sarno C, Luisetto I, Zurlo F, Licoccia S, Di Bartolomeo E. Lanthanum chromite based composite anodes for dry reforming of methane. Int J Hydrogen Energy

2018;43:14742–50. https://doi.org/10.1016/j.ijhydene.2018.06.021.
[133] Kong X, Tian Y, Zhou X, Wu X, Zhang J. Surface tuned La0.9Ca0.1Fe0.9Nb0.1O3-δ based anode for direct methane solid oxide fuel cells by infiltration method. Electrochim Acta 2017;234:71–81. https://doi.org/10.1016/j.electacta.2017.03.046.
[134] Zhou N, Yin Y-M, Chen Z, Song Y, Yin J, Zhou D, et al. A Regenerative Coking and Sulfur Resistant Composite Anode with Cu Exsolution for Intermediate Temperature Solid Oxide Fuel Cells. J Electrochem Soc 2018;165:F629–34. https://doi.org/10.1149/2.0841809jes.
[135] Zhao J, Pu Y, Li L, Zhou W, Guo Y. Efficient Ferrite-Based Perovskite Anode for Solid Oxide Fuel Cells with A-Site and B-Site Co-exsolution. Energy and Fuels 2020;34:10100–8. https://doi.org/10.1021/acs.energyfuels.0c02140.
[136] Zhang W, Wang H, Guan K, Meng J, Wei Z, Liu X, et al. Enhanced Anode Performance and Coking Resistance by in Situ Exsolved Multiple-Twinned Co-Fe Nanoparticles for Solid Oxide Fuel Cells. ACS Appl Mater Interfaces 2020;12:461–73. https://doi.org/10.1021/acsami.9b14655.
[137] Wang W, Zhu C, Xie K, Gan L. High performance, coking-resistant and sulfur-tolerant anode for solid oxide fuel cell. J Power Sources 2018;406:1–6. https://doi.org/10.1016/j.jpowsour.2018.10.040.
[138] Peng X, Tian Y, Liu Y, Wang W, Jing chen, Li J, et al. A double perovskite decorated carbon-tolerant redox electrode for symmetrical SOFC. Int J Hydrogen Energy 2020;45:14461–9. https://doi.org/10.1016/j.ijhydene.2020.03.151.
[139] Ding H, Fang S, Yang Y, Yang Y, Wu W, Tao Z. High-performing and stable electricity generation by ceramic fuel cells operating in dry methane over 1000 hours. J Power Sources 2018;401:322–8. https://doi.org/10.1016/j.jpowsour.2018.08.084.
[140] Qiu P, Yang X, Wang W, Wei T, Lu Y, Lin J, et al. Redox-Reversible Electrode Material for Direct Hydrocarbon Solid Oxide Fuel Cells. ACS Appl Mater Interfaces 2020;12:13988–95. https://doi.org/10.1021/acsami.0c00922.
[141] Lin Y, Zhan Z, Barnett SA. Improving the stability of direct-methane solid oxide fuel cells using anode barrier layers. J Power Sources 2006;158:1313–6. https://doi.org/10.1016/j.jpowsour.2005.09.060.
[142] Rosensteel WA, Babiniec SM, Storjohann DD, Persky J, Sullivan NP. Use of anode barrier layers in tubular solid-oxide fuel cells for robust operation on hydrocarbon fuels. J Power Sources 2012;205:108–13. https://doi.org/10.1016/j.jpowsour.2012.01.035.
[143] Zhan Z, Barnett SA. An octane-fueled solid oxide fuel cell. Science (80-)

2005;308:844–7. https://doi.org/10.1126/science.1109213.

[144] Zhao J, Xu X, Li M, Zhou W, Liu S, Zhu Z. Coking-resistant Ce0.8Ni0.2O2-δ internal reforming layer for direct methane solid oxide fuel cells. Electrochim Acta 2018;282:402–8. https://doi.org/10.1016/j.electacta.2018.06.088.

[145] Chien AC, Lin EY, Lai AD. Aid of a metallic functional layer on Ni/YSZ anode for Direct Methane Fuel Cell. Int J Hydrogen Energy 2020;45:23526–32. https://doi.org/10.1016/j.ijhydene.2020.06.169.

[146] Zhao J, Xu X, Zhou W, Blakey I, Liu S, Zhu Z. Proton-conducting la-doped ceria-based internal reforming layer for direct methane solid oxide fuel cells. ACS Appl Mater Interfaces 2017;9:33758–65. https://doi.org/10.1021/acsami.7b07938.

[147] Lv X, Chen H, Zhou W, Cheng F, Li SD, Shao Z. Direct-methane solid oxide fuel cells with an in situ formed Ni–Fe alloy composite catalyst layer over Ni–YSZ anodes. Renew Energy 2020;150:334–41. https://doi.org/10.1016/j.renene.2019.12.126.

[148] Chen Y, deGlee B, Tang Y, Wang Z, Zhao B, Wei Y, et al. A robust fuel cell operated on nearly dry methane at 500 °C enabled by synergistic thermal catalysis and electrocatalysis. Nat Energy 2018;3:1042–50. https://doi.org/10.1038/s41560-018-0262-5.

[149] Ye XF, Wang SR, Wang ZR, Xiong L, Sun XF, Wen TL. Use of a catalyst layer for anode-supported SOFCs running on ethanol fuel. J Power Sources 2008;177:419–25. https://doi.org/10.1016/j.jpowsour.2007.11.054.

[150] Liu X, Zhan Z, Meng X, Huang W, Wang S, Wen T. Enabling catalysis of Ru-CeO2 for propane oxidation in low temperature solid oxide fuel cells. J Power Sources 2012;199:138–41. https://doi.org/10.1016/j.jpowsour.2011.09.072.

[151] da Silva AAA, Steil MC, Tabuti FN, Rabelo-Neto RC, Noronha FB, Mattos L V., et al. The role of the ceria dopant on Ni / doped-ceria anodic layer cermets for direct ethanol solid oxide fuel cell. Int J Hydrogen Energy 2021;46:4309–28. https://doi.org/10.1016/j.ijhydene.2020.10.155.

[152] Augusto BL, Noronha FB, Fonseca FC, Tabuti FN, Colman RC, Mattos L V. Nickel/gadolinium-doped ceria anode for direct ethanol solid oxide fuel cell. Int J Hydrogen Energy 2014;39:11196–209. https://doi.org/10.1016/j.ijhydene.2014.05.088.

[153] Chang H, Chen H, Shao Z, Shi J, Bai J, Li S-D. In situ fabrication of (Sr,La)FeO 4 with CoFe alloy nanoparticles as an independent catalyst layer for direct methane-based solid oxide fuel cells with a nickel cermet anode. J Mater Chem A 2016;4:13997–4007. https://doi.org/10.1039/C6TA04639H.

[154] Majewski AJ, Dhir A. Direct Utilization of Methane in Microtubular-SOFC. J Electrochem Soc 2016;163:F272–7. https://doi.org/10.1149/2.1051603jes.
[155] Lu X, Li T, Bertei A, Cho JIS, Heenan TMM, Rabuni MF, et al. The application of hierarchical structures in energy devices: New insights into the design of solid oxide fuel cells with enhanced mass transport. Energy Environ Sci 2018;11:2390–403. https://doi.org/10.1039/c8ee01064a.
[156] Chen B, Xu H, Ni M. Modelling of finger-like channelled anode support for SOFCs application. Sci Bull 2016;61:1324–32. https://doi.org/10.1007/s11434-016-1131-x.
[157] Wang J, Fan D, Yu L, Wei T, Hu X, Ye Z, et al. Efficient conversion of methane into power via microchanneled solid oxide fuel cells. J Power Sources 2020;453:227848. https://doi.org/10.1016/j.jpowsour.2020.227848.
[158] Li T, Lu X, Rabuni MF, Rabuni MF, Wang B, Farandos NM, et al. High-performance fuel cell designed for coking-resistance and efficient conversion of waste methane to electrical energy. Energy Environ Sci 2020;13:1879–87. https://doi.org/10.1039/d0ee00070a.
[159] Hagen A, Barfod R, Vang Hendriksen P, Liu YL, Ramousse S. Effect of operational conditions on long-term stability of SOFCs. Proc - Electrochem Soc 2005;PV 2005-07:503–13. https://doi.org/10.1149/200507.0503pv.
[160] Duan C, Kee RJ, Zhu H, Karakaya C, Chen Y, Ricote S, et al. Highly durable, coking and sulfur tolerant, fuel-flexible protonic ceramic fuel cells. Nature 2018;557:217–22. https://doi.org/10.1038/s41586-018-0082-6.
[161] Sumi H, Yamaguchi T, Shimada H, Fujishiro Y, Awano M. Internal Partial Oxidation Reforming of Butane and Steam Reforming of Ethanol for Anode-supported Microtubular Solid Oxide Fuel Cells. Fuel Cells 2017;17:875–81. https://doi.org/10.1002/fuce.201700154.
[162] Chen Y, Lu M, Yang H, Yao Y, Tao T, Lu S, et al. 80 Hours operation of a tubular solid oxide fuel cell using propane/air. Appl Energy 2020;272:115099. https://doi.org/10.1016/j.apenergy.2020.115099.
[163] Hong JE, Usman M, Lee SB, Song RH, Lim TH. Thermally self-sustaining operation of tubular solid oxide fuel cells integrated with a hybrid partial oxidation reformer using propane. Energy Convers Manag 2019;189:132–42. https://doi.org/10.1016/j.enconman.2019.04.001.
[164] Zhan Z, Liu J, Barnett SA. Operation of anode-supported solid oxide fuel cells on propane-air fuel mixtures. Appl Catal A Gen 2004;262:255–9.

https://doi.org/10.1016/j.apcata.2003.11.033.
[165] Zhan Z, Barnett SA. Use of a catalyst layer for propane partial oxidation in solid oxide fuel cells. Solid State Ionics 2005;176:871–9. https://doi.org/10.1016/j.ssi.2004.12.005.
[166] He Z, Li C, Chen C, Tong Y, Luo T, Zhan Z. Membrane-assisted propane partial oxidation for solid oxide fuel cell applications. J Power Sources 2018;392:200–5. https://doi.org/10.1016/j.jpowsour.2018.04.085.
[167] Huang TJ, Wu CY, Wang CH. Fuel processing in direct propane solid oxide fuel cell and carbon dioxide reforming of propane over Ni-YSZ. Fuel Process Technol 2011;92:1611–6. https://doi.org/10.1016/j.fuproc.2011.04.007.
[168] Thieu CA, Park S, Kim H, Ji H Il, Lee JH, Yoon KJ, et al. Improved electrochemical performance and durability of butane-operating low-temperature solid oxide fuel cell through palladium infiltration. Int J Energy Res 2020;44:9995–10007. https://doi.org/10.1002/er.5547.
[169] Yang L, Wang S, Blinn K, Liu M, Liu Z, Cheng Z, et al. Enhanced Sulfur and Coking Tolerance of a Mixed Ion Conductor for SOFCs: BaZr0.1Ce0.7Y0.2-xYbxO3-. Science (80-) 2009;326:126–9. https://doi.org/10.1126/science.1174811.
[170] Sumi H, Suda E, Mori M, Weber A. Infiltration of Lanthanum Doped Ceria into Nickel-Zirconia Anodes for Direct Butane Utilization in Solid Oxide Fuel Cells. J Electrochem Soc 2019;166:F301–5. https://doi.org/10.1149/2.0891904jes.
[171] Sumi H, Yamaguchi T, Shimada H, Hamamoto K, Suzuki T, Barnett SA. Direct Butane Utilization on Ni-(Y2O3)0.08(ZrO2)0.92-(Ce0.9Gd0.1)O1.95 Composite Anode-Supported Microtubular Solid Oxide Fuel Cells. Electrocatalysis 2017;8:288–93. https://doi.org/10.1007/s12678-017-0369-7.
[172] Sumi H, Yamaguchi T, Hamamoto K, Suzuki T, Fujishiro Y. Impact of direct butane microtubular solid oxide fuel cells. J Power Sources 2012;220:74–8. https://doi.org/10.1016/j.jpowsour.2012.07.106.
[173] Thieu CA, Ji H Il, Kim H, Yoon KJ, Lee JH, Son JW. Palladium incorporation at the anode of thin-film solid oxide fuel cells and its effect on direct utilization of butane fuel at 600 °C. Appl Energy 2019;243:155–64. https://doi.org/10.1016/j.apenergy.2019.03.203.
[174] Yang L, Choi Y, Qin W, Chen H, Blinn K, Liu M, et al. Promotion of water-mediated carbon removal by nanostructured barium oxide/nickel interfaces in solid oxide fuel cells. Nat Commun 2011;2. https://doi.org/10.1038/ncomms1359.
[175] Zhang Y, Yu F, Wang X, Zhou Q, Liu J, Liu M. Direct operation of Ag-based anode

solid oxide fuel cells on propane. J Power Sources 2017;366:56–64. https://doi.org/10.1016/j.jpowsour.2017.08.111.

[176] Xu N, Zhu T, Yang Z, Han M. Co-synthesis of LSCFN-GDC electrode for symmetric solid oxide fuel cell running on propane. Electrochim Acta 2018;265:259–64. https://doi.org/10.1016/j.electacta.2017.12.096.

[177] Lai KY, Manthiram A. Self-Regenerating Co-Fe Nanoparticles on Perovskite Oxides as a Hydrocarbon Fuel Oxidation Catalyst in Solid Oxide Fuel Cells. Chem Mater 2018;30:2515–25. https://doi.org/10.1021/acs.chemmater.7b04569.

[178] Zhan Z, Barnett SA. Solid oxide fuel cells operated by internal partial oxidation reforming of iso-octane. J Power Sources 2006;155:353–7. https://doi.org/10.1016/j.jpowsour.2005.04.015.

[179] Zhan Z, Barnett SA. Operation of ceria-electrolyte solid oxide fuel cells on iso-octane-air fuel mixtures. J Power Sources 2006;157:422–9. https://doi.org/10.1016/j.jpowsour.2005.08.008.

[180] Liu M, Choi YM, Yang L, Blinn K, Qin W, Liu P, et al. Direct octane fuel cells: A promising power for transportation. Nano Energy 2012;1:448–55. https://doi.org/10.1016/j.nanoen.2012.02.006.

[181] Yamaji K, Kishimoto H, Xiong Y, Horita T, Sakai N, Brito ME, et al. Feasibility of Ni-based cermet anode for direct HC SOFCs: Fueling ethane at a low S/C condition to Ni-ScSZ anode-supported cell. J Power Sources 2006;159:885–90. https://doi.org/10.1016/j.jpowsour.2005.12.087.

[182] Gao Y, Neal L, Ding D, Wu W, Baroi C, Gaffney AM, et al. Recent Advances in Intensified Ethylene Production - A Review. ACS Catal 2019;9:8592–621. https://doi.org/10.1021/acscatal.9b02922.

[183] Yang X, Wei T, Chi B, Pu J, Li J. Lanthanum manganite-based perovskite as a catalyst for co-production of ethylene and hydrogen by ethane dehydrogenation. J Catal 2019;377:629–37. https://doi.org/10.1016/j.jcat.2019.08.008.

[184] Li J, Hou J, Xi X, Lu Y, Li M, Fan Y, et al. Cogeneration of ethylene and electricity in symmetrical protonic solid oxide fuel cells based on a La0.6Sr0.4Fe0.8Nb0.1Cu0.1O3-: δelectrode. J Mater Chem A 2020;8:25978–85. https://doi.org/10.1039/d0ta08974e.

[185] Liu S, Chuang KT, Luo J-L. Double-Layered Perovskite Anode with in Situ Exsolution of a Co–Fe Alloy To Cogenerate Ethylene and Electricity in a Proton-Conducting Ethane Fuel Cell. ACS Catal 2016;6:760–8. https://doi.org/10.1021/acscatal.5b02296.

[186] Liu S, Liu Q, Fu XZ, Luo JL. Cogeneration of ethylene and energy in protonic fuel cell

with an efficient and stable anode anchored with in-situ exsolved functional metal nanoparticles. Appl Catal B Environ 2018;220:283–9. https://doi.org/10.1016/j.apcatb.2017.08.051.

[187] Hook A, Massa JD, Celik FE. Effect of Tin Coverage on Selectivity for Ethane Dehydrogenation over Platinum-Tin Alloys. J Phys Chem C 2016;120:27307–18. https://doi.org/10.1021/acs.jpcc.6b08407.

[188] Fu XZ, Luo JL, Sanger AR, Danilovic N, Chuang KT. An integral proton conducting SOFC for simultaneous production of ethylene and power from ethane. Chem Commun 2010;46:2052–4. https://doi.org/10.1039/b926928b.

[189] Weckhuysen BM, Schoonheydt RA. Alkane dehydrogenation over supported chromium oxide catalysts. Catal Today 1999;51:223–32. https://doi.org/10.1016/S0920-5861(99)00047-4.

[190] Norby T. Solid-state protonic conductors: Principles, properties, progress and prospects. Solid State Ionics 1999;125:1–11. https://doi.org/10.1016/S0167-2738(99)00152-6.

[191] Li JH, Fu XZ, Zhou GH, Luo JL, Chuang KT, Sanger AR. FeCr2O4 nanoparticles as anode catalyst for ethane proton conducting fuel cell reactors to coproduce ethylene and electricity. Adv Phys Chem 2011;2011. https://doi.org/10.1155/2011/407480.

[192] Fu XZ, Lin JY, Xu S, Luo JL, Chuang KT, Sanger AR, et al. CO2 emission free co-generation of energy and ethylene in hydrocarbon SOFC reactors with a dehydrogenation anode. Phys Chem Chem Phys 2011;13:19615–23. https://doi.org/10.1039/c1cp22837d.

[193] Lin JY, Shao L, Si FZ, Liu SB, Fu XZ, Luo JL. Co2CrO4 Nanopowders as an Anode Catalyst for Simultaneous Conversion of Ethane to Ethylene and Power in Proton-Conducting Fuel Cell Reactors. J Phys Chem C 2018;122:4165–71. https://doi.org/10.1021/acs.jpcc.7b11680.

[194] Liu S, Behnamian Y, Chuang KT, Liu Q, Luo JL. A-site deficient La0.2Sr0.7TiO3-δ anode material for proton conducting ethane fuel cell to cogenerate ethylene and electricity. J Power Sources 2015;298:23–9. https://doi.org/10.1016/j.jpowsour.2015.08.032.

[195] Cimenti M, Alzate-Restrepo V, Hill JM. Direct utilization of methanol on impregnated Ni/YSZ and Ni-Zr0.35Ce0.65O2/YSZ anodes for solid oxide fuel cells. J Power Sources 2010;195:4002–12. https://doi.org/10.1016/j.jpowsour.2009.12.119.

[196] Elharati MA, Dewa M, Bkour Q, Mohammed Hussain A, Miura Y, Dong S, et al. Internal Reforming Solid Oxide Fuel Cell System Operating under Direct Ethanol Feed

Condition. Energy Technol 2020;8:1–11. https://doi.org/10.1002/ente.202000350.

[197] Dalena F, Senatore A, Marino A, Gordano A, Basile M, Basile A. Methanol Production and Applications: An Overview. Elsevier B.V.; 2018. https://doi.org/10.1016/B978-0-444-63903-5.00001-7.

[198] Bozzano G, Manenti F. Efficient methanol synthesis: Perspectives, technologies and optimization strategiesa. Prog Energy Combust Sci 2016;56:71–105. https://doi.org/10.1016/j.pecs.2016.06.001.

[199] Palo DR, Dagle RA, Holladay JD. Methanol steam reforming for hydrogen production. Chem Rev 2007;107:3992–4021. https://doi.org/10.1021/cr050198b.

[200] Cimenti M, Hill JM. Thermodynamic analysis of solid oxide fuel cells operated with methanol and ethanol under direct utilization, steam reforming, dry reforming or partial oxidation conditions. J Power Sources 2009;186:377–84. https://doi.org/10.1016/j.jpowsour.2008.10.043.

[201] Sasaki K, Watanabe K, Teraoka Y. Direct-Alcohol SOFCs: Current-Voltage Characteristics and Fuel Gas Compositions. J Electrochem Soc 2004;151:A965. https://doi.org/10.1149/1.1756884.

[202] Jiang Y, Virkar A V. A High Performance, Anode-Supported Solid Oxide Fuel Cell Operating on Direct Alcohol. J Electrochem Soc 2001;148:A706. https://doi.org/10.1149/1.1375166.

[203] Liu M, Peng R, Dong D, Gao J, Liu X, Meng G. Direct liquid methanol-fueled solid oxide fuel cell. J Power Sources 2008;185:188–92. https://doi.org/10.1016/j.jpowsour.2008.06.076.

[204] Meng X, Zhan Z, Liu X, Wu H, Wang S, Wen T. Low-temperature ceria-electrolyte solid oxide fuel cells for efficient methanol oxidation. J Power Sources 2011;196:9961–4. https://doi.org/10.1016/j.jpowsour.2011.08.002.

[205] Qu J, Wang W, Chen Y, Wang F, Ran R, Shao Z. Ethylene glycol as a new sustainable fuel for solid oxide fuel cells with conventional nickel-based anodes. Appl Energy 2015;148:1–9. https://doi.org/10.1016/j.apenergy.2015.03.051.

[206] Eigenbrodt BC, Pomfret MB, Steinhurst DA, Owrutsky JC, Walker RA. Direct, in situ optical studies of Ni-YSZ anodes in solid oxide fuel cells operating with methanol and methane. J Phys Chem C 2011;115:2895–903. https://doi.org/10.1021/jp109292r.

[207] Jeon OS, Lee JG, Ji Y, Lee SH, Kwon O, Kim JP, et al. Effects of dispersed copper nanoparticles on Ni-ceria based dry methanol fuelled low temperature solid oxide fuel cells. RSC Adv 2019;9:6320–7. https://doi.org/10.1039/c8ra07586g.

[208] Saunders GJ, Preece J, Kendall K. Formulating liquid hydrocarbon fuels for SOFCs. J Power Sources 2004;131:23–6. https://doi.org/10.1016/j.jpowsour.2004.01.040.

[209] Jang DY, Koo J, Choi HR, Kim JW, Jeong HJ, Prinz FB, et al. Coke-Free Oxidation of Methanol in Solid Oxide Fuel Cells with Heterogeneous Nickel-Palladium Catalysts Prepared by Atomic Layer Deposition. ACS Sustain Chem Eng 2020;8:10529–35. https://doi.org/10.1021/acssuschemeng.0c03020.

[210] Ru Y, Sang J, Xia C, Wei WCJ, Guan W. Durability of direct internal reforming of methanol as fuel for solid oxide fuel cell with double-sided cathodes. Int J Hydrogen Energy 2020;45:7069–76. https://doi.org/10.1016/j.ijhydene.2019.12.222.

[211] Li P, Wang R, Yan F. Effect of Pr addition into Ni based anode on direct methanol fueled solid oxide fuel cell. J Electroanal Chem 2020;859:113846. https://doi.org/10.1016/j.jelechem.2020.113846.

[212] Yao X, Fan L, Gan T, Hou N, Li P, Zhao Y, et al. Coking-resistant NbOx-Ni-Ce0.8Sm0.2O1.9 anode material for methanol-fueled solid oxide fuel cells. Int J Hydrogen Energy 2018;43:12748–55. https://doi.org/10.1016/j.ijhydene.2018.03.186.

[213] Li P, Fang L, Hou N, Li J, Yao X, Gan T, et al. Improved Performance of Ni-Mo Based Anode for Direct Methanol Solid Oxide Fuel Cells with the Addition of Rare Earth Oxides. J Electrochem Soc 2017;164:F1142–8. https://doi.org/10.1149/2.1021712jes.

[214] Li P, Yu B, Li J, Yao X, Zhao Y, Li Y. Improved activity and stability of Ni-Ce0.8Sm0.2O1.9 anode for solid oxide fuel cells fed with methanol through addition of molybdenum. J Power Sources 2016;320:251–6. https://doi.org/10.1016/j.jpowsour.2016.04.100.

[215] Ding G, Gan T, Yu J, Li P, Yao X, Hou N, et al. Carbon-resistant Ni1-xCox-Ce0.8Sm0.2O1.9 anode for solid oxide fuel cells fed with methanol. Catal Today 2017;298:250–7. https://doi.org/10.1016/j.cattod.2017.03.060.

[216] de Araujo Guilherme A, Dantas PVF, Padilha CE de A, dos Santos ES, de Macedo GR. Ethanol production from sugarcane bagasse: Use of different fermentation strategies to enhance an environmental-friendly process. J Environ Manage 2019;234:44–51. https://doi.org/10.1016/j.jenvman.2018.12.102.

[217] Taghizadeh-Alisaraei A, Motevali A, Ghobadian B. Ethanol production from date wastes: Adapted technologies, challenges, and global potential. Renew Energy 2019;143:1094–110. https://doi.org/10.1016/j.renene.2019.05.048.

[218] Vaidya PD, Rodrigues AE. Insight into steam reforming of ethanol to produce hydrogen for fuel cells. Chem Eng J 2006;117:39–49. https://doi.org/10.1016/j.cej.2005.12.008.

[219] Cimenti M, Hill JM. Direct utilization of methanol and ethanol in solid oxide fuel cells using Cu-Co(Ru)/Zr0.35Ce0.65O2-δ anodes. J Power Sources 2010;195:3996–4001. https://doi.org/10.1016/j.jpowsour.2009.12.122.

[220] Sharma YC, Kumar A, Prasad R, Upadhyay SN. Ethanol steam reforming for hydrogen production: Latest and effective catalyst modification strategies to minimize carbonaceous deactivation. Renew Sustain Energy Rev 2017;74:89–103. https://doi.org/10.1016/j.rser.2017.02.049.

[221] Moraes TS, Neto RCR, Ribeiro MC, Mattos LV, Kourtelesis M, Verykios X, et al. Effects of ceria morphology on catalytic performance of Ni/CeO2 catalysts for low temperature steam reforming of ethanol. Top Catal 2015;58:281–94. https://doi.org/10.1007/s11244-015-0369-x.

[222] Huang B, Wang SR, Liu RZ, Wen TL. Preparation and performance characterization of the Fe-Ni/ScSZ cermet anode for oxidation of ethanol fuel in SOFCs. J Power Sources 2007;167:288–94. https://doi.org/10.1016/j.jpowsour.2007.02.075.

[223] Farrell B, Linic S. Direct electrochemical oxidation of ethanol on SOFCs: Improved carbon tolerance of Ni anode by alloying. Appl Catal B Environ 2016;183:386–93. https://doi.org/10.1016/j.apcatb.2015.11.002.

[224] Ye XF, Huang B, Wang SR, Wang ZR, Xiong L, Wen TL. Preparation and performance of a Cu-CeO2-ScSZ composite anode for SOFCs running on ethanol fuel. J Power Sources 2007;164:203–9. https://doi.org/10.1016/j.jpowsour.2006.10.056.

[225] Ye XF, Wang SR, Hu Q, Chen JY, Wen TL, Wen ZY. Improvement of Cu-CeO2 anodes for SOFCs running on ethanol fuels. Solid State Ionics 2009;180:276–81. https://doi.org/10.1016/j.ssi.2008.11.010.

[226] Huang B, Wang SR, Liu RZ, Ye XF, Nie HW, Sun XF, et al. Performance of La0.75Sr0.25Cr0.5Mn0.5O3−δ perovskite-structure anode material at lanthanum gallate electrolyte for IT-SOFC running on ethanol fuel. J Power Sources 2007;167:39–46. https://doi.org/10.1016/j.jpowsour.2007.02.022.

[227] Monteiro NK, Noronha FB, Da Costa LOO, Linardi M, Fonseca FC. A direct ethanol anode for solid oxide fuel cell based on a chromite-manganite with catalytic ruthenium nanoparticles. Int J Hydrogen Energy 2012;37:9816–29. https://doi.org/10.1016/j.ijhydene.2012.03.157.

[228] Jiang SP, Ye Y, He T, Ho SB. Nanostructured palladium-La0.75Sr0.25Cr0.5Mn0.5O3/Y2O3-ZrO2 composite anodes for direct methane and ethanol solid oxide fuel cells. J Power Sources 2008;185:179–82.

https://doi.org/10.1016/j.jpowsour.2008.06.099.
[229] Ye XF, Wang SR, Wang ZR, Hu Q, Sun XF, Wen TL, et al. Use of La0.75Sr0.25Cr0.5Mn 0.5O3 materials in composite anodes for direct ethanol solid oxide fuel cells. J Power Sources 2008;183:512–7. https://doi.org/10.1016/j.jpowsour.2008.05.064.
[230] Huang B, Zhu X jian, Hu W qi, Wang Y yun, Yu Q chun. Characterization of the Ni-ScSZ anode with a LSCM-CeO2 catalyst layer in thin film solid oxide fuel cell running on ethanol fuel. J Power Sources 2010;195:3053–9. https://doi.org/10.1016/j.jpowsour.2009.11.126.
[231] Ye XF, Wang SR, Hu Q, Wang ZR, Wen TL, Wen ZY. Improvement of multi-layer anode for direct ethanol Solid Oxide Fuel Cells. Electrochem Commun 2009;11:823–6. https://doi.org/10.1016/j.elecom.2009.02.003.
[232] Hahn TA. Thermal expansion of copper from 20 to 800 k - standard reference material 736. J Appl Phys 1970;41:5096–101. https://doi.org/10.1063/1.1658614.
[233] Wang Y, Liu ZK, Chen LQ. Thermodynamic properties of Al, Ni, NiAl, and Ni3Al from first-principles calculations. Acta Mater 2004;52:2665–71. https://doi.org/10.1016/j.actamat.2004.02.014.
[234] Hayashi H, Kanoh M, Quan CJ, Inaba H, Wang S, Dokiya M, et al. Thermal expansion of Gd-doped ceria and reduced ceria. Solid State Ionics 2000;132:227–33. https://doi.org/10.1016/s0167-2738(00)00646-9.
[235] Mori M, Yamamoto T, Itoh H, Inaba H, Tagawa H. Thermal Expansion of Nickel-Zirconia Anodes in Solid Oxide Fuel Cells during Fabrication and Operation. J Electrochem Soc 1998;145:1374–81. https://doi.org/10.1149/1.1838468.
[236] Liao M, Wang W, Ran R, Shao Z. Development of a Ni-Ce0.8Zr0.2O2 catalyst for solid oxide fuel cells operating on ethanol through internal reforming. J Power Sources 2011;196:6177–85. https://doi.org/10.1016/j.jpowsour.2011.03.018.
[237] Lo Faro M, Reis RM, Saglietti GGA, Oliveira VL, Zignani SC, Trocino S, et al. Solid oxide fuel cells fed with dry ethanol: The effect of a perovskite protective anodic layer containing dispersed Ni-alloy @ FeOx core-shell nanoparticles. Appl Catal B Environ 2018;220:98–110. https://doi.org/10.1016/j.apcatb.2017.08.010.
[238] Sun LL, Liu LL, Luo LH, Wu YF, Shi JJ, Cheng L, et al. Facile synthesis of flower-like Pd catalyst for direct ethanol solid oxide fuel cell. Ranliao Huaxue Xuebao/Journal Fuel Chem Technol 2016;44:607–12. https://doi.org/10.1016/s1872-5813(16)30027-5.
[239] Nobrega SD, Gelin P, Georges S, Steil MC, Augusto BL, Noronha FB, et al. A Fuel-

Flexible Solid Oxide Fuel Cell Operating in Gradual Internal Reforming. J Electrochem Soc 2014;161:F354–9. https://doi.org/10.1149/2.107403jes.

[240] Steil MC, Nobrega SD, Georges S, Gelin P, Uhlenbruck S, Fonseca FC. Durable direct ethanol anode-supported solid oxide fuel cell. Appl Energy 2017;199:180–6. https://doi.org/10.1016/j.apenergy.2017.04.086.

[241] Zhang B, Tang X, Li Y, Cai W, Xu Y, Shen W. Steam reforming of bio-ethanol for the production of hydrogen over ceria-supported Co, Ir and Ni catalysts. Catal Commun 2006;7:367–72. https://doi.org/10.1016/j.catcom.2005.12.014.

[242] Wang W, Su C, Ran R, Zhao B, Shao Z, O. Tade M, et al. Nickel-based anode with water storage capability to mitigate carbon deposition for direct ethanol solid oxide fuel cells. ChemSusChem 2014;7:1719–28. https://doi.org/10.1002/cssc.201301341.

[243] Wang W, Chen Y, Wang F, Tade MO, Shao Z. Enhanced electrochemical performance, water storage capability and coking resistance of a Ni+BaZr0.1Ce0.7Y0.1Yb0.1O3-δ anode for solid oxide fuel cells operating on ethanol. Chem Eng Sci 2015;126:22–31. https://doi.org/10.1016/j.ces.2014.12.011.

[244] Giddey S, Badwal SPS, Kulkarni A, Munnings C. A comprehensive review of direct carbon fuel cell technology. Prog Energy Combust Sci 2012;38:360–99. https://doi.org/10.1016/j.pecs.2012.01.003.

[245] Duan N, Xue Y, Ma J, Han Y, Xu M, Chi B, et al. Liquid antimony-silver alloys as anodes for direct carbon solid oxide fuel cells. J Power Sources 2018;397:170–6. https://doi.org/10.1016/j.jpowsour.2018.07.011.

[246] Ma M, Qiao J, Yang X, Xu C, Ren R, Sun W, et al. Enhanced Stability and Catalytic Activity on Layered Perovskite Anode for High-Performance Hybrid Direct Carbon Fuel Cells. ACS Appl Mater Interfaces 2020;12:12938–48. https://doi.org/10.1021/acsami.0c02866.

[247] Gür TM. Critical review of carbon conversion in “carbon fuel cells.” Chem Rev 2013;113:6179–206. https://doi.org/10.1021/cr400072b.

[248] Nakagawa N, Ishida M. Performance of an internal direct-oxidation carbon fuel cell and its evaluation by graphic exergy analysis. Ind Eng Chem Res 1988;27:1181–5. https://doi.org/10.1021/ie00079a016.

[249] Xie Y, Tang Y, Liu J. A verification of the reaction mechanism of direct carbon solid oxide fuel cells. J Solid State Electrochem 2013;17:121–7. https://doi.org/10.1007/s10008-012-1866-5.

[250] Yu F, Zhang Y, Yu L, Cai W, Yuan L, Liu J, et al. All-solid-state direct carbon fuel

cells with thin yttrium-stabilized-zirconia electrolyte supported on nickel and iron bimetal-based anodes. Int J Hydrogen Energy 2016;41:9048–58. https://doi.org/10.1016/j.ijhydene.2016.04.063.

[251] Xie Y, Cai W, Xiao J, Tang Y, Liu J, Liu M. Electrochemical gas-electricity cogeneration through direct carbon solid oxide fuel cells. J Power Sources 2015;277:1–8. https://doi.org/10.1016/j.jpowsour.2014.12.016.

[252] Xie Y, Lu Z, Ma C, Xu Z, Tang Y, Ouyang S, et al. High-performance gas–electricity cogeneration using a direct carbon solid oxide fuel cell fueled by biochar derived from camellia oleifera shells. Int J Hydrogen Energy 2020;45:29322–30. https://doi.org/10.1016/j.ijhydene.2020.07.214.

[253] Xu H, Chen B, Liu J, Ni M. Modeling of direct carbon solid oxide fuel cell for CO and electricity cogeneration. Appl Energy 2016;178:353–62. https://doi.org/10.1016/j.apenergy.2016.06.064.

[254] Zhou M, Wang X, Zhang Y, Qiu Q, Liu M, Liu J. Effect of counter diffusion of CO and CO2 between carbon and anode on the performance of direct carbon solid oxide fuel cells. Solid State Ionics 2019;343:115127. https://doi.org/10.1016/j.ssi.2019.115127.

[255] Tang Y, Liu J. Effect of anode and Boudouard reaction catalysts on the performance of direct carbon solid oxide fuel cells. Int J Hydrogen Energy 2010;35:11188–93. https://doi.org/10.1016/j.ijhydene.2010.07.068.

[256] Zhu Y, Zhou W, Ran R, Chen Y, Shao Z, Liu M. Promotion of Oxygen Reduction by Exsolved Silver Nanoparticles on a Perovskite Scaffold for Low-Temperature Solid Oxide Fuel Cells. Nano Lett 2016;16:512–8. https://doi.org/10.1021/acs.nanolett.5b04160.

[257] Li C, Shi Y, Cai N. Performance improvement of direct carbon fuel cell by introducing catalytic gasification process. J Power Sources 2010;195:4660–6. https://doi.org/10.1016/j.jpowsour.2010.01.083.

[258] Jiao Y, Xue X, An W, Julião PSB, Wang W, Yang G, et al. Purified high-sulfur coal as a fuel for direct carbon solid oxide fuel cells. Int J Energy Res 2019;43:2501–13. https://doi.org/10.1002/er.4004.

[259] Xu K, Dong J, Li X, Wang J, Hu Z, Li A, et al. Evaluation of biomass and its thermal decomposition products as fuels for direct carbon fuel cells. Biomass and Bioenergy 2019;130:105359. https://doi.org/10.1016/j.biombioe.2019.105359.

[260] Li J, Wei B, Wang C, Zhou Z, Lü Z. High-performance and stable

La0.8Sr0.2Fe0.9Nb0.1O3-Δanode for direct carbon solid oxide fuel cells fueled by activated carbon and corn straw derived carbon. Int J Hydrogen Energy 2018;43:12358–67. https://doi.org/10.1016/j.ijhydene.2018.04.176.

[261] Cai W, Cao D, Zhou M, Yan X, Li Y, Wu Z, et al. Sulfur-tolerant Fe-doped La0·3Sr0·7TiO3 perovskite as anode of direct carbon solid oxide fuel cells. Energy 2020;211:118958. https://doi.org/10.1016/j.energy.2020.118958.

[262] Cai W, Zhou M, Cao D, Yan X, Li Q, Lü S, et al. Ni-doped A-site-deficient La0.7Sr0.3Cr0.5Mn0.5O3-δ perovskite as anode of direct carbon solid oxide fuel cells. Int J Hydrogen Energy 2020;45:21873–80. https://doi.org/10.1016/j.ijhydene.2020.05.266.

[263] Qiao J, Chen H, Wang Z, Sun W, Li H, Sun K. Enhancing the Catalytic Activity of Y0.08Sr0.92TiO3-δAnodes through in Situ Cu Exsolution for Direct Carbon Solid Oxide Fuel Cells. Ind Eng Chem Res 2020;59:13105–12. https://doi.org/10.1021/acs.iecr.0c02203.

[264] Tang H, Yu F, Wang Y, Xie Y, Meng X, Sun H, et al. Enhancing the Power Output of Direct Carbon Solid Oxide Fuel Cell Using Ba-Loaded Activated Carbon Fuel. Energy Technol 2019;7:1–8. https://doi.org/10.1002/ente.201800885.

[265] Cai W, Liu J, Yu F, Zhou Q, Zhang Y, Wang X, et al. A high performance direct carbon solid oxide fuel cell fueled by Ca-loaded activated carbon. Int J Hydrogen Energy 2017;42:21167–76. https://doi.org/10.1016/j.ijhydene.2017.03.229.

[266] Yu F, Han T, Wang Y, Xie Y, Zhang J, Sun H, et al. Performance improvement of a direct carbon solid oxide fuel cell via strontium-catalyzed carbon gasification. Int J Hydrogen Energy 2020;45:23368–77. https://doi.org/10.1016/j.ijhydene.2020.06.065.

[267] Jiao Y, Wang C, Zhang L, An W, Zhou N, Yang G, et al. A steel slag–derived Boudouard reaction catalyst for improved performance of direct carbon solid oxide fuel cells. Int J Energy Res 2019;43:6970–82. https://doi.org/10.1002/er.4715.

[268] Li X, Zhu Z, De Marco R, Bradley J, Dicks A. Evaluation of raw coals as fuels for direct carbon fuel cells. J Power Sources 2010;195:4051–8. https://doi.org/10.1016/j.jpowsour.2010.01.048.

[269] Wu H, Xiao J, Zeng X, Li X, Yang J, Zou Y, et al. A high performance direct carbon solid oxide fuel cell – A green pathway for brown coal utilization. Appl Energy 2019;248:679–87. https://doi.org/10.1016/j.apenergy.2019.04.104.

[270] Guo M, Song W, Buhain J. Bioenergy and biofuels: History, status, and perspective. Renew Sustain Energy Rev 2015;42:712–25.

https://doi.org/10.1016/j.rser.2014.10.013.
[271] Yu F, Wang Y, Xie Y, Zhang W, Zhang J, Meng X, et al. A Microtubular Direct Carbon Solid Oxide Fuel Cell Operated on the Biochar Derived from Pepper Straw. Energy Technol 2020;8:2–9. https://doi.org/10.1002/ente.201901077.
[272] Qiu Q, Zhou M, Cai W, Zhou Q, Zhang Y, Wang W, et al. A comparative investigation on direct carbon solid oxide fuel cells operated with fuels of biochar derived from wheat straw, corncob, and bagasse. Biomass and Bioenergy 2019;121:56–63. https://doi.org/10.1016/j.biombioe.2018.12.016.
[273] Cai W, Liu J, Liu P, Liu Z, Xu H, Chen B, et al. A direct carbon solid oxide fuel cell fueled with char from wheat straw. Int J Energy Res 2019;43:2468–77. https://doi.org/10.1002/er.3968.
[274] Xie Y, Xiao J, Liu Q, Wang X, Liu J, Wu P, et al. Highly efficient utilization of walnut shell biochar through a facile designed portable direct carbon solid oxide fuel cell stack. Energy 2021;227:120456. https://doi.org/10.1016/j.energy.2021.120456.
[275] Wu H, Xiao J, Hao S, Yang R, Dong P, Han L, et al. In-situ catalytic gasification of kelp-derived biochar as a fuel for direct carbon solid oxide fuel cells. J Alloys Compd 2021;865:158922. https://doi.org/10.1016/j.jallcom.2021.158922.
[276] Dudek M, Adamczyk B, Sitarz M, Śliwa M, Lach R, Skrzypkiewicz M, et al. The usefulness of walnut shells as waste biomass fuels in direct carbon solid oxide fuel cells. Biomass and Bioenergy 2018;119:144–54. https://doi.org/10.1016/j.biombioe.2018.09.026.
[277] Wang C, Lü Z, Su C, Li J, Cao Z, Zhu X, et al. Effects of discharge mode and fuel treating temperature on the fuel utilization of direct carbon solid oxide fuel cell. Int J Hydrogen Energy 2019;44:1174–81. https://doi.org/10.1016/j.ijhydene.2018.11.073.
[278] Xu K, Dong J, Hu H, Zhu X, Yao H. Effect of Ash Components on the Performance of Solid Oxide Electrolyte-Based Carbon Fuel Cells. Energy and Fuels 2018;32:4538–46. https://doi.org/10.1021/acs.energyfuels.7b03068.
[279] Guo Y, Pan Z, An L. Carbon-free sustainable energy technology: Direct ammonia fuel cells. J Power Sources 2020;476:228454. https://doi.org/10.1016/j.jpowsour.2020.228454.
[280] Siddiqui O, Dincer I. A review and comparative assessment of direct ammonia fuel cells. Therm Sci Eng Prog 2018;5:568–78. https://doi.org/10.1016/j.tsep.2018.02.011.
[281] Valera-Medina A, Xiao H, Owen-Jones M, David WIF, Bowen PJ. Ammonia for power. Prog Energy Combust Sci 2018;69:63–102. https://doi.org/10.1016/j.pecs.2018.07.001.

[282] Ganley JC, Thomas FS, Seebauer EG, Masel RI. A priori catalytic activity correlations: The difficult case of hydrogen production from ammonia. Catal Letters 2004;96:117–22. https://doi.org/10.1023/B:CATL.0000030108.50691.d4.

[283] Cinti G, Discepoli G, Sisani E, Desideri U. SOFC operating with ammonia: Stack test and system analysis. Int J Hydrogen Energy 2016;41:13583–90. https://doi.org/10.1016/j.ijhydene.2016.06.070.

[284] Ma Q, Peng RR, Tian L, Meng G. Direct utilization of ammonia in intermediate-temperature solid oxide fuel cells. Electrochem Commun 2006;8:1791–5. https://doi.org/10.1016/j.elecom.2006.08.012.

[285] Suryanto BHR, Matuszek K, Choi J, Hodgetts RY, Du H, Bakker JM, et al. Nitrogen reduction to ammonia at high efficiency and rates based on a phosphonium proton shuttle. Science (80-) 2021;372:1187–91. https://doi.org/10.1126/science.abg2371.

[286] Wojcik A, Middleton H, Damopoulos I, Van Herle J. Ammonia as a fuel in solid oxide fuel cells. J Power Sources 2003;118:342–8. https://doi.org/10.1016/S0378-7753(03)00083-1.

[287] Pelletier L, McFarlan A, Maffei N. Ammonia fuel cell using doped barium cerate proton conducting solid electrolytes. J Power Sources 2005;145:262–5. https://doi.org/10.1016/j.jpowsour.2005.02.040.

[288] Ma Q, Peng R, Lin Y, Gao J, Meng G. A high-performance ammonia-fueled solid oxide fuel cell. J Power Sources 2006;161:95–8. https://doi.org/10.1016/j.jpowsour.2006.04.099.

[289] Zhang L, Yang W. Direct ammonia solid oxide fuel cell based on thin proton-conducting electrolyte. J Power Sources 2008;179:92–5. https://doi.org/10.1016/j.jpowsour.2007.12.061.

[290] Maffei N, Pelletier L, McFarlan A. A high performance direct ammonia fuel cell using a mixed ionic and electronic conducting anode. J Power Sources 2008;175:221–5. https://doi.org/10.1016/j.jpowsour.2007.09.040.

[291] Xie K, Ma Q, Lin B, Jiang Y, Gao J, Liu X, et al. An ammonia fuelled SOFC with a BaCe0.9Nd0.1O3-δ thin electrolyte prepared with a suspension spray. J Power Sources 2007;170:38–41. https://doi.org/10.1016/j.jpowsour.2007.03.059.

[292] Meng G, Jiang C, Ma J, Ma Q, Liu X. Comparative study on the performance of a SDC-based SOFC fueled by ammonia and hydrogen. J Power Sources 2007;173:189–93. https://doi.org/10.1016/j.jpowsour.2007.05.002.

[293] Ma Q, Ma J, Zhou S, Yan R, Gao J, Meng G. A high-performance ammonia-fueled

SOFC based on a YSZ thin-film electrolyte. J Power Sources 2007;164:86–9. https://doi.org/10.1016/j.jpowsour.2006.09.093.

[294] ZHANG L, CONG Y, YANG W, LIN L. A Direct Ammonia Tubular Solid Oxide Fuel Cell. Chinese J Catal 2007;28:749–51. https://doi.org/10.1016/S1872-2067(07)60062-X.

[295] Fuerte A, Valenzuela RX, Escudero MJ, Daza L. Ammonia as efficient fuel for SOFC. J Power Sources 2009;192:170–4. https://doi.org/10.1016/j.jpowsour.2008.11.037.

[296] Lin Y, Ran R, Guo Y, Zhou W, Cai R, Wang J, et al. Proton-conducting fuel cells operating on hydrogen, ammonia and hydrazine at intermediate temperatures. Int J Hydrogen Energy 2010;35:2637–42. https://doi.org/10.1016/j.ijhydene.2009.04.019.

[297] Liu L, Sun K, Wu X, Li X, Zhang M, Zhang N, et al. Improved performance of ammonia-fueled solid oxide fuel cell with SSZ thin film electrolyte and Ni-SSZ anode functional layer. Int J Hydrogen Energy 2012;37:10857–65. https://doi.org/10.1016/j.ijhydene.2012.04.101.

[298] Yang J, Akagi T, Okanishi T, Muroyama H, Matsui T, Eguchi K. Catalytic influence of oxide component in Ni-based cermet anodes for ammonia-fueled solid oxide fuel cells. Fuel Cells 2015;15:390–7. https://doi.org/10.1002/fuce.201400135.

[299] Yang J, Molouk AFS, Okanishi T, Muroyama H, Matsui T, Eguchi K. Electrochemical and catalytic properties of Ni/BaCe0.75Y0.25O3-δ anode for direct ammonia-fueled solid oxide fuel cells. ACS Appl Mater Interfaces 2015;7:7406–12. https://doi.org/10.1021/acsami.5b01048.

[300] Miyazaki K, Okanishi T, Muroyama H, Matsui T, Eguchi K. Development of Ni–Ba(Zr,Y)O3 cermet anodes for direct ammonia-fueled solid oxide fuel cells. J Power Sources 2017;365:148–54. https://doi.org/10.1016/j.jpowsour.2017.08.085.

[301] Molouk AFS, Okanishi T, Muroyama H, Matsui T, Eguchi K. Electrochemical and Catalytic Behaviors of Ni–YSZ Anode for the Direct Utilization of Ammonia Fuel in Solid Oxide Fuel Cells. J Electrochem Soc 2015;162:F1268–74. https://doi.org/10.1149/2.1011510jes.

[302] Kishimoto M, Furukawa N, Kume T, Iwai H, Yoshida H. Formulation of ammonia decomposition rate in Ni-YSZ anode of solid oxide fuel cells. Int J Hydrogen Energy 2017;42:2370–80. https://doi.org/10.1016/j.ijhydene.2016.11.183.

[303] Park BK, Barnett SA. Boosting solid oxide fuel cell performance: Via electrolyte thickness reduction and cathode infiltration. J Mater Chem A 2020;8:11626–31. https://doi.org/10.1039/d0ta04280c.

[304] Stoeckl B, Subotić V, Preininger M, Schwaiger M, Evic N, Schroettner H, et al. Characterization and performance evaluation of ammonia as fuel for solid oxide fuel cells with Ni/YSZ anodes. Electrochim Acta 2019;298:874–83. https://doi.org/10.1016/j.electacta.2018.12.065.

[305] Wang Y, Gu Y, Zhang H, Yang J, Wang J, Guan W, et al. Efficient and durable ammonia power generation by symmetric flat-tube solid oxide fuel cells. Appl Energy 2020;270:115185. https://doi.org/10.1016/j.apenergy.2020.115185.

[306] Miyazaki K, Muroyama H, Matsui T, Eguchi K. Impact of the ammonia decomposition reaction over an anode on direct ammonia-fueled protonic ceramic fuel cells. Sustain Energy Fuels 2020;4:5238–46. https://doi.org/10.1039/d0se00841a.

[307] Wang Y, Yang J, Wang J, Guan W, Chi B, Jia L, et al. Low–Temperature Ammonia Decomposition Catalysts for Direct Ammonia Solid Oxide Fuel Cells. J Electrochem Soc 2020;167:064501. https://doi.org/10.1149/1945-7111/ab7b5b.

[308] Xu Q, Xia L, He Q, Guo Z, Ni M. Thermo-electrochemical modelling of high temperature methanol-fuelled solid oxide fuel cells. Appl Energy 2021;291:116832. https://doi.org/10.1016/j.apenergy.2021.116832.

[309] Molouk AFS, Yang J, Okanishi T, Muroyama H, Matsui T, Eguchi K. Comparative study on ammonia oxidation over Ni-based cermet anodes for solid oxide fuel cells. J Power Sources 2016;305:72–9. https://doi.org/10.1016/j.jpowsour.2015.11.085.

[310] Okanishi T, Okura K, Srifa A, Muroyama H, Matsui T, Kishimoto M, et al. Comparative Study of Ammonia-fueled Solid Oxide Fuel Cell Systems. Fuel Cells 2017;17:383–90. https://doi.org/10.1002/fuce.201600165.

[311] Itagaki Y, Cui J, Ito N, Aono H, Yahiro H. Effect of Ni-loading on Sm-doped CeO2 anode for ammonia-fueled solid oxide fuel cell. J Ceram Soc Japan 2018;126:870–6. https://doi.org/10.2109/jcersj2.18033.

[312] Kishimoto M, Muroyama H, Suzuki S, Saito M, Koide T, Takahashi Y, et al. Development of 1 kW-class Ammonia-fueled Solid Oxide Fuel Cell Stack. Fuel Cells 2020;20:80–8. https://doi.org/10.1002/fuce.201900131.

[313] He F, Gao Q, Liu Z, Yang M, Ran R, Yang G, et al. A New Pd Doped Proton Conducting Perovskite Oxide with Multiple Functionalities for Efficient and Stable Power Generation from Ammonia at Reduced Temperatures. Adv Energy Mater 2021;2003916:1–10. https://doi.org/10.1002/aenm.202003916.

[314] Hashinokuchi M, Yokochi R, Akimoto W, Doi T, Inaba M, Kugai J. Enhancement of anode activity at Ni/Sm-doped CeO2 cermet anodes by Mo addition in NH3-fueled

solid oxide fuel cells. Solid State Ionics 2016;285:222–6. https://doi.org/10.1016/j.ssi.2015.07.021.

[315] Schüth F, Palkovits R, Schlögl R, Su DS. Ammonia as a possible element in an energy infrastructure: Catalysts for ammonia decomposition. Energy Environ Sci 2012;5:6278–89. https://doi.org/10.1039/c2ee02865d.

[316] Song Y, Li H, Xu M, Yang G, Wang W, Ran R, et al. Infiltrated NiCo Alloy Nanoparticle Decorated Perovskite Oxide: A Highly Active, Stable, and Antisintering Anode for Direct-Ammonia Solid Oxide Fuel Cells. Small 2020;16:1–8. https://doi.org/10.1002/smll.202001859.

[317] Akimoto W, Fujimoto T, Saito M, Inaba M, Yoshida H, Inagaki T. Ni-Fe/Sm-doped CeO2 anode for ammonia-fueled solid oxide fuel cells. Solid State Ionics 2014;256:1–4. https://doi.org/10.1016/j.ssi.2013.12.026.

[318] Hashinokuchi M, Zhang M, Doi T, Inaba M. Enhancement of anode activity and stability by Cr addition at Ni/Sm-doped CeO2 cermet anodes in NH3-fueled solid oxide fuel cells. Solid State Ionics 2018;319:180–5. https://doi.org/10.1016/j.ssi.2018.02.015.

[319] Hill AK, Torrente-Murciano L. Low temperature H2 production from ammonia using ruthenium-based catalysts: Synergetic effect of promoter and support. Appl Catal B Environ 2015;172–173:129–35. https://doi.org/10.1016/j.apcatb.2015.02.011.

[320] Yang J, Molouk AFS, Okanishi T, Muroyama H, Matsui T, Eguchi K. A Stability Study of Ni/Yttria-Stabilized Zirconia Anode for Direct Ammonia Solid Oxide Fuel Cells. ACS Appl Mater Interfaces 2015;7:28701–7. https://doi.org/10.1021/acsami.5b11122.

[321] Stoeckl B, Preininger M, Subotić V, Megel S, Folgner C, Hochenauer C. Towards a wastewater energy recovery system: The utilization of humidified ammonia by a solid oxide fuel cell stack. J Power Sources 2020;450. https://doi.org/10.1016/j.jpowsour.2019.227608.

[322] Hagen A, Langnickel H, Sun X. Operation of solid oxide fuel cells with alternative hydrogen carriers. Int J Hydrogen Energy 2019;44:18382–92. https://doi.org/10.1016/j.ijhydene.2019.05.065.

Table 1. Electrochemical performances of methane-fuelled SOFCs.

Fuel	Configuration: anode/electrolyte/cathode (thickness, μm)	Maximum power density (mW cm^{-2})	Stability characteristic	Ref.
Thermodynamics				
Methane-steam mixture (S/C: 2)	Flat-tube cell with symmetric double-sided cathodes: Ni-YSZ(1000)/Ni-YSZ(15)/YSZ(15)/GDC(3)/LSCF(15)	~360 under 0.7 V at 850 ℃	Stable for 190 h under 0.257 A cm^{-2} at 750 ℃	[65]
Air-diluted natural gas (O/C: 0.8)	Anode-supported button cell: Ni-YSZ/YSZ/GDC-LSCF	~560 under 0.8 V at 800 ℃	Stable for 100 under 0.5 A cm^{-2} at 800 ℃	[49]
Upgraded-biogas (O/C: 0.4)	Anode-supported button cell: Ni-YSZ/YSZ/GDC-LSCF	~320 under 0.8 V at 800 ℃	Stable for 200 under 0.5 A cm^{-2} at 800 ℃	[49]
Methane-air mixture (100 SCCM air, 500 SCCM methane)	Button cell: Ni-YSZ(500)/Ni-YSZ(20)/YSZ(12)/LSM-YSZ(30)		Stable for 100 under 0.6 V at 800 ℃	[55]
Kinetics				
Methane-steam mixture	Circular shaped planar electrolyte-supported cell: NiO(5)/Au-Ni-GDC(15)/GDC(5)/YSZ(90)/LSM-YSZ(15)/LSM(15)		Stable for over 200 h under 0.81 V at 850 ℃	[98]
Methane-steam mixture (S/C: 0.3)	Button cell: Au-Ni-GDC/YSZ(150)/LSM		Stable for 192 h under 0.7 V at 800 ℃	[99]
Simulated biogas	Button cell: Ag-Ni-YSZ(700)/YSZ(20)/LSM-YSZ(10)	102 at 750 ℃	50 h with the degradation rate of 0.793 mV h^{-1} under 0.2 A cm^{-2} at 750 ℃	[102]
Simulated biogas	Button cell: Sn-Ni-YSZ(700)/YSZ(20)/LSM-YSZ(10)	272 at 750 ℃	50 h with the degradation rate of 0.298 mV h^{-1} under 0.2 A cm^{-2} at 750 ℃	[102]
Methane	Button cell: 5Sn-Ni-SDC(490)/SDC(115)/BSCF(45)	600 at 700 ℃	72 h with the degradation of 1.5% under 0.3 A at 600 ℃	[105]
Wet methane (3 vol% steam)	Button cell: $Ni_{0.9}Fe_{0.1}$(1000)/Ni-SDC(10)/SDC(10)/LSM-BSCF	1010 at 650 ℃	50 h with the degradation of 7.7% under 0.4 A cm^{-2} at 650 ℃	[106]
Simulated biogas	Button cell: Cu-Ni-YSZ(700)/YSZ(20)/LSM-YSZ(10)	85 at 750 ℃	50 h with the degradation rate of 6.2 mV h^{-1} under 0.2 A cm^{-2} at 750 ℃	[102]
Methane	Anode-supported button cell: Cu-Ni-SDC/YSZ(16)/SDC(8)/LSCF(25)	424 at 700 ℃	Stable for 15 h under 0.5 A cm^{-2} at 700 ℃	[107]
Wet methane (3 vol% steam)	Anode-supported button cell: CaO-Ni-SDC/SDC/LSCF-SSC	1051 at 700 ℃	70 h with the degradation rate of 0.65 mV h^{-1} under 0.3 A cm^{-2} at 650 ℃	[100]
Wet methane (3 vol% steam)	Anode-supported button cell: BaO-Ni-SDC/SDC/LSCF-SSC	563 at 700 ℃		[100]
Wet methane (3 vol% steam)	Button cell: MgO-Ni-SDC(35)/LDC/LSGM(220)/SCCO-SDC(35)	714 at 800 ℃	330 h with the degradation of 15% under 0.8 V at 800 ℃	[109]

Wet methane (3 % steam)	Anode-supported button cell: $Ni_{0.875}Cu_{0.1}Mg_{0.025}O$-SDC/SDC/LSCF-SDC	670 at 700 °C	100 h with the degradation of less than 7% under 0.3 A cm^{-2} at 700 °C	[110]
Wet methane	Button cell:GDC-Ni-YSZ(300)/YSZ(30)/YSZ-LSF(70)	428 at 750 °C	170 h with little degradation under 0.25 A cm^{-2} at 750 °C	[112]
Methane	Button cell: Ni-SDC(600)/SDC(31)/SSC-SDC(160)	697 at 700 °C	100 h with the degradation rate of 1.33 mV h^{-1} under 0.35 A cm^{-2} at 700 °C	[113]
Methane-air mixture (40 SCCM oxygen, 80 SCCM methane)	Anode-supported button cell: Ni-GDC/GDC/LSCF-GDC	1350 at 650 °C; 1100 at 600 °C	530 h with the degradation of 0.91% under OCV condition at 650 °C	[56]
Wet methane	Anode-supported button cell: Ni-$Ce_{0.9}Ca_{0.1}O_{2-\delta}$/YSZ(9)/SDC(5)/LSCF(10)	618 at 800 °C	30 h with the degradation rate of 1.1 mV h^{-1} under 0.5 A cm^{-2} at 800 °C	[115]
Methane	Button cell: Cu-CeO_2-YSZ(140)/YSZ(110)/LSM-YSZ(30)	70 at 800 °C		[117]
Methane	Button cell: Cu-Fe-CeO_2-YSZ(140)/YSZ(110)/LSM-YSZ(30)	90 at 800 °C	46 h with the degradation of 20% under 0.6 V at 800 °C	[117]
Methane	Button cell: CeO_2-Cu(30)/10Sc1CeSZ-CeO_2/10Sc1CeSZ(150)/LSM(30)	34.2 at 850 °C		[118]
Methane	Button cell: CeO_2-Cu-Co(30)/10Sc1CeSZ-CeO_2/10Sc1CeSZ(150)/LSM(30)	446.4 at 850 °C		[118]
Methane	Button cell: Cu-CeO_2-YSZ(130)/YSZ(180)/LSM-YSZ(185)	~110 at 800 °C		[119]
Wet methane (3 % steam)	Button cell: LSFT/SDC/YSZ(500)/LSM-YSZ	121 at 850 °C	Stable for 24 h under 0.2 A cm^{-2} at 850 °C	[127]
Wet methane (3 % steam)	Button cell: SFNM20(10)/LSGM(200)/PBCO(20)	380 at 800 °C; 276 at 700 °C	Stable for 200 h under 0.6 A cm^{-2} at 700 °C	[128]
Methane	Electrolyte-supported button cell: PBFN(20)/LSGM/PBCO(20)	577 at 800 °C; 418 at 750 °C	Stable for 300 h under 0.35, 0.7 and 0.84 A cm^{-2} at 700 °C	[129]
Methane	Button cell: LSFMn-Ni-GDC(53)/GDC(430)/LSFCo-GDC(20)	119 at 800 °C	33 h with the degradation of 17% under 0.5 V at 800 °C	[130]
Methane	Button cell: Ni-CeO_2-impregnated LSTA(540)/YSZ(900)/LSM-YSZ/LSM	490 at 900 °C		[131]
Methane	Button cell: Ni-LCFNb-SDC-SSZ(65)/SSZ(70)/LSM(15)	729 at 850 °C; 507 at 800 °C	Stable for 100 h under 0.2 A cm^{-2} at 800 °C	[133]
Methane	Button cell: Ni-infiltrated BSFM/GDC/SSZ(200)/GDC/LSCF-GDC	194 at 800 °C	70 h with the degradation rate of 0.135 mV h^{-1} under 0.2 A cm^{-2} at 800 °C	[135]
Methane	Button cell: $Cu_{0.5}Fe_{0.5}$-LSCM-SDC/LSGM(300)/LSM-SDC	640 at 850 °C	Stable for 100 h under 0.4 A cm^{-2} at 850 °C	[137]
Wet methane	Button cell: R-SCMF0.05(20)/SDC/LSGM(300)/LSCF	652.3 at 850 °C; 532.9 at 800 °C	50 h with the degradation rate of 0.018% h^{-1} under 0.2 A cm^{-2} at 700 °C	[136]

Structure				
Wet methane (3 % steam)	Button cell: PBFM(25)/LSGM(200)/PBFM(25)	340 at 800 °C; 193 at 750 °C	Stable for 280 h under 0.6 A cm^{-2} at 800 °C	[139]
Methane	Button cell: nanoparticle-infiltrated PBFM(25)/LSGM(200)/nanoparticle-infiltrated PBFM(25)	390 at 800 °C; 300 at 750 °C	Stable for 1060 h under 1 A cm^{-2} at 800 °C	[139]
Methane	Button cell: RP-SCFM-CFA(20)/LSGM(300)/SCFM(20)	401 at 850 °C; 271 at 800 °C	Stable for 130 h under 0.4 A cm^{-2} at 800 °C	[140]
Synthetic natural gas	Anode-supported button cell: SLT/Ni-SDC/Ni-YSZ/YSZ/LSM-YSZ	~540 at 800 °C	Stable for 80 h at 800 °C	[88]
Methane	Microtubular cell: Al_2O_3(160)/Ni-SDC(20)/SDC(10)/PBCO(15)	790 at 700 °C	Stable for 50 h under OCV condition at 700 °C	[87]
Methane	Microtubular cell: $NiAl_2O_4$(150)/Ni-SDC(20)/SDC(10)/PBCO(13)	870 at 700 °C	Stable for 50 h under OCV condition at 700 °C	[87]
Wet methane	Button cell: PSZ-CeO_2/Ni-YSZ(700)/YSZ/LSCF-GDC/LSCF	800 at 800 °C	Stable for 155 h under 0.6 A cm^{-2} at 750 °C	[141]
Wet biogas (63% methane, 34% carbon dioxide, 3% steam)	Anode-supported tubular cell: SLT-YSZ/Ni-YSZ/YSZ/LSM-YSZ	264 at 800 °C	Stable for 280 h under 0.2, 0.15 and 0.1 A cm^{-2} at 850 °C	[142]
Wet methane (3 mol% steam)	Anode-supported button cell: $Ce_{0.8}Ni_{0.2}O_{2-\delta}$ (45)/Ni-SDC/SDC/BSCF	664 at 650 °C	50 h with the degradation rate of 0.438 mV h^{-1} under 0.2 A cm^{-2} at 650 °C	[144]
Methane	Button cell: Cu-Ni/Ni-YSZ(750)/YSZ(40)/YSZ-LSM(40)/LSM(50)	~280 at 800 °C		[145]
Wet methane (3 mol% steam)	Anode-supported button cell: Ni-$La_2Ce_2O_7$(10)/Ni-SDC/SDC/BSCF	699 at 650 °C	26 h with the degradation rate of 1.061 mV h^{-1} under 0.2 A cm^{-2} at 650 °C	[146]
Wet methane (3 mol% steam)	Anode-supported button cell: Ni-$La_{1.95}Sm_{0.05}Ce_2O_7$(10)/Ni-SDC/SDC/BSCF	639 at 650 °C	26 h with the degradation rate of 0.843 mV h^{-1} under 0.2 A cm^{-2} at 650 °C	[146]
Methane	Anode-supported button cell: Ni-$La_2Ce_2O_7$(10)/Ni-SDC/SDC/BSCF	671 at 650 °C	26 h with little degradation under 0.2 A cm^{-2} at 650 °C	[146]
Methane	Anode-supported button cell: Ni-$La_{1.95}Sm_{0.05}Ce_2O_7$(10)/Ni-SDC/SDC/BSCF	599 at 650 °C	26 h with the little degradation under 0.2 A cm^{-2} at 650 °C	[146]
Wet methane (3% steam)	Anode-supported button cell: $La_{0.7}Sr_{0.3}Fe_{0.8}Ni_{0.2}O_{3-\delta}$ (30)/Ni-YSZ/YSZ(30)/LSM-YSZ	688 at 850 °C; 421 at 800 °C	110 h with little degradation under 0.335 A cm^{-2} at 800 °C	[147]
Methane-air mixture (70% air)	Anode-supported button cell: $La_{0.7}Sr_{0.3}Fe_{0.8}Ni_{0.2}O_{3-\delta}$ (30)/Ni-YSZ/YSZ(30)/LSM-YSZ	539 at 850 °C; 356 at 800 °C	120 h with little degradation under 0.335 A cm^{-2} at 800 °C	[147]
Wet methane (3.5 vol% steam)	Button cell: $Ce_{0.90}Ni_{0.05}Ru_{0.05}O_2$/Ni-BZCYYb(800)/Ni-	370 at 500 °C	Stable for 550 h under 0.75 V at 550 °C	[148]

	BZCYYb(10)/SDC(15)/PrOx infiltrated PBSCF(25)			
Wet methane (3 % steam)	Anode-supported Button cell: $La_{0.6}Sr_{0.4}Co_{0.2}Fe_{0.8}O_{3-\delta}$(70)/$Al_2O_3$(1200)//Ni-YSZ/YSZ(33)/YSZ-LSM	660 at 850 ℃	Stable for 116 h under 0.333 A cm^{-2} at 800 ℃	[153]
Methane	Anode-supported button cell: CeO_2-Ni-GDC with microchannels/GDC/GDC-BSCF	545 at 600 ℃	Stable for 65 h under 1.3 A cm^{-2} at 600 ℃	[157]
Methane	Anode-supported microtubular cell: Cu-CeO_2-YSZ with microchannels/YSZ(10)/LSM-YSZ	160 at 750 ℃	Stable for 30 h under 0.7 V at 750 ℃	[116]
Methane-carbon dioxide mixture	Anode-supported tubular cell: Ni-YSZ with 6 sub-channels/YSZ(4.5)/GDC(4.5)/GDC-LSCF(25)	1770, 2030 and 2220 in the mixture fuels with methane concentrations of 10%, 15% and 20% at 750 ℃	Over 500 h with the degradation rate of 0.02 A cm^{-2} kh^{-1} in the methane and carbon dioxide (1:1 ratio) under 0.7 V at 700 ℃	[158]

Table 2. Electrochemical performances of higher hydrocarbon-fuelled SOFCs.

Fuel	Configuration: anode/electrolyte/cathode (thickness, μm)	Maximum power density (mW cm^{-2})	Stability characteristic	Ref.
Butane-oxygen mixture (O/C: 1.5)	Microtubular cell: Ni-GDC(640)/YSZ(10)/GDC(1)/LSCF-GDC(20)	213 at 650 ℃	Stable for 100 h under 0.1 A cm^{-2} at 650 ℃	[161]
Propane-air mixture (1/7.1, 12vol% propane)	Inner reformer + tubular cell: Ni-YSZ(600)/YSZ(5)/GDC(1)/LSCF(30)	670 at 700 ℃	80 h with the degradation of 20% under 0.7 V at 700 ℃	[162]
Propane-air mixture (10.7% propane)	Anode supported button cell: Ru-CeO_2(30)/PSZ-CeO_2(300)/Ru-CeO_2(30)/Ni-SDC/Ni-SDC(12)/SDC(6)/LSCF-SDC/LSCF	395 at 500 ℃; 280 at 450 ℃		[150]
Propane-air mixture	Oxygen-permeable membrane reactor + button cell: Ni-YSZ(900)/YSZ(12)/LSM-YSZ(25)	675 at 800 ℃	Stable for 45 h under 0.7 V at 800 ℃	[166]
Propane-air mixture (C/O: 1.04)	Reformer + tubular cell stack: Ni-YSZ(890)/Ni-YSZ(15)/YSZ(6)/LSM-YSZ-LSCF	11.9 W at 780 ℃		[163]
Propane-oxygen mixture (10.7% propane, 18.7% oxygen)	Anode-supported button cell: Ni-YSZ/YSZ/LSCF-GDC/LSCF	~700 at 790 ℃	Stable for 100 h	[164]
Propane-oxygen mixture (10.7% propane, 18.7% oxygen)	Button cell: Ru-CeO_2(20)/PSZ(650)/Ni-YSZ(650)/YSZ(10)/LSCF-GDC/LSCF	480 at 750 ℃		[165]
Propane-carbon dioxide mixture (5% propane)	Anode-supported button cell: Ni-YSZ/YSZ/LSM		Stable for 3 h under 0.12 A cm^{-2} at 800 ℃	[167]

Wet propane (3 vol% steam)	Button cell: Ni-BZCYYb/GDC(5)/YSZ(150)/GDC(5)/LSCF		Stable for 100 h under 0.3 A cm^{-2} at 750 °C	[169]
Wet butane (20% butane, 3% steam)	Microtubular cell: Ni-GDC(200)/YSZ(5)/GDC(1)/LSCF-GDC(20)	251 at 615 °C	Stable for 100 h under 0.1 A cm^{-2} at 615 °C	[170]
Wet butane (20% butane, 3% steam)	Microtubular cell: LDC-infiltrated Ni-GDC(200)/YSZ(5)/GDC(1)/LSCF(20)	374 at 615 °C	Stable for 100 h under 0.1 A cm^{-2} at 615 °C	[170]
Wet butane (17% butane, 3% steam)	Microtubular cell: Ni-GDC(200)/YSZ(5)/GDC(1)/LSCF(20)	~260 at 610 °C	Stable for 24 h under 0.2 A cm^{-2} at 610 °C	[172]
Wet butane (10% butane, 4% steam)	Microtubular cell: Ni-GDC(400)/YSZ(5)/GDC(1)/LSCF-GDC(20)	~130 at 600 °C	Stable for 100 h under 0.15 A cm^{-2} at 600 °C	[171]
Butane-steam mixture (S/C: 3)	Button cell: Pd-infiltrated Ni-YSZ(1000)/Ni-YSZ(2)/YSZ(1)/GDC(0.2)/LSC(3)	946 at 600 °C	100 h with the degradation rate of 14% 100 h^{-1} under 0.15 A cm^{-2} at 600 °C	[168]
Butane	Button cell: Pd-infiltrated Ni-YSZ(870)/Ni-YSZ/YSZ(1)/GDC(0.2)/LSC(3)	486 at 600 °C	Failed at 30 h under 0.15 A cm^{-2} at 600 °C	[173]
Propane	Button cell: BaO-deposited Ni-YSZ(600)/YSZ(15)/SDC(3)/LSCF(30)	880 at 750 °C	Stable for 100 h under 0.5 A cm^{-2} at 750 °C	[174]
Propane	Tubular cell: Ag-GDC(15)/YSZ(200)/Ag-GDC	~120 at 800 °C	Stable for 160 h under 0.103 A cm^{-2} at 800 °C	[175]
Wet propane	Button cell: RP-PSFR-FRA-GDC/LSGM(300)/LSCF-GDC	500 at 800 °C	Stable for 50 h under 0.15 A cm^{-2} at 750 °C	[126]
Wet propane (3% steam)	Button cell: LSCFN-GDC/GDC(10)/YSZ(200)/GDC(10)/LSCFN-GDC	324 at 850 °C	Stable for 100 h under 0.4 A cm^{-2} at 850 °C	[176]
Wet propane (3% steam)	Button cell: LSCrFeCo10-GDC(20)/LSGM(250)/LSCF-GDC(30)	700 at 850 °C; 490 at 800 °C	Stable for 840 h with 2 reoxidation processes under 0.2 A cm^{-2} at 700 °C	[177]
Octane-air-carbon dioxide mixture (5% *iso*-octane, 9% air, 86% carbon dioxide)	Anode-supported button cell: Ru-CeO_2/PSZ(500)/Ru-CeO_2/Ni-YSZ/YSZ/LSCF-SDC	~640 at 770 °C	Stable for 50 h under OCV condition at 770 °C	[143]
Octane-air mixture (6% *iso*-octane)	Button cell: Ru-CeO_2(10)/PSZ/Ru-CeO_2(20)/Ni-YSZ(600)/Ni-YSZ(15)/YSZ(7)/LSCF-SDC/LSCF	~750 at 790 °C	Stable for 50 h under 0.6 A cm^{-2} at 790 °C	[178]
Octane-air mixture (6% *iso*-octane)	Button cell: Ru-CeO_2(10)/PSZ/Ru-CeO_2(20)/Ni-GDC(600)/Ni-GDC(15)/GDC(10)/LSCF-SDC/LSCF	~610 at 590 °C	Stable for 50 h under 0.8 A cm^{-2} at 590 °C	[178]
Octane-air mixture (6% *iso*-octane)	Anode supported button cell: Ru-CeO_2(10)/PSZ-CeO_2(300)/Ru-CeO_2(20)/Ni-SDC/Ni-SDC/SDC/LSCF-SDC/LSCF	600 at 590 °C	Stable for 50 h under 0.8 A cm^{-2} at 590 °C	[179]

Wet octane (3 v% steam, 6.5% *iso*-octane)	Button cell: Ni-YSZ-BZY(800)/Ni-YSZ (15)/YSZ(15)/LSCF(50)	600 at 750 ℃; 100 at 600 ℃	Stable for 100 h under 0.7 V at 750 ℃	[180]

Table 3. Summary of SOFCs on ethane for power and chemical.

Fuel	Configuration: anode/electrolyte/cathode (thickness, μm)	Maximum power density (mW cm^{-2}) and ethene yield	Stability characteristic	Ref.
Ethane	Electrode-supported button cell: Pt-BCYN/BCYN(50)/Pt-BCYN	173 and 20.7% at 650℃; 237 and 32.9% at 700 ℃		[188]
Ethane	Button cell: Cu-Cr_2O_3(20)/BCZY(800)/Pt	170 and 39% at 700 ℃	Stable for 240 h under ~0.12 W cm^{-2} at 700 ℃	[192]
Ethane	Button cell: Co-Cr_2O_3/BCZY(1000)/Pt	132 and 19% at 650 ℃; 173 and 32% at 700 ℃		[193]
Ethane	Button cell: $FeCr_2O_4$-BCZY/BCZY(900)/LSF-BCZY	160 and 27.3% at 700 ℃; 240 and 39.7% at 750 ℃		[191]
Ethane	Button cell: LST_A-Cr_2O_3-Cu/BCZY(400)/GDC(8)/LSCF-BCZY	320 and 27.7% at 750 ℃	Stable for 100 h under 0.45 A cm^{-2} at 700 ℃	[194]
Ethane	Button cell: P-PSCFM/BCZY(300)/GDC(2)/LSCF-BCZY	348.84 and 41.5% at 750 ℃	Stable for 100 h under 0.65 A cm^{-2} at 750 ℃	[185]
Ethane	Electrolyte-supported button cell: Co-SMCFO-BCZY/BCZY/LSCF-BCZY	268 and 37.8% at 750 ℃; 219 and 26.5 at 700 ℃	Stable for 50 h under 0.39 A cm^{-2} at 700 ℃	[186]
Ethane	Button cell: LSFNCu(35)/BZCYYb(300)/LSFNCu(35)	90 and 40.4% at 750 ℃	Stable for 40 h under 0.5 V at 750 ℃	[184]

Table 4. Electrochemical performances of alcohol-fuelled SOFCs.

Fuel	Configuration: anode/electrolyte/cathode (thickness, μm)	Maximum power density (mW cm^{-2})	Stability characteristic	Ref.
Methanol	Button cell: Ni-YSZ(1000)/Ni-YSZ(20)/YSZ(10)/LSM-YSZ(20)/LSM(80)	1300 at 800 ℃; 600 at 650 ℃		[202]
Methanol	Anode-supported button cell: Ni-SDC/SDC(24)/SSC-SDC	698 at 650 ℃; 430 at 600 ℃	Stable for 160 h under 0.5 V at 550, 600 and 650 ℃	[203]
Methanol	Button cell: Ni-SDC(600)/SDC(6)/LSCF-SDC	820 at 600 ℃; 520 at 550 ℃	Stable for 60 h under 0.8 A cm^{-2} at 600 ℃	[204]
Methanol-steam mixture (S/C: 2)	Flat-tube cell with symmetric double-sided cathodes: Ni-YSZ(600)/Ni-YSZ(20)/YSZ(9)/GDC(3)/LSCF-GDC(30)	12 W at 750 ℃	Stable for 120 h under 0.221 A cm^{-2} at 750 ℃	[210]
Methanol	Button cell: Ni-Cu-SDC(300)/Ni-Cu-SDC(10)/GDC(10)/LSCF-SDC(10)	420 at 550 ℃	Stable for 55 h under 0.6 V at 550 ℃	[207]

Methanol	Button cell: Pd-Ni/GDC(400)/LSCF-SDC	~9 at 450 ℃	40 h with little degradation under 0.4 V at 450 ℃	[209]
Ethanol-steam mixture (S/C: 2)	Microtubular cell: Ni-GDC(640)/YSZ(10)/GDC(1)/LSCF-GDC(20)	180 at 650 ℃	Stable for 100 h under 0.1 A cm^{-2} at 650 ℃	[161]
Ethanol-steam mixture (volume ratio: 2:1)	Button cell: $Fe_{0.5}Ni_{0.5}$-ScSZ(1000)/ScSZ(15)/PCM(20)	460 at 850 ℃; 265 at 800 ℃		[222]
Ethanol	Button cell: Sn-Ni-YSZ(500)/YSZ(15)/LSM-YSZ(50)	~180 at 740 ℃		[223]
Ethanol-steam mixture (volume ratio: 2:1)	Button cell: Cu-CeO_2-ScSZ(600)/ScSZ(20)/PCM(30)	222 at 800 ℃	Stable for 50 h under 0.5 V at 800 ℃	[224]
Ethanol-steam mixture (volume ratio: 2:1)	Button cell: Cu-CeO_2-YSZ(600)/Ni-ScSZ/ScSZ(40)/PCM	438 at 800 ℃	Stable for 50 h under 0.7 V at 800 ℃	[225]
Ethanol-steam mixture (volume ratio: 2:1)	Button cell: LSCM(65)/LSGM(600)PCM	160 at 850 ℃; 101 at 800 ℃	Stable for 60 h under about 55 mW cm^{-2} at 750 ℃	[226]
Ethanol	Button cell: Pd-LSCM-YSZ/YSZ(1000)/Pt	111 at 800 ℃		[228]
Ethanol	Button cell: LSCM-Ru(10)/Ni-YSZ(7)/YSZ(500)/LSM	~80 at 950 ℃		[227]
Ethanol-steam mixture (volume ratio: 2:1)	Button cell: Cu-LSCM-ScSZ(600)/ScSZ(20)/PCM(30)	84 at 800 ℃	Stable for 12 h under 0.6 V at 800 ℃	[229]
Ethanol-steam mixture (volume ratio: 2:1)	Button cell: Cu-LSCM-YSZ(20)/Ni-YSZ(500)/Ni-ScSZ(20)/ScSZ(20)/PCM(20)	384 at 800 ℃	Stable for 120 h under 0.7 V at 800 ℃	[229]
Ethanol-steam mixture (volume ratio: 2:1)	Button cell: LSCM-CeO_2(8)/Ni-ScSZ(800)/ScSZ(15)/PCM(20)	669 at 850 ℃	Stable for 216 h under 0.6 V at 700 ℃	[230]
Ethanol-steam mixture (volume ratio: 2:1)	Button cell: Cu-CeO_2(30)/Ni-YSZ(600)/ScSZ(15)/PCM(40)	566 at 800 ℃	Gradual degradation due to delamination under 0.6 V at 800 ℃	[149]
Ethanol-steam mixture (volume ratio: 2:1)	Button cell: Cu-CeO_2(20)/Ni-CeO_2(20)/Ni-YSZ(600)/Ni-ScSZ(15)/ScSZ(15)/PCM(20)	519 at 800 ℃	Stable for about 210 h under 0.7 V at 750 ℃	[231]
Ethanol	Anode-supported button cell: Ni-modified LSFCO-GDC(4)/YDC/YSZ/LSFC	650 at 800 ℃	Stable for 400 h under 0.8 V at 800 ℃	[237]
Ethanol-steam mixture (molar ratio: 2.3:1)	Button cell: Ni–$Ce_{0.8}Zr_{0.2}O_2$/Ni-YSZ/YSZ/SDC/SDC-BSCF	536 at 700 ℃; 334 at 650 ℃		[236]
Ethanol	Button cell: Pd(10)/Ni-YSZ(500)/YSZ(20)/Pt(20)	196 at 750 ℃	Stable for 59 h under OCV condition at 750 ℃	[238]
Ethanol	Button cell: Ni-GDC/Ni-YSZ/YSZ(500)/LSM	70 under 0.7 V at 850 ℃	Stable for 50 h under 0.7 V at 850 ℃	[152]
Ethanol	Button cell: Ni-ZDC(25)/Ni-YSZ/Ni-YSZ/YSZ(500)/YSZ-LSM/LSM	100 under 0.6 V at 850 ℃	Stable for 85 h under 0.6 V at 850 ℃	[151]

Steam-ethanol mixture (S/C: 3.1)	Electrolyte-supported cell: Rh-$Ce_{0.75}Zr_{0.25}O_2$/Ni-YSZ(30)/YSZ/SDC/LSCF(30)		Stable for 60 h under 20 mA at 800 ℃	[196]
Ethanol	Button cell: Ir-GDC(25)/Ni-YSZ(600)/YSZ(10)/GDC/LSCF	420 under 0.6 V at 850 ℃	Stable for 700 h under 0.6 V at 850 ℃	[240]
Ethanol-steam mixture (molar ratio: 1:1)	Anode-supported button cell: Ni-BZCY/SDC(20)/BSCF or SSC(20)	750 at 750 ℃; 391 at 550 ℃	Stable for 180 h under 300 mA cm^{-2} at 600 ℃	[242]
Ethanol	Anode-supported button cell: Ni-BZCYYb/SDC(20)/BSCF or SSC(15)	953 at 750 ℃; 519 at 600 ℃	Stable for 100 h under 300 mA cm^{-2} at 600 ℃	[243]

Table 5. Electrochemical performances of solid carbon-fuelled SOFCs.

Fuel	Configuration: anode/electrolyte/cathode (thickness, μm)	Operating temperature (℃)	Maximum power density (mW cm^{-2})	Discharging duration	Fuel utilization	Ref.
Activated carbon	Button cell: LSFNb(20)/SDC(20)/ScSZ(400)/LSM-ScSZ	850	302.8	~18 h at 227 mA cm^{-2}	25%	[260]
Ca-loaded activated carbon	Button cell: LSFT-GDC(25)/YSZ(200)/LSCF-GDC	850	292	~4.8 h at 350 mA cm^{-2}		[261]
Fe-loaded activated carbon	Button cell: N-LSCM-YSZ(35)/YSZ(300)/LSCF-GDC	850	153	12 h at 180 mA cm^{-2}	33.6%	[262]
Activated carbon-carbonate mixture	Button cell: $YST_{0.9}Cu_{0.1}$-GDC/LSGM(300)/LSCF	800	366	30 h at 200 mA cm^{-2}		[263]
Ca-loaded activated carbon	Button cell: Ag-GDC(20)/YSZ(300)/Ag-GDC	850	373	8.11 h at 364 mA cm^{-2}	18.2%	[265]
Ba-loaded activated carbon	Button cell: Ag-GDC(40)/YSZ(400)/Ag-GDC	850	328.4	28.76 h at 250 mA cm^{-2}	16%	[264]
Sr-loaded coconut active charcoal	Button cell: Ag-GDC(32)/YSZ(450)/Ag-GDC(32)	850	316	22.68 h at 250 mA cm^{-2}	18.3%	[266]
Steel slag-loaded activated charcoal	Button cell: Ni-YSZ(430)/YSZ(35)/LSM(30)	825	159	~3.3 h at 52.1 mA cm^{-2}	46.43%	[267]
Purified High sulfur coal	Button cell: Ni-YSZ(470)/YSZ/LSM	850	~115	11.2 h at 50 mA cm^{-2}	40%	[258]
Brown coal char	Button cell: Ag-GDC(13)/YSZ(450)/Ag-GDC	850	221	13.73 h at 400 mA cm^{-2}	61.5%	[269]
Raw brown coal	Button cell: Ag-GDC(13)/YSZ(450)/Ag-GDC	850	211.4	4.14 h at 400 mA cm^{-2}	18.5%	[269]
Pepper straw char	Microtubular cell: Ag-GDC(30)/YSZ(280)/LSM(60)	850	217	21 h at 100 mA	44.4%	[271]
Bagasse char	Button cell: Ag-GDC(35)/YSZ(370)/Ag-GDC(35)	800	260	22 h at 140 mA cm^{-2}	19.8%	[272]
Corncob char	Button cell: Ag-GDC(35)/YSZ(370)/Ag-GDC(35)	800	204	24 h at 140 mA cm^{-2}	21.4%	[272]
Wheat straw char	Button cell: Ag-GDC(35)/YSZ(370)/Ag-GDC(35)	800	187	15 h at 140 mA cm^{-2}	13.4%	[272]
Ca-loaded Wheat straw char	Button cell: Ag-GDC(21)/YSZ(200)/Ag-GDC	800	258	10.2 h at 300 mA cm^{-2}	33.3%	[273]
Fe-loaded walnut shell char	Tubular cell: Ag-GDC/YSZ(192)/Ag-GDC	800	205			[274]
Corn straw char	Button cell: LSFNb(20)/SDC(20)/ScSZ(400)/LSM-ScSZ	850	218.5	~21 h at 227 mA cm^{-2}	30%	[260]

Kelp char	Button cell: Ag-GDC(20)/YSZ(400)/Ag-GDC(20)	850	285	2.81 h at 350 mA cm^{-2}	10.7%	[275]

Table 6. Stability capacities of ammonia-fuelled SOFCs.

Fuel	Configuration: anode/electrolyte/cathode (thickness, μm)	Operating temperature (°C)	Stability characteristic	Ref.
Ammonia	Anode-supported planar cell: Ni-YSZ/Ni-YSZ/YSZ/LSM-YSZ	850	1500 h with the degradation rate of 2-4% kh^{-1} under 1 A cm^{-2}	[322]
Ammonia	200 W-class planar cell stack: Ni-YSZ(1000)/Ni-YSZ(7)/ZrO_2-based oxide(7)/Perovskite-type oxide(30)	770	1000 h with the comparable degradation rate to hydrogen fuel under 30 A	[310]
Ammonia-steam mixture	10-planar-cell stack: Ni-GDC(40)/ScSZ(165)/LSM-ScSZ(45)	835	1000 h with the degradation rate of 1.1% kh^{-1} under 0.226 A cm^{-2}	[321]
Ammonia	30-planar-cell stack: Ni-YSZ(1000)/Ni-YSZ(7)/ZrO_2-based oxide(7)/LaNiO-based perovskite(30)	750	Stable for 1000 h under 0.316 A cm^{-2}	[312]
Ammonia	Button cell: Ni-SDC(700)/SDC(50)/SSC-SDC	600	Stable for 50 h under 0.36 A cm^{-2}	[284]
Ammonia-nitrogen mixture	Flat-tube cell with the Ba-Ni-YSZ catalyst: Ni-YSZ(100)/YSZ(10)/LSM-YSZ(25)	750	50 h with the degradation of 0.47% under 0.2 A cm^{-2}	[307]
Ammonia-nitrogen mixture	Button cell: $Ni_{97}Cr_3$-SDC(30)/LSGM(500)/SSC(10)	600	30 h with the degradation of 4% under OCV condition	[318]
Ammonia	Button cell: LSTNC-SDC(30)/SDC(350)/SSC(20)	700	120 h with the degradation rate of 0.89 mV h^{-1} under 0.1 A cm^{-2}	[316]